COPPE
Instituto Alberto Luiz Coimbra de Pós-Graduação e Pesquisa de Engenharia
UFRJ

MODELING OF CHO CELL BATCH AND FED-BATCH CULTURES USING A DYNAMIC FLUX BALANCE ANALYSIS APPROACH AND A GENOME-SCALE METABOLIC MODEL

Jasper Hendrik Moltrecht

Dissertação de Mestrado apresentada ao Programa de Pós-graduação em Engenharia Química, COPPE, da Universidade Federal do Rio de Janeiro, como parte dos requisitos necessários à obtenção do título de Mestre em Engenharia Química.

Orientadores: Leda dos Reis Castilho
Argimiro Resende Secchi

Rio de Janeiro
Dezembro de 2017

MODELING OF CHO CELL BATCH AND FED-BATCH CULTURES USING A DYNAMIC FLUX BALANCE ANALYSIS APPROACH AND A GENOME-SCALE METABOLIC MODEL

Jasper Hendrik Moltrecht

DISSERTAÇÃO SUBMETIDA AO CORPO DOCENTE DO INSTITUTO ALBERTO LUIZ COIMBRA DE PÓS-GRADUAÇÃO E PESQUISA DE ENGENHARIA (COPPE) DA UNIVERSIDADE FEDERAL DO RIO DE JANEIRO COMO PARTE DOS REQUISITOS NECESSÁRIOS PARA A OBTENÇÃO DO GRAU DE MESTRE EM CIÊNCIAS EM ENGENHARIA QUÍMICA.

Examinada por:

Profa. Leda dos Reis Castilho, Dr.-Ing

Prof. Argimiro Resende Secchi, D.Sc.

Profa. Maria Alice Zarur Coelho, D.Sc.

Eng. Alvio Figueredo Cardero, D.Sc.

RIO DE JANEIRO, RJ – BRASIL
DEZEMBRO DE 2017

Moltrecht, Jasper Hendrik

Modeling of CHO cell batch and fed-batch cultures using a dynamic flux balance analysis approach and a genome-scale metabolic model/Jasper Hendrik Moltrecht. – Rio de Janeiro: UFRJ/COPPE, 2017.

XIII, 96 p.: il.; 29, 7cm.

Orientadores: Leda dos Reis Castilho
Argimiro Resende Secchi

Dissertação (mestrado) – UFRJ/COPPE/Programa de Engenharia Química, 2017.

Referências Bibliográficas: p. 77 – 85.

1. Dynamic flux balance analysis. 2. Genome-scale metabolic model. 3. CHO cell metabolism. 4. Monoclonal antibodies. I. Castilho, Leda dos Reis *et al.* II. Universidade Federal do Rio de Janeiro, COPPE, Programa de Engenharia Química. III. Título.

Resumo da Dissertação apresentada à COPPE/UFRJ como parte dos requisitos necessários para a obtenção do grau de Mestre em Ciências (M.Sc.)

MODELAGEM DE CULTIVOS EM BATELADA E BATELADA ALIMENTADA DE CÉLULAS CHO PRODUTORES DE UM ANTICORPO MONOCLONAL USANDO A ABORDAGEM DINÂMICA DO BALANÇO DE FLUXOS

Jasper Hendrik Moltrecht

Dezembro/2017

Orientadores: Leda dos Reis Castilho
Argimiro Resende Secchi

Programa: Engenharia Química

Apresenta-se, nesta dissertação, a modelagem dinâmica de cultivos de células CHO produtores de um anticorpo monoclonal em batelada simples e batelada alimentada. Foi usada a abordagem dinâmica do balanço de fluxos (DFBA) para modelar o metabolismo de células CHO em escala genômica. Foram conduzidos três cultivos em biorreator para obter dados sobre a dinâmica do processo, um cultivo em batelada simples, outro em batelada alimentada com alimentação em pulsos e o terceiro em batelada alimentada com alimentação contínua. Amostras diárias foram retiradas e as concentrações dos metabólitos principais (concentração de células viáveis, glicose, lactato, anticorpo e 19 aminoácidos) foram analisados. Esses dados forneceram a base para a modelagem do processo. O modelo consiste de três partes: um modelo dinâmico do reator, um modelo em estado pseudo-estacionário do metabolismo intracelular em escala genômica, e um bloco cinético determinando as taxas máximas de consumo de substratos. O mesmo conjunto de parâmetros foi usado para simular os três diferentes modos de operação. O modelo foi capaz de prever satisfatoriamente o comportamento dinâmico do crescimento celular e de metabólitos chave.

Abstract of Dissertation presented to COPPE/UFRJ as a partial fulfillment of the requirements for the degree of Master of Science (M.Sc.)

MODELING OF CHO CELL BATCH AND FED-BATCH CULTURES USING A DYNAMIC FLUX BALANCE ANALYSIS APPROACH AND A GENOME-SCALE METABOLIC MODEL

Jasper Hendrik Moltrecht

December/2017

Advisors: Leda dos Reis Castilho
Argimiro Resende Secchi

Department: Chemical Engineering

In this work, the dynamic modeling of antibody-producing CHO cells in batch and fed-batch cultures was realized. A dynamic flux balance analysis approach (DFBA) was applied on a genome-scale metabolic model (GEM) of the CHO cell metabolism. Three cell cultures in a lab-scale bioreactor were carried out: a batch culture, a fed-batch culture with pulse feeding and a fed-batch culture with continuous feeding. Daily samples were taken and analyzed for the concentrations of the main metabolites, including 19 amino acids. These data provided a base to identify key phenomena, fit the parameters and validate the model. The DFBA model was formulated in three parts: a reactor-scale dynamic model representing the mass balances of the analyzed species, a pseudo steady-state model of the intracellular metabolism (the GEM), and a kinetic model which was used to determine the maximal possible substrate uptake rates. The same set of parameters was used to simulate the three distinct operation modes. The model was able to represent satisfactorily the cellular growth and the metabolism of key metabolites.

Contents

List of Figures

List of Tables

Nomenclature

$(\bullet)^\intercal$	transpose matrix/vector of $\bullet$, p. 24
K_m	Michaelis-Menten constant, p. 21
Q	quadratic objective matrix, p. 27
Q_{feed}	continuous feed rate, p. 42
S	stoichiometric matrix, p. 23
Z	value of the objective function, p. 27
$\frac{d(\bullet)}{dt}$	time derivative of $\bullet$, p. 24
$\gamma_{cell,dry}$	specific cell dry mass, p. 39
$[\bullet]$	concentration of $\bullet$ p. 23
μ	net growth rate, p. 42
c	vector of linear objectives, p. 26
k_d	specific death rate, p. 42
lb_i	lower bound of flux i, p. 27
pK_a	acid dissociation constant, p. 18
ub_i	upper bound of flux i, p. 27
v	flux distribution, p. 24
v_i	flux i of the flux distribution v, p. 27
v_{max}	maximum reaction rate, p. 20

Abbreviatons

AOS	Alternative optimal solutions, p. 29
CHO	Chinese hamster ovary, p. 1
COPPE	Instituto Alberto Luiz Coimbra de Pós-graduação e Pesquisa de Engenharia, p. 5
DFBA	Dynamic flux balance analysis, p. 4
FBA	Flux balance analysis, p. 4
FBcont	Fed-batch cultivation with continuous feed, p. 50
FBpulse	Fed-batch cultivation with pulse feed, p. 50
FVA	Flux variability analysis, p. 29
GDH	Glutamate dehydrogenase, p. 14
GEM	Genome-scale metabolic model, p. 3
GLUT	Glucose transporters, p. 9
GPR	Gene-protein-reaction, p. 3
HPLC	High-performance liquid chromatography, p. 37
LECC	Laboratório de Engenharia de Cultivos Celulares, p. 5
LP	Linear programming, p. 26
ME	Malic enzyme, p. 14
NLP	Nonlinear programming, p. 32
ODE	Ordinary differential equation, p. 24
PC	Pyruvate carboxylase, p. 12
PDH	Pyruvate dehydrogenase, p. 12

PEPCK	Phosphoenolpyruvate carboxykinase, p. 14
QP	Quadratic Programming, p. 27
TA	Transamination (pathways), p. 14
TCA	Tricarboxylic acid, p. 8
UFRJ	Universidade Federal do Rio de Janeiro, p. 5
NH_3	Ammonia, p. 13
NH_4^+	Ammonium ion, p. 17
alaTA	Alanine transaminase, p. 14
mAb	Monoclonal antibody, p. 1

Chapter 1

Introduction

1.1 Motivation

Chinese hamster ovary (CHO) cell lines dominate large-scale manufacturing of biopharmaceuticals due to their capacity to correctly produce folded proteins that present proper posttranslational modifications for human use (Castilho, 2016). Of all biopharmaceutical products approved, more than one third are produced in CHO cells (Figure 1.1). Among these biopharmaceuticals (including recombinant hormones, antibodies, blood factors and enzymes), monoclonal antibody (mAb) products are the leading product class, approved for treatment of a wide range of diseases, such as cancer, autoimmune disorders and multiple sclerosis (Ecker et al., 2015).

In 2013, global revenues of the biopharmaceutical market accounted for US $163 billion, which is around 20 % of the total pharmaceutical market (Walsh, 2014). The biopharmaceutical sector has been growing with annual rates of more than 8 %, which is over two-fold the growth rate of the pharmaceutical sector (Walsh, 2014). Of the 10 best-sold pharmaceutical drugs in 2016, seven were biologics, five were produced in CHO cells and five were monoclonal antibodies, as shown in Table 1.1.

In Brazil, biopharmaceuticals are only available by importation of the final product or of the active ingredient, leading to a huge financial burden for the

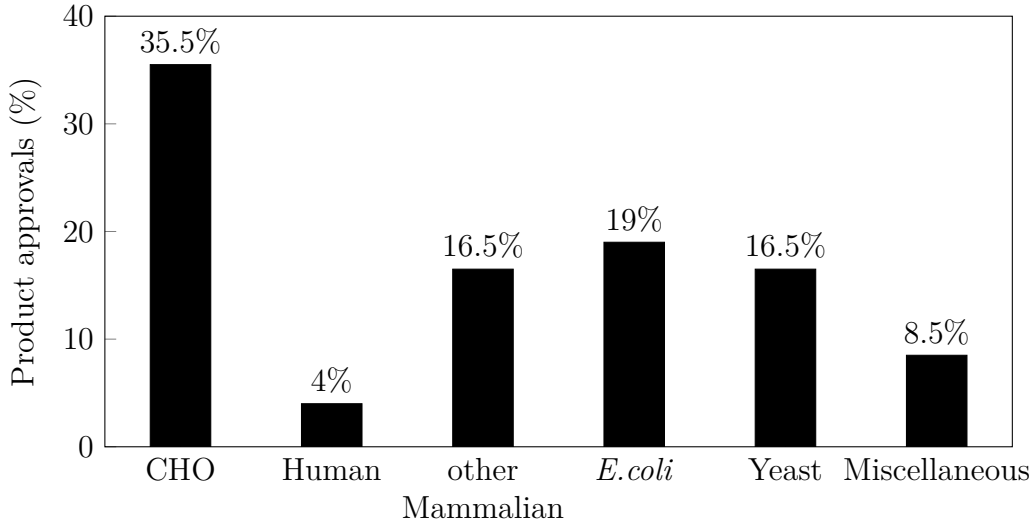

Figure 1.1: Expression systems used to manufacture biopharmaceutical products approved between 1982 and 2014. for different expression systems employed. The data are expressed as a percentage of total biopharmaceutical product approvals. CHO cells are with 35.5 % of total product approvals the dominant expression system. Adapted from Walsh (2014).

Table 1.1: Top ten pharmaceutical drugs by revenue in 2016. Data from the Genetic Engineering & Biotechnology News (Philippidis, 2017).

Name	Company	Type	Expression System	Sales in Billion US$
Humira	AbbVie Inc.	mAb	**CHO**	16.078
Harvoni	Gilead Sciences	Small Molecule	—	9.081
Enbrel	Amgen Pfizer	Fusion Protein	**CHO**	8.874
Rituxan	Roche	mAb	**CHO**	8.583
Remicade	Johnson & Johnson	mAb	Murine Myeloma	7.829
Revlimid	Celgene	Small Molecule	—	6.974
Avastin	Roche	mAb	**CHO**	6.751
Herceptin	Roche	mAb	**CHO**	6.751
Lantus	Sanofi	Protein	*E.coli*	6.054
Prevnar 13	Pfizer	Vaccine	*S. pneumoniae*	5.718

Ministry of Health and for public spending (Neto, 2016). Thus, the establishment of a local production of biosimilars (off-patent biopharmaceuticals) is of great public and economic interest (Ledford, 2010).

Process optimization in the biopharmaceutical industry, in contrast to the chemical or petrochemical industry, remains mainly empirical. This can be explained by the great complexity of biological systems and thus the difficulties to describe them in mathematic terms, leading to two major disadvantages: first, empiric process optimization is based on cost-, labor- and time-intensive experimental work. Second, it does not consider interactions between operation parameters. Conversely, mathematical models based on experimental data and biologic knowledge can provide an *in silico* platform for process analysis and optimization (Koumpouras, 2012).

Traditionally, phenomena in biology have been studied using reductionist approaches, meaning that complex systems were first reduced into smaller problems, which were then analyzed individually (Trewavas, 2006). However, it has been found that the organization and interconnectivity of entire biological systems are as important as the comprehension of the functioning of its parts (Chuang et al., 2010). The need of such holistic approach in biotechnology, and the broad availability of high-throughput genomic and proteomic data, led to the emerging of systems biology in the beginning of the 21st century. Systems biology studies complex biological systems based on molecular-level understanding of its structure and dynamic behavior, with the purpose to formulate representative mathematical models of the system (Ideker et al., 2001; Kitano, 2002).

Genome-scale metabolic models (GEMs) are a powerful tool provided by systems biology. A GEM is a complete reconstruction of the biochemical reaction network that operates in a cell. GEMs are based on biochemical, genetic, and genomic data structured in mathematical terms (Palsson, 2015). They are consistent in mass and energy balances and thus stoichiometrically balanced. Further, the gene-protein-reaction (GPR) relationships are annotated and included (Zhang and Hua,

2016). GEMs have been used successfully in studies about gene lethality (Blank et al., 2005), metabolic pathway evolution (Pál et al., 2006), metabolic engineering strategies (Bro and Nielsen, 2004) and the interpretation of cultivation data (Teusink et al., 2006), among others (Santos et al., 2011).

Considering the great scale of GEMs, traditional theory-based model approaches based on biophysical equations prove themselves inconvenient, as they rely on difficult-to-measure kinetic parameters (Orth et al., 2010). In contrast, constrained-based modeling approaches, such as flux balance analysis (FBA) , can be applied to GEMs without requiring much input data. FBA is a method to simulate the metabolism of a cell, based on its biochemical reaction network (Santos et al., 2011). It combines the stoichiometry of the metabolic network with a pseudo steady state assumption of the intracellular metabolism and certain biological constraints to transform the problem into a set of linear equations. Then, using an optimization approach, the flow of metabolites (or "fluxes") through the metabolic network is determined. Thus, predictions of the growth rate and the usage of certain metabolic pathways can be made (Orth et al., 2010).

However, the application of classic FBA is limited to a particular steady state of the system. The need to study the dynamics of the metabolic network led to the development of an extension of FBA: dynamic flux balance analysis (DFBA) (Mahadevan et al., 2002). DFBA considers the influence of environmental conditions on the intracellular metabolism, commonly in the form of substrate kinetics. This allows the analysis of interactions between the cellular metabolism and its extracellular environment, and thus predictions of substrate, biomass and product concentrations in dynamic cultures (Höffner et al., 2013).

Even though several studies successfully applied DFBA to bacteria (Oddone et al., 2009; Zhuang et al., 2011) and yeast (Hjersted and Henson, 2009; Hjersted et al., 2007), only very few attempts to model the dynamics of animal cell cultures were made, and none of them using a genome-scale metabolic model. This makes this work a pioneer study in the field.

Currently, several projects of the Cell Culture Engineering Laboratory (LECC) at the Alberto Luiz Coimbra Institute for Graduate Studies and Research in Engineering (COPPE) of the Federal University of Rio de Janeiro (UFRJ) involve CHO cells as expression system for biopharmaceutical products. The ambition of these projects is to expand biopharmaceutical manufacturing in Brazil, and thus ease the burden of public spending. These projects could greatly benefit from a robust model, which is investigated in this work.

1.2 Objective

The global objective of this work is to model the production of a monoclonal antibody expressed in CHO cells, using a dynamic flux balance analysis (DFBA) approach, in order to then use a dynamic optimization approach to define the optimal feeding strategy for the process. This involves the following specific objectives:

(i) To obtain representative data for the process dynamics: quantification of main metabolite concentrations for different feeding strategies;

(ii) To create the DFBA model: find a genome-scale metabolic model (GEM) of the CHO cell, define kinetic flux constraints and objective functions, estimate model parameters.

1.3 Structure of the thesis

This thesis is structured in five chapters. In Chapter 1 the reader is briefly introduced to the main topics, motivations and objectives of this work. Chapter 2 discusses the current knowledge about CHO cells as expression system for biopharmaceuticals, their metabolism, genome-scale metabolic models (GEMs) and dynamic flux balance analysis. The third chapter explains the methodology for both the experimental and the computational part of this work. In Chapter 4 the obtained results

are described and compared with previous results of other authors. Further, the innovation is clarified and strengths and weaknesses are discussed critically. In the fifth and last chapter, the conclusions are drawn and ideas for future work are raised.

Chapter 2

Literature review

2.1 CHO cells as expression system

Chinese hamsters (*Cricetulus griseus*) are a species of rodents native to Northern China. They were used as laboratory animals in different areas of biomedical research since 1919. In 1957 the isolation of an ovary from *Cricetulus griseus* led to the establishment of the first continuous Chinese hamster ovary (CHO) cell line, which is known as CHO.K1 and gave rise to other CHO cell lines derived from it. CHO cell lines have emerged as the dominant host cell line in biopharmaceutical manufacturing, producing more than one third of all recombinant protein therapeutics (Walsh, 2014).

The preference for CHO cells in the biopharmaceutical industry is explained by their high efficiency in producing human-compatible therapeutic proteins and continued approval by the regulatory agencies (Kildegaard et al., 2013). CHO cells are robust, highly adaptable and can be easily cultured in suspension, allowing very high cell densities and product titers in large scale processes (Jayapal et al., 2007). Moreover, they are capable to correctly fold and post-translationally modify recombinant proteins leading to human-compatible therapeutic proteins with a high biological activity (Ghaderi et al., 2012). Most of viral agents that are pathogenic to humans are not able to propagate in CHO cells, thus they assure high product safety (Wiebe et al., 1989). Furthermore, the selection of stable clones and amplification

of genes in CHO cells is effective, and thus genetic modification of CHO cells is well established (Jayapal et al., 2007). Last but not least, downstream processes for CHO cell products are well characterized, permitting high final product purity (Wurm, 2005). Thus, the use of CHO cells brings advantages in all steps of biopharmaceutical manufacturing: cell line development, large scale production, downstream processing, product safety and regulatory approval (Kim et al., 2012).

2.2 Cellular metabolism

Metabolism is the integration of all biochemical processes that occur within a cell in order to provide chemical energy and sustain growth. The chemical reactions can be arranged in metabolic pathways, which describe how one metabolite is transformed into another by a series of enzyme-catalyzed reactions. The metabolism of a cell consists of hundreds of pathways which are interconnected by thousands of enzymes and metabolites - and thus form a complex metabolic network (Amable and Butler, 2008).

The main carbon and energy sources of animal cells are the monosaccharide sugar glucose and amino acids, especially glutamine, which is also the cell's main nitrogen source (Häggström, 2000). Glucose is mainly metabolized in glycolysis, a pathway that consists of a chain of reactions leading to the formation of ATP, the metabolisms energy *currency*, pyruvate and other metabolic intermediates. Glucose can also be metabolized in the pentose phosphate pathway. Pyruvate can be further processed in the aerobic tricarboxylic acid (TCA) cycle, providing NADH and $FADH_2$, which are fed into the oxidative phosphorylation pathway, the cells respiratory system, where they give riste to the generation of large amounts of ATP. Pyruvate can also be transformed into lactate by the enzyme lactate dehydrogenase (LDH). Glutamine plays an important role in energy and nitrogen metabolism, since its carbon molecules can be completely oxidized to CO_2 in the TCA cycle and oxidative phosphorylation, and its amino groups are used to synthesize other amino acids or converted to ammonia.

To become a continuous cell line used for the industrial production of biopharmaceuticals, mammalian cells undergo a process called transformation, which gives them the capacity to grow indefinitely. During transformation the cells suffer genetic alterations, causing a de-regulation of the mechanisms that control the cell cycle, and thus leading to uncontrolled proliferation. However, the mutations also affect the metabolism of continuous cell lines, causing an excessive glucose and glutamine metabolism that exceeds purely biosynthetic requirements. This also contributes to the formation of large amounts of metabolic byproducts, such as lactate, ammonia and alanine (Amable and Butler, 2008; Häggström, 2000).

2.2.1 Glucose metabolism

Extracellular glucose is transported by membrane proteins, called glucose transporters (GLUT), to the cytoplasm of the cell, where it is rapidly phosphorylated to glucose-6-phosphate by the enzyme hexokinase. This reaction is the first step of glycolysis, a pathway that provides the cell with energy, in the form of ATP, and metabolic intermediates. However, glucose-6-phosphate can also be metabolized via the hexose monophosphate shunt (HMS), which forms together with the pentose phosphate pathway (PPP) and a part of glycolysis the pentose phosphate cycle. The products of this cycle, nicotinamide adenine dinucleotide phosphate (NADPH) and ribose-5-phosphate, are important for biosynthesis and the synthesis of nucleotides and nucleic acids, respectively (Häggström, 2000). However, studies in hybridoma cells reported that often more than 90 % of glucose consumed enters the glycolytic pathway, and only a small proportion the HMS (Neermann and Wagner, 1996; Petch and Butler, 1994).

Glycolysis is a sequence of enzyme-catalyzed reactions that metabolize one molecule of glucose to two molecules of pyruvate. During glycolysis two molecules of ATP are consumed, and four provided, leading to a net balance of two molecules of ATP (Figure 2.1). Thus, glycolysis is the source of cytosolic ATP (Amable and Butler, 2008). However, it is also the source of fructose 6-phosphate,

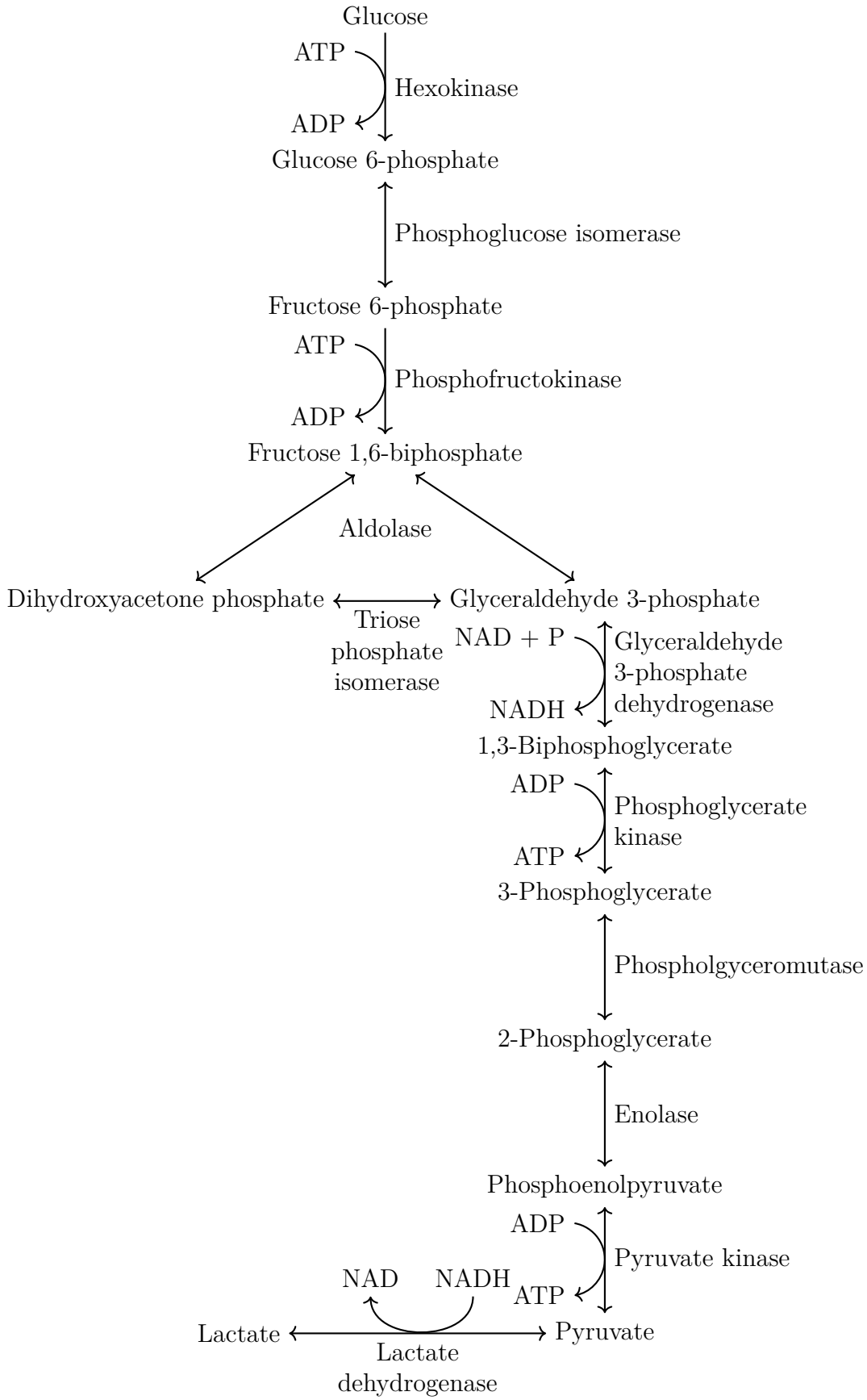

Figure 2.1: An overview of glycolysis, the pathway by which glucose is degraded to pyruvate. Aldolase converts one six-carbon molecule into two, three-carbon molecules. Thus, the reactions following glyceraldehyde 3-phosphate occur twice.

dihydroxyacetone phosphate and 3-phosphoglycerate, precursors for the synthesis of amino sugars, glycerol-3-phosphate, and the amino acids serine and glycine. A sufficient supply of these metabolites is necessary to sustain the fast growth of a continuous cell line (Häggström, 2000).

Both glycolysis and the pathway for serine and glycine synthesis reduce NAD to NADH. Thus, a source of NAD is needed for the functioning of these two pathways. There are two ways to regenerate the NAD in the cytosol: first, shuttle mechanisms that indirectly transport NADH into the mitochondria and NAD into the cytosol; second, the reduction of pyruvate to lactate by the enzyme lactate dehydrogenase (LDH), which consumes NADH and releases NAD (Häggström, 2000).

Redox shuttle systems, such as the malate-citrate shuttle, the glycerol-phosphate shuttle and the malate-aspartate shuttle, allow the indirect transportation of NADH from cytosol into mitochondria and NAD in the opposite direction through the impermeable mitochondrial membrane. In the mitochondria, NADH enters the respiratory chain, where its oxidation to NAD occurs (Altamirano et al., 2013).

2.2.2 Tricarboxylic acid cycle

The tricarboxylic acid (TCA) cycle consists of a chain of reactions, which occur exclusively in the mitochondria. It provides precursor metabolites for anabolism and the redox cofactors NADH and $FADH_2$, which are used in the respiration chain to generate large amounts of ATP. It is the major source of metabolic energy for mammalian cells (Häggström, 2000).

Important participants of the TCA cycle are citrate, isocitrate, oxaloacetate and alpha-ketoglutarate. Citrate is the precursor of acetyl coenzyme A (acetyl CoA) in the cytosol, which is needed for the synthesis of fatty acids. Isocitrate, when transported to the cytosol, can be metabolized by the cytosolic isocitrate dehydrogenase to produce NADPH. Oxaloacetate and alpha-ketoglutarate are precursors for aspartate/asparagine and glutamate biosynthesis, respectively. However, it is more probable that glutamate enters the TCA cycle through this

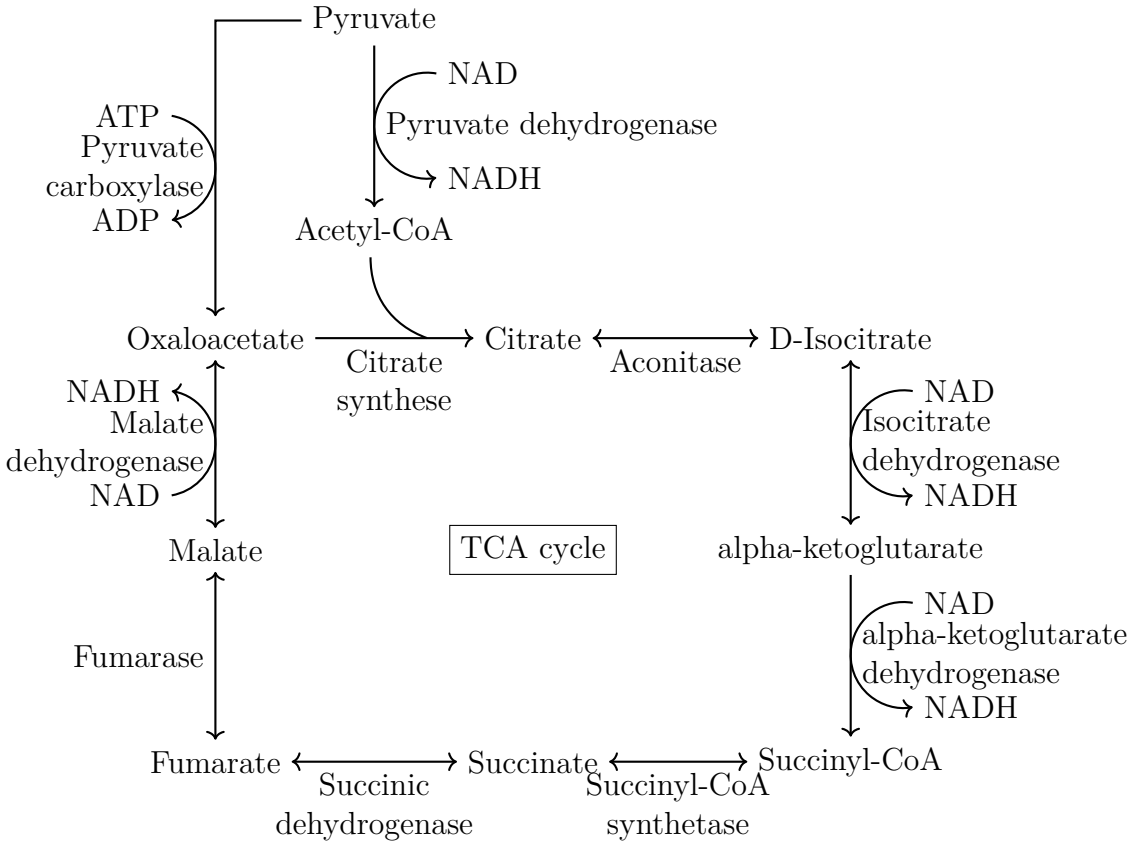

Figure 2.2: An overview of the TCA cycle. Pyruvate, the end product of glycolysis, connects the TCA cycle with the glucose metabolism by means of the enzymes pyruvate dehydrogenase and carboxylase.

reversible reaction catalyzed by glutamate dehydrogenase as part of glutamine metabolism (Häggström, 2000). Figure 2.2 shows a schematic diagram of the TCA cycle.

The TCA cycle is linked to glycolysis by two key enzymes: pyruvate dehydrogenase and pyruvate carboxylase (PC). In the mitochondria, pyruvate dehydrogenase (PDH) transforms pyruvate into acetyl CoA, which enters the TCA cycle to form citrate. The reaction catalyzed by pyruvate dehydrogenase is essentially irreversible (Amable and Butler, 2008). Other than from glycolysis, acetyl CoA can also originate from fatty acids or the breakdown of the amino acids leucine and isoleucine. If going through the full TCA cycle, acetyl CoA is completely oxidized to carbon dioxide and water, unfolding the full energetic potential of glucose.

However, it was found that the influx of pyruvate into the TCA cycle was

extremely low in continuous cell lines: only 0.2 % to 0.6 % of total glucose metabolized were estimated to enter the TCA cycle of the cells (Fitzpatrick et al., 1993; Petch and Butler, 1994). Further, Neermann and Wagner (1996) reported the lack of PDH activity in CHO.K1 cells. Thus, pyruvate is metabolized to lactate in the cytosol, which is then secreted to the extracellular environment. Consequently, the full energetic potential of glucose is not unfolded. Reasons for this could be (1) pyruvate unavailability due to LDH overactivity, (2) a low level of PDH expression, (3) inhibition of PDH activity by high mitochondrial NADH levels as result of the glutamine metabolism, or (4) a combination of these factors (Häggström, 2000).

Pyruvate carboxylase (PC) is a shortcut from pyruvate to oxaloacetate in the TCA cycle. Oxaloacetate is an important precursor for aspartate, which in turn can be further metabolized to purines, pyrimidines and the amino acid asparagine. Thus, the action of PC allows the substitution of oxaloacetate withdrawn from the TCA cycle for anabolism. It enables the synthesis of aspartate directly from glucose (Häggström, 2000). However, the lack of PC was reported in continuous cell lines, such as CHO.K1 (Neermann and Wagner, 1996), myeloma (Vriezen and van Dijken, 1998) and murine hybridoma (Mancuso et al., 1994). Consequently, oxaloacetate has to be supplied by glutamine metabolism.

2.2.3 Glutamine metabolism

Glutamine is the amino acid with the highest consumption rates in mammalian cell lines, plays important roles in energy and carbon metabolism and is the main source of nitrogen. Its metabolism generates energy and provides precursors for biosynthesis. It acts as nitrogen donor in the synthesis of pyrimidine, purine, amino sugars, NAD and asparagine (Häggström, 2000).

Glutamine metabolism occurs mainly in mitochondria and consists of a mixture of different pathways. The first step is the conversion of glutamine and H_2O to glutamate and ammonia (NH_3), catalyzed by the enzyme phosphate-activated glutaminase (PAG). Glutamate is then processed in two major pathways: the

glutamate dehydrogenase (GDH) pathway and the transamination (TA) pathways. In both cases the immediate product of glutamate is alpha-ketoglutarate, and thus a connection to the TCA is established. The difference is the destiny of the amino group, which is cleaved in the reactions (Altamirano et al., 2013).

In the GDH pathway, the deamination occurs by releasing a further ammonium ion. The formed alpha-ketoglutarate can then be used freely in the intermediate metabolism, for example, it can be oxidized completely in the TCA cycle to H_2O and CO_2, providing energy. It can also leave the TCA cycle as malate to form pyruvate and even lactate. The conversion from malate to pyruvate can occur in mitochondria, involving the malic enzyme II (ME-II), or in the cytosol, where it is catalyzed by the enzymes phosphoenolpyruvate carboxykinase (PEPCK) or the cytosolic malic enzyme I (ME-I) (Altamirano et al., 2013). However, in CHO and other cell lines, a deficiency of PEPCK (Fitzpatrick et al., 1993; Neermann and Wagner, 1996) and a significant activity of ME-I was shown (Bonarius et al., 2001; Quek et al., 2010).

In the TA pathways, the amino group cleaved in the reaction of glutamate to alpha-ketoglutarate is transferred to pyruvate or to oxaloacetate, to yield the amino acids alanine and aspartate, respectively (Figure 2.3). Thus it can be distinguished between two different TA pathways, catalyzed by the enzymes alanine transaminase (alaTA) and aspartate transaminase. Both pyruvate and oxaloacetate are substrates of the TCA cycle, so the addition of the glutamate carbon as alpha-ketoglutarate to the cycle is coupled with the removal of another carbon. Therefore, the TA pathways have a closed loop structure, and cannot lead to complete oxidation nor to lactate formation. Hence, the possible energy yield of TA pathways is smaller than of the GDH pathway (Altamirano et al., 2013).

Mitochondrial oxaloacetate is presumably the most important intermediate of glutamine metabolism, being the precursor for aspartate, which in turn can be further metabolized to purines, pyrimidines and the amino acid asparagine. As discussed earlier, the enzyme PC, which enables the supply of oxaloacetate from

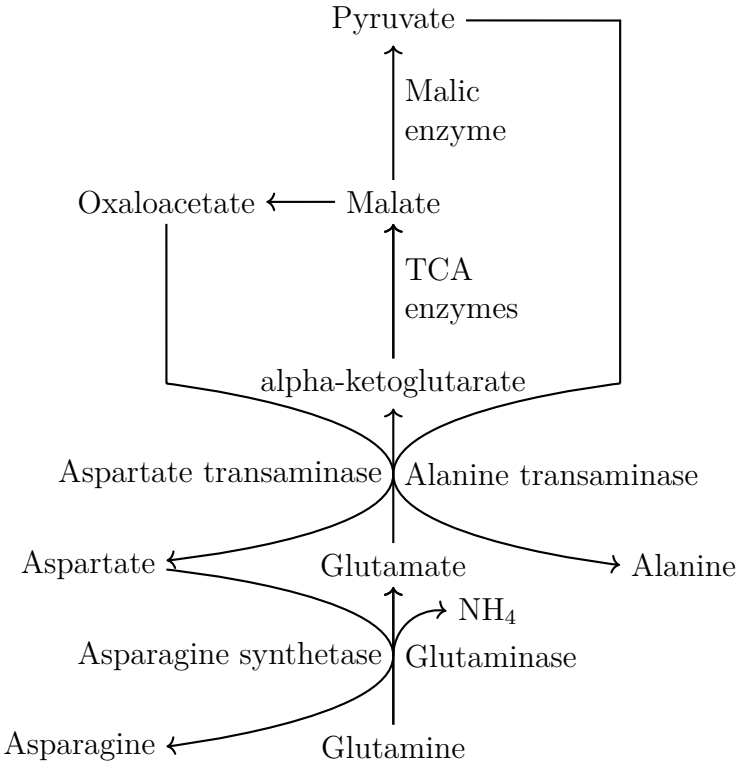

Figure 2.3: Overview of the transamination pathways. On the right is the alaTA pathway and on the left the aspTA pathway. If aspartate is further metabolized to asparagine, no ammonia is formed at all. Adapted from Häggström (2000).

glucose, is not present in continuous cell lines. Furthermore, the activity of the amino acid transport system X_{AG}^-, responsible for the importation of glutamate and aspartate from the extracellular space, was found to be extremely low in continuous cell lines (Bussolati et al., 1993; Longo et al., 1988). Consequently, glutamine metabolism may be fundamental for continuous cell lines to obtain these amino acids (Häggström, 2000).

2.2.4 Lactate metabolism

As explained earlier, lactate is a metabolic byproduct, which is generated from pyruvate by the enzyme lactate dehydrogenase (LDH), and can be a product both of glucose and glutamine metabolism. An excessive lactate production has been observed in continuous cell lines, which is the result of the deregulated metabolism of glucose and glutamine. The production of lactate is associated with an unfavorable energy metabolism, as the complete oxidation of pyruvate yields a far greater amount

of ATP. Moreover, lactate is secreted by the cell and accumulates in the culture medium, causing an acidification of the medium if not controlled. When there is pH control, it can give rise to an increase in osmolality. Furthermore, high lactate concentrations were found to inhibit both cell growth and productivity even at constant pH (Amable and Butler, 2008).

The high lactate generation in continuous cell lines can have various explanations which were partially mentioned above and have been summarized by Amable and Butler (2008):

(i) conversion of pyruvate to lactate occurs to regenerate NADH in the cytosol required for the high glycolytic flux;

(ii) limitation of the indirect transport of NAD through the malate/aspartate shuttle to the mitochondria by a low concentration of cytosolic and a high concentration of mitochondrial aspartate;

(iii) accumulation of malate in the mitochondria due to glutamine metabolism may further limit the flux through the malate/aspartate shuttle;

(iv) saturation of the respiratory system with NADH due to glutamine metabolism;

(v) suppression of the respiratory system due to low availability of ADP, as large amounts of ADP are consumed in glycolysis;

(vi) high activity of lactate dehydrogenase and low activity of pyruvate dehydrogenase;

(vii) lack of enzymatic activity of the enzymes linking the glycolysis pathway with the TCA cycle, such as pyruvate dehydrogenase and pyruvate carboxylase.

Summarizing, lactate is the end product of an incomplete oxidative metabolism, associated with high glucose and glutamine consumption in continuous cell lines.

Lactate consumption in CHO cells

However, a metabolic shift from lactate production to net lactate consumption was observed in several CHO cell lines (Luo et al., 2011; Martínez et al., 2013; Nolan and Lee, 2011; Zagari et al., 2013). The cells are able to import extracellular lactate to the cytosol where lactate dehydrogenase catalyzes the reverse reaction, consuming

lactate and producing pyruvate. Then, pyruvate may be further metabolized in the cell.

Zagari et al. (2013) stated that lactate is strongly produced in both parental CHO-S cells and a non-recombinant subclone when the key substrates glucose and glutamine are available in high concentrations, but suddenly consumed when there is depletion of both of these substrates. They found that high lactate production is associated with a reduced mitochondrial oxidative metabolism and assumed that mitochondria play a key role in the regulation of the metabolic shift.

Luo et al. (2011) studied the metabolic shift in antibody producing CHO cell lines derived from CHO DUK-XB11 cells. They observed that the energy metabolism of the cells was less effective while they produced lactate, and that glucose was primarily metabolized to pyruvate, sorbitol, lactate and other glycolytic intermediates, but did not supply the TCA cycle. Thus, they stated glycolysis as the main energy source of the cells. Further, they also associated the lactate metabolic shift with the capacity of the oxidative metabolism.

Martínez et al. (2013) used a flux balance analysis approach to compare the energy metabolism of CHO during lactate production and lactate consumption. Their CHO-XL99 cells underwent the metabolic shift from lactate production to lactate consumption upon glucose depletion. They found that cells consuming lactate generate six times more ATP per carbon molecule than lactate producing cells. Further, they stated that the majority of acetyl-CoA formed by pyruvate dehydrogenase (PDH) was used for fatty acid production while producing lactate, in contrast to the lactate consumption phase, where it was mostly oxidized in the TCA cycle.

2.2.5 Ammonia

Ammonia (NH_3) and ammonium ions (NH_4^+) are considered highly toxic to mammalian cells. Even small concentrations of ammonia, between 2 mM to 5 mM, cause inhibition in growth and productivity (Glacken, 1988). The origin of ammonia

in cell cultures lies in glutamine metabolism: one ammonium ion is released in the reaction from glutamine to glutamate, and another one when glutamate is processed in the GDH pathway. Further, glutamine also suffers thermal degradation, releasing ammonia (Amable and Butler, 2008).

The negative effects of ammonia are attributed to intracellular pH changes. The relative concentrations of NH_3 and NH_4^+ can be calculated with the Henderson-Hasselbalch equation:

$$pH = pK_a + \log_{10}\left(\frac{[NH_3]}{[NH_4^+]}\right) \tag{2.1}$$

At a temperature of 37 °C the acid dissociation constant pK_a lies between 8.80 and 8.95 (Bates and Pinching, 1949), and thus at a physiological pH of around 7.2, NH_3 only constitutes a small proportion of the total concentration of NH_3 and NH_4^+. The cell membranes are impermeable to NH_4^+ but allow the diffusion of the uncharged NH_3. This diffusion is driven by the concentration gradient over the membrane, and thus new equilibria between NH_3 and NH_4^+ in the different cell compartments and the medium are instantaneously established. Some of the NH_4^+ released in mitochondria as function of glutamine metabolism give up their protons and become NH_3, in order to satisfy the chemical equilibrium. This, however, changes the transmembrane concentration gradient, resulting in an outflow of NH_3 to the cytosol and then to the extracellular environment. As the proton is left behind, this leads to an acidification of the cytoplasm and the mitochondrial matrix, and an alkalinization of the extracellular environment. Additionally, NH_4^+ can be transported back to the cytosol by carrier proteins, thus forming a cycle with NH_3 diffusion, which leads to a further pH decrease (Figure 2.4). Besides the pH modifications, this process also causes a perturbation of the transcellular ionic gradient (Amable and Butler, 2008; Häggström, 2000).

Further toxic effects of excessive ammonium include the enzymatic inhibition of parts of glycolysis, the TCA cycle, the PPC and glutamine metabolism, an increase in alanine secretion and it can affect the glycolisation pattern of recombinant proteins

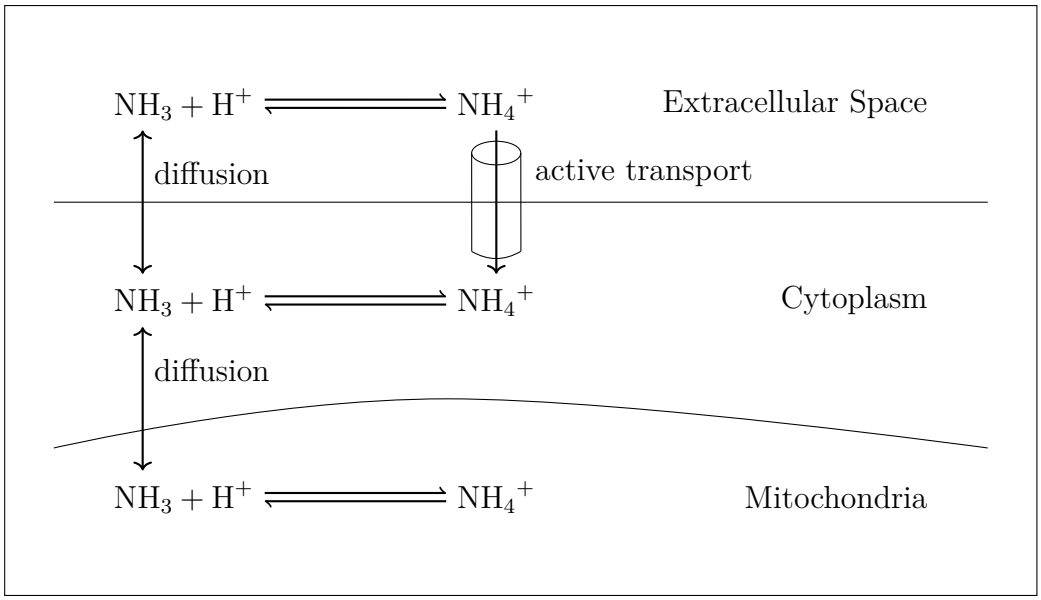

Figure 2.4: Effects of ammonia and ammonium on mammalian cell cultures. NH_3 is able to freely diffuse between the cell compartments, NH_4^+ not. Further production of NH_4^+ due to glutamine metabolism thus leads to a pH decrease in the mitochondria. Adapted from Amable and Butler (2008).

(Amable and Butler, 2008; Nam et al., 2008). The latter is especially important for the production of proteins with a complex three-dimensional structure such as monoclonal antibodies, as protein glycosylation plays critical roles in protein folding, activity and immunogenicity (Jenkins and Curling, 1994).

2.3 Enzyme kinetics

As mentioned before, the cellular metabolism is fundamentally based on enzyme-catalyzed reactions. Enzymes are macromolecular biological catalysts, mostly proteins, that accelerate chemical reactions by factors of millions. Their catalytic activity is essential for biological systems, as in their absence most metabolic processes would not occur at rates fast enough to sustain life. Another key attribute of enzymes is their high specificity towards both the reactions that they catalyze and their choice of substrate (Berg et al., 2002).

The catalytic efficiency of enzymes is based on intermolecular forces. They bind to substrates to form an enzyme-substrate complex and arrange the substrates in an optimal orientation for the chemical reaction. Doing so they stabilize the transition

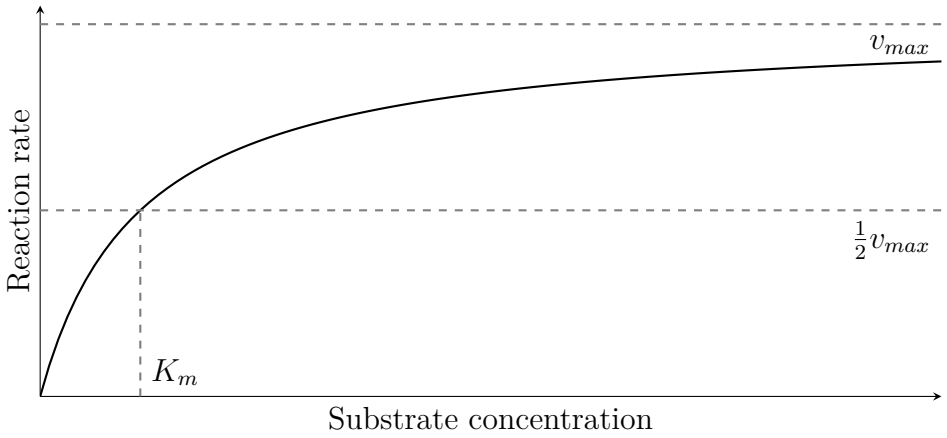

Figure 2.5: Michaelis–Menten saturation curve showing the relation between the substrate concentration and reaction rate of a single-substrate enzyme catalyzed reaction.

state and thus lower the activation energy of the reaction. During this process the enzyme does not undergo any permanent chemical change and is not used up (Berg et al., 2002).

Enzyme-catalyzed reactions display saturation kinetics with the turnover rate of the enzyme as limiting factor. The functional dependency of the reaction rate on the substrate concentration of a single-substrate enzyme catalyzed reaction is described in Figure 2.5. For relatively low substrate concentrations the reaction rate of an enzyme increases linearly with substrate concentration, as encounters between enzyme and substrate become more frequent. However, for higher substrate concentrations, not the substrate concentration, but the availability of active sites on the enzyme becomes the limiting factor. Thus, the reaction rate asymptotically approaches a theoretical maximum, which is reached when all active sites of the enzyme are constantly occupied (Berg et al., 2002).

This kinetic behavior was described in mathematical terms by Michaelis and Menten (1913). The Michaelis-Menten equation describes the reaction rate v as a function of the substrate concentration $[S]$, as follows:

$$v = \frac{v_{max}\,[S]}{K_m + [S]} \tag{2.2}$$

where v_{max} represents the maximum velocity that the enzyme can achieve, at

saturating substrate concentrations. K_m is the Michaelis-Menten constant, which shows the substrate concentration for which the reaction rate of an enzyme is equal to one half of v_{max}, thus indicating how quickly the enzyme becomes saturated with the substrate. Knowing these properties helps to predict the behavior of an enzyme in a cell under different conditions. Furthermore, these information can be utilized in the dynamic modeling of cell culture processes to describe the maximum possible uptake rate of a certain substrate, based on its concentration.

Further, enzymatic activity is strongly influenced by environmental conditions such as pH and temperature (Berg et al., 2002). Thus it is of great importance for studies of the metabolism that these factors are well measured and controlled.

2.4 Modeling of cell culture processes

Mammalian cell culture processes are extremely complex, and a large number of process parameters influence growth and product formation. For manufacturing, it is important to determine the optimal conditions to efficiently provide a safe and affordable product. Currently, process identification and optimization is mainly based on empiric experimental work, which is expensive, time consuming and labor intensive (Koumpouras, 2012). Further, interactions and mechanisms between process parameters often cannot be identified by pure statistical analysis of experimental data (Yahia et al., 2015). Conversely, mathematical models can provide an *in silico* platform for process analysis, simulation and optimization.

Mathematical models for animal cell culture and biosystems in general can be classified as unstructured and structured, segregated and unsegregated models. Unstructured models consider the cell as a black box, while structured models also consider intracellular reactions. Unsegregated models consider the cell population homogeneous in regard to cell age, size, growth rate and metabolic state. In contrast, segregated models describe the biochemical activities of distinct parts of the population as function of cell cycles or age of cells (Tziampazis and Sambanis, 1994; Yahia et al., 2015).

However, due to the high complexity and interactivity of biological systems, their representation as robust mathematical models remains challenging. There are several limitations of theory-based modeling approaches in biologic systems, as described by Palsson (2015):

(i) The complexity of the intracellular chemical environment makes the formulation of descriptive equations difficult.

(ii) Accurate numerical values for all parameters of the equations are necessary, but not available.

(iii) Evolution leads to genetic variation and thus diversity in a population. Consequently living systems are time-variant and parameters change over the course of time.

A more convenient modeling approach, able to represent different phenotypes and functional states of organisms, is based on genome-scale metabolic reconstructions and constraint-based network analysis. These topics will be discussed in the next two sections.

2.5 Genome-scale metabolic models

Genome-scale metabolic models (GEMs) are mathematical reconstructions of metabolic networks, consisting of all biochemical reactions, metabolites and genes involved in the metabolism of a specific organism. They contain biophysical constraints on the metabolic system, such as limitations in nutrient uptake rates, stoichiometric coefficients and reversibility of reactions (King et al., 2016). Furthermore, information about enzyme interactions and cellular localization of each reaction is included (Feist et al., 2009). GEMs can be used for detailed analysis of the metabolic potential of the organism, process optimization and cell engineering (Hefzi et al., 2016; King et al., 2016).

2.5.1 The stoichiometric matrix S

The central part of a GEM is the stoichiometric matrix S. It represents the stoichiometry of the chemical equations in the reaction network. It is an $m \times n$ matrix, consisting of m rows of reactions and n columns of compounds. Each entry of the matrix is an integer, the stoichiometric coefficient which associates a compound to a reaction. Thus, each row represents a global mass balance for an intracellular metabolite, and every column describes a chemical reaction with elemental balancing (Krömer et al., 2014; Palsson, 2015).

In Figure 2.6, the reaction map of a simple open network is shown. The network considers four metabolites (A, B, C, D), three intracellular reactions (v_{1-3}) and three exchange reactions e_{1-3}. First, the metabolites A and B enter the system by exchange reactions e_1 and e_2. Then, intracellular reactions v_1 and v_2 lead to conversion of A and B, respectively, to metabolite C, which is further processed by reaction v_3 to form metabolite D. Finally, the exchange reaction e_3 transports D to the extracellular space. The reaction rates v and e, called "fluxes", typically have the dimension of moles per time per gram of dry biomass (e.g $\mathrm{mmol\,h^{-1}\,gDM^{-1}}$).

The network can be described as a system of mass balance equations, and more specifically, considering that the intracellular metabolite concentrations may change

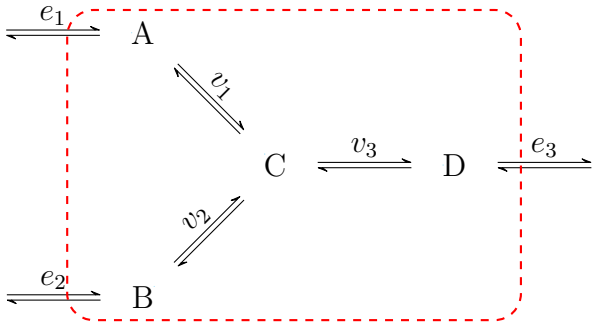

Figure 2.6: Example of a simple reaction network involving the metabolites A, B, C and D, the intra-compartment reactions v and the exchange reactions e. The red line depicts the compartment border.

over time, as system of ordinary differential equations (ODEs):

$$\begin{aligned}
\frac{d[A]}{dt} &= e_1 - v_1 \\
\frac{d[B]}{dt} &= e_2 - v_2 \\
\frac{d[C]}{dt} &= v_1 + v_2 - v_3 \\
\frac{d[D]}{dt} &= v_3 - e_3
\end{aligned} \tag{2.3}$$

By definition, producing reactions receive a positive, and consuming reactions a negative annotation in the respective conservation equation of the system (Krömer et al., 2014). By allowing positive or negative values for the reactions, reversible reactions are unified in a unique reaction. In general, this reaction system can be described in a form:

$$\frac{d[M]}{dt} = Sv \tag{2.4}$$

where $\frac{d[M]}{dt}$ is an $n \times 1$ array containing the time derivations of metabolite concentrations, S the $m \times n$ stoichiometric matrix and v an $m \times 1$ array of all reaction rates, called flux distribution (Krömer et al., 2014).

Applying this to the prior analyzed network (Figure 2.6), we obtain the time derivation array $M = [A, B, C, D]^\intercal$, the flux distribution $v = [e_1, e_2, v_1, v_2, v_3, e_3]^\intercal$ and the stoichiometric matrix

$$S = \begin{array}{c} \begin{matrix} e_1 & e_2 & v_1 & v_2 & v_3 & e_3 \end{matrix} \\ \begin{pmatrix} 1 & 0 & -1 & 0 & 0 & 0 \\ 0 & 1 & 0 & -1 & 0 & 0 \\ 0 & 0 & 1 & 1 & -1 & 0 \\ 0 & 0 & 0 & 0 & 1 & -1 \end{pmatrix} \end{array} \begin{matrix} \\ \text{A} \\ \text{B} \\ \text{C} \\ \text{D} \end{matrix}$$

where each row corresponds to the mass balance of a metabolite.

Beyond the stoichiometric matrix, a GEM contains a gene-reaction association matrix with information about genes and their interactions with the reactions, the

charge and structural formula of each metabolite, cellular compartments and vectors of upper and lower bounds for all reaction rates (Hefzi et al., 2016).

2.6 Constrained-based modeling

As mentioned earlier, theory-based modeling approaches are of limited use for GEMs for several reasons. First, they require complete knowledge about the process and thus a great number of parameters which are not available in literature. Then, theory-based approaches attempt to find a single, exact solution (see Figure 2.7a). This is inconvenient for the analysis of biological networks, as the network may express the same function in different and equivalent ways (Palsson, 2015).

This behavior is better represented by constrained-based approaches, built on the assumption that the functional capabilities of a biological system are constrained by its environment, genetics, and by physico-chemical laws (Bordbar et al., 2014). These constraints define a solution space containing all feasible functional states (see Figure 2.7b), in contrast to the solution point of theory-based approaches.

The most relevant constraint types for the dynamic modeling of metabolic networks are stoichiometric constraints, thermodynamic constraints, and capacity constraints, expressed in the form of mass balances, reaction irreversibility and highest possible reaction rate, respectively (Orth et al., 2010).

The mathematical implementation of these constraints and flux balance analysis (FBA), a method to simulate the flow of metabolites through a metabolic network, are discussed in the next section. Then, for illustrative purposes, FBA is applied to a simple example network. Subsequently, the origin of nonunique solutions is discussed.

2.6.1 Flux balance analysis

Flux balance analysis (FBA) is a constrained-based modeling approach, used to analyze the reaction flux distribution of a metabolic network (Krömer et al.,

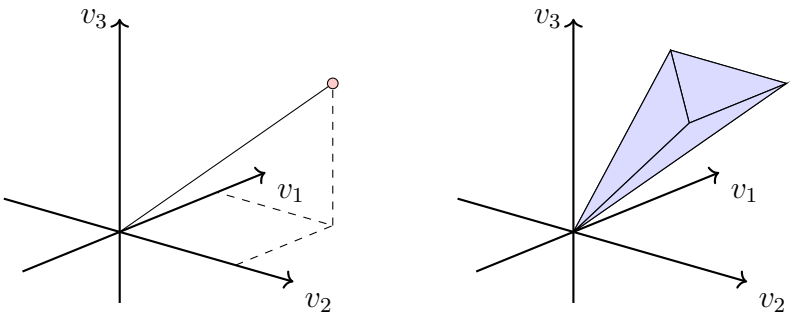

(a) Theory-based analysis (b) Constrained-based analysis

Figure 2.7: Theory- vs constrained-based analysis. Theory-based analysis leads to a single solution, while constraints define a range of possible solutions, a solution space. Adapted from Palsson (2015).

2014). In FBA, a pseudo steady state of the intracellular metabolism is considered, assuming that the intracellular metabolite concentrations do not change over time. This implies for Equation 2.4 that the derivatives of the intracellular metabolites M on the left-hand side are all equal to zero, reducing the original ODE system to a system of linear equations:

$$0 = Sv \tag{2.5}$$

Consequently, the metabolite concentrations are no longer considered and the flux distribution v now contains the unknown variables v_i of the system. In genome-scale metabolic networks the number of unknown variables is significantly greater than the number of linear independent mass balance equations, and thus the flux distribution can be obtained by formulating an optimization. This optimization problem can be formulated as follows:

$$\begin{aligned} \max_{v} \quad & Z = c^{\intercal} v \\ \text{subject to} \quad & Sv = 0 \\ & lb \leq v \leq ub \end{aligned} \tag{2.6}$$

being Z the objective function of an linear programming (LP) problem, where c is a vector of weights, indicating how much each flux v_i of the flux distribution

v contributes to Z. The optimization problem is subject to the mass balance constraints imposed by the multiplication of the stoichiometric matrix S and the flux distribution v, and the capacity constraints in form of lower and upper bounds lb_i and ub_i for reaction flux v_i (Orth et al., 2010). The objective function Z has to be formulated in regard to the organism and its specific evolutionary *purpose* (Palsson, 2015). In most cases, the maximization or minimization of a single or a number of reaction fluxes, for example biomass or product formation, is chosen (Krömer et al., 2014). Other common objective functions are the production or consumption of ATP or a specific metabolite (Gianchandani et al., 2010). By solving the optimization problem the flux distribution v of the metabolic network is obtained.

Another objective function that can be considered is the principle of enzyme efficiency maximization (Holzhütter, 2004; Sánchez et al., 2014; Schuetz et al., 2012), which can be applied by minimizing the total sum of weighted square fluxes, as there exist - due to reaction reversibility - both positive and negative annotated fluxes. This objective function can be implemented as quadratic programming (QP) problem. Thus, this QP problem can be formulated as follows:

$$\begin{aligned} \min_{v} \quad & Z = \tfrac{1}{2} v^{\intercal} Q v \\ \text{subject to} \quad & Sv = 0 \\ & lb \leq v \leq ub \end{aligned} \tag{2.7}$$

being Q an $m \times m$ quadratic objective matrix. By defining Q as the identity matrix, the square of the Euclidean norm of the flux vector is minimized (Palsson, 2015).

FBA of the example network

For illustrative purposes, FBA will now be applied step by step to the example network in Figure 2.6. As there are no constraints, the flux distribution of the network may lie at any point, as shown in Figure 2.8a. However, by considering pseudo steady state and applying the mass balance constraint $0 = Sv$, the ODE in

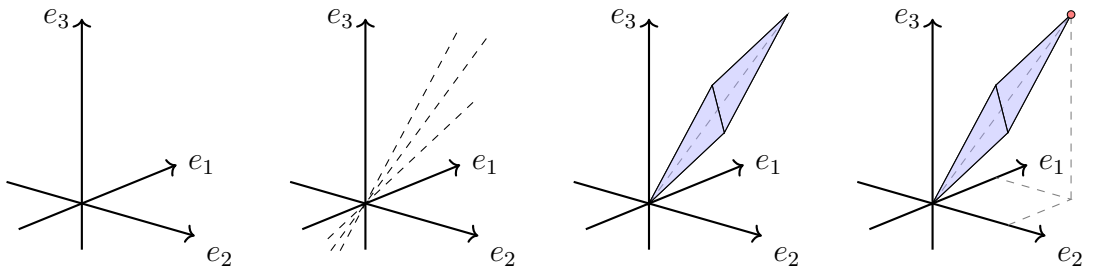

Figure 2.8: Application of constraints and FBA on the example network. **(a)** Unconstrained solution space **(b)** Mass balance constraints imposed by $0 = Sv$ **(c)** Thermodynamic and capacity constraints $0 \leq v_i \leq v_{max}$ **(d)** Maximization of objective function $Z = e_3$.

Equation 2.3 is transformed into the following system of linear equations:

$$\begin{aligned} 0 &= e_1 - v_1 \\ 0 &= e_2 - v_2 \\ 0 &= v_1 + v_2 - v_3 \\ 0 &= v_3 - e_3 \end{aligned} \tag{2.8}$$

As there are more unknown reactions than linear-independent mass balance equations, the system is over-defined and has infinite linear-dependent solutions, which can be displayed as a unbounded convex cone as in Figure 2.8b. As the solution can be both positive and negative, the convex cone also extends to the negative space.

Now, the exchange reactions $e_{1,2,3}$ are considered thermodynamically irreversible. Thus, the thermodynamic constraints $0 \geq e_{1,2,3}$ are introduced to the system. There is no information available about the reversibility of the intracellular reactions $v_{1,2,3}$, but, the mass balances in Equation 2.8 impose $e_1 = v_1$, $e_2 = v_2$ and $e_3 = v_3$. Consequently, the solution of the system is now limited to the positive convex cone.

Then, biochemical knowledge about the reactions e_1 and e_2 allows us to introduce capacity constraints for these reactions. For this example, a maximal reaction rate of $1\,\mathrm{mmol\,g^{-1}\,h^{-1}}$ for the reactions e_1 and e_2 is assumed. In Figure 2.8c it is shown

how the thermodynamic and capacity constraints transform the solution space in a bounded convex subset.

Last but not least, the FBA requires the formulation of a biological meaningful objective function for the resolution of the system. Here, the maximization of e_3 is chosen. For this simple system, the solution can be easily determined by examining the equation $e_3 = e_1 + e_2$ from the mass balances in Equation 2.8. As e_1 and e_2 are both limited to $1\,\mathrm{mmol\,g^{-1}\,h^{-1}}$ by the capacity constraints, the maximum of e_3 is $2\,\mathrm{mmol\,g^{-1}\,h^{-1}}$ and the flux distribution $v = [e_1, e_2, v_1, v_2, v_3, e_3]^\intercal$ is defined as $v = [1, 1, 1, 1, 2, 2]^\intercal$. The result of this FBA is described in Figure 2.8d.

Alternative optimal solutions and flux variability analysis

Constraint-based optimization problems can have multiple solutions with the same numerical value of the objective function, but different flux distributions (Palsson, 2015). To study these alternative optimal solutions (AOS) , the capacity constraint $e_3 \leq 1.5\,\mathrm{mmol\,g^{-1}\,h^{-1}}$ is introduced to the example FBA. As a result, the objective function of the FBA is now limited to this value, which can be achieved through different combinations of e_1 and e_2. Thus, multiple flux distributions are possible for the same objective function. This can be visualized in Figure 2.9.

An approach to study alternative optimal solutions is flux variability analysis (FVA) (Mahadevan and Schilling, 2003). FVA evaluates the minimum and maximum range of fluxes for a given cellular objective. After the resolution of the FBA, the objective function value of the FBA is introduced as constraint for the FVA and each flux is maximized and minimized. Thus, the maximum and minimum values of each flux of interest for a fixed cellular objective are obtained and the phenomenon of AOS can be studied. The occurrence of AOS increases rapidly with the network size.

This can be applied to the example examined earlier: a new inequality constraint $e_3 \geq 1.5\,\mathrm{mmol\,g^{-1}\,h^{-1}}$ (the solution of the FBA) is introduced and then the other fluxes, e_1 and e_2 are separately both maximized and minimized. Doing so, the

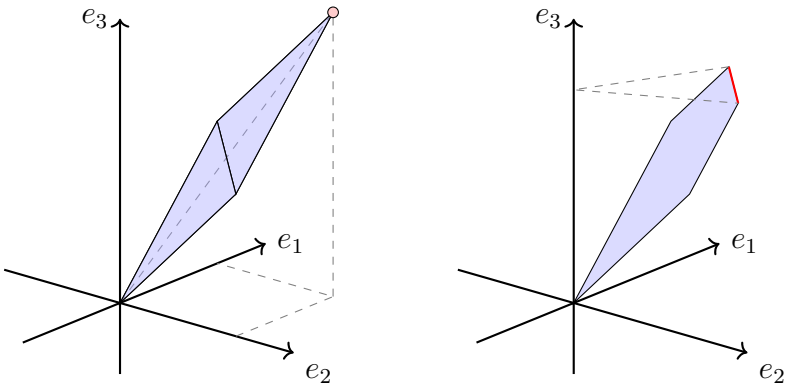

(a) Single solution (b) Multiple solutions

Figure 2.9: Example of multiple optimal solutions. In **(a)** the maximization of e_3 leads to an unique solution, in **(b)** there are multiple solutions with the same value of the objective function.

minimum values $e_{1,min} = 0.5$, $e_{2,min} = 0.5$ and the maximum values $e_{1,max} = 1.0$, $e_{2,max} = 1.0$ mmol g^{-1} h^{-1} are obtained.

In the case of a quadratic objective function, such as the principle of enzyme efficiency maximization, a quadratic constraint in the form $\frac{1}{2}v^\intercal Qv + c^\intercal v \leq \beta$ must be introduced for the FVA, where β is the value of the objective function of the FBA. If the objective function of the FBA was maximization, the constraint must be formulated as $\frac{1}{2}v^\intercal Qv + c^\intercal v \geq \beta$. In the FVA the objective function is linear, thus the optimization problem can be formulated as a second-order cone program (SOCP). SOCP problems can be solved efficiently by interior point methods (Alizadeh and Goldfarb, 2003).

2.6.2 Dynamic flux balance analysis

Dynamic flux balance analysis (DFBA) is an extension of classic FBA which allows the analysis of interactions between the cellular metabolism and its extracellular environment, and thus predictions of substrate, biomass and product concentrations in dynamic cultures (Höffner et al., 2013). It is based on the assumption that the intracellular metabolism instantaneously reaches a new equilibrium after an environmental perturbation. Thus, DFBA maintains the pseudo steady state assumption for the intracellular metabolism, but considers dynamics of extracellular

metabolite concentrations (Antoniewicz, 2013).

The dynamics of the extracellular environment in DFBA are represented in the form of ordinary differential equations, describing the mass balance of each process state variables of interest. The intracellular metabolism is described by the FBA simulation (Höffner et al., 2013). DFBA then introduces two types of interactions between the extracellular (ODE) and intracellular (FBA) environments.

First, the exchange fluxes calculated in the FBA problem enter in the right-hand side of the ODE system, multiplied by the current biomass concentration (FBA fluxes are expressed as amount of moles per time per amount of biomass). Thus, metabolites consumed by the cell cause a decrease in their extracellular concentration, and metabolites produced an increase.

Second, the influence of changes in the extracellular metabolite concentrations on the intracellular metabolism is expressed as a functional dependency on the substrate concentrations (Höffner et al., 2013). This is accomplished by updating the flux constraints of the FBA problem based on enzyme kinetics. For illustrative purposes, consider the example of a concentration drop of a certain substrate, whose cellular uptake rate is a function of its concentration: As the concentration drops, the availability of the substrate decreases and consequently the uptake reaction rate is limited. This implies for the FBA simulation that the constraint of this uptake flux is tightened, which narrows down the solution space of the optimization problem. The mathematical formulation of DFBA is shown schematically in Figure 2.10.

Other types of culture dynamics have also been introduced into DFBA in the form of transcriptional regulatory constraints (Covert et al., 2001) and time-dependent objective functions (Vargas et al., 2011).

There are three different approaches to simulate DFBA models: the static optimization approach (Mahadevan et al., 2002), the dynamic optimization approach (Mahadevan et al., 2002) and the direct approach (Höffner et al., 2013).

For the static optimization approach the culture time is divided in a number of fixed time intervals. At the start of each time interval, the constraints of the FBA are

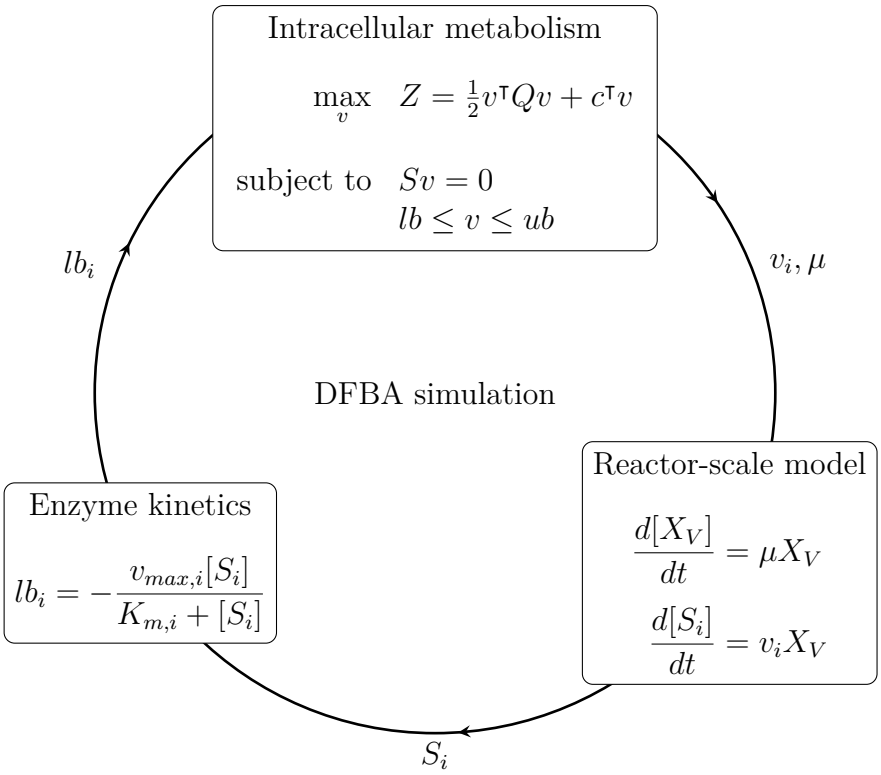

Figure 2.10: A schematic flowchart of DFBA simulation: The intracellular metabolism is described by the FBA simulation and the reactor-scale model is represented in the form of mass balances. The flux values obtained by the FBA enter the mass balances and enzyme kinetics redefine the minimal substrate uptake rates as the substrate concentrations change dynamically.

updated based on the extracellular metabolite concentrations, and the FBA problem is solved. Then, the ODEs are integrated with the fixed FBA solution for the full time interval. This process is repeated until reaching the end of the simulation time (Mahadevan et al., 2002). A disadvantage of this approach is that the simulation sensitivity depends strongly on the time interval size, so that a too large step size makes the simulation inaccurate. A small step size, however, may require a high computation time (Höffner et al., 2013).

The dynamic optimization approach proposes a dynamic optimization problem for the whole culture time, which is then transformed into a nonlinear programming (NLP) problem by orthogonal collocation. This NLP problem is solved once and time profiles of fluxes and metabolite levels are obtained (Mahadevan et al., 2002). Even though this approach only involves the solution of one optimization problem, the solution of NLP problems is more complicated in comparison to LP

problems. Further, the number of variables and constraints increases rapidly with time discretization, which limits the application of this approach to small-scale metabolic models (Gomez et al., 2014; Höffner et al., 2013).

A third alternative is the direct approach, in which the FBA problem is embedded in the right-hand side of the ordinary differential equations. Then, an implicit ODE integrator with adaptive step size for error control is used to integrate the system. However, there are two problems associated that can lead to failure during the simulation: First, the FBA problem can become infeasible during integration, which will lead to failure of the integrator. Second, the solution set of the FBA problem and thus the right-hand side of the ODE system may be nonunique at some time point. Numerical integrators can not handle this situation as they encounter discontinuities when decreasing step-size (Gomez et al., 2014).

These two problems have been addressed by transforming the ODE system and its embedded optimization problem in a system of differential algebraic equations (DAEs) and applying lexicographic optimization to all exchange fluxes of interest, respectively. Lexicographic optimization implies maximizing or minimizing each flux of interest in a specific order, and after each step fixing the result of that flux with an equality constraint for the next steps. Thus, a unique solution for all exchange fluxes is guaranteed (Gomez et al., 2014; Höffner et al., 2013).

However, the lexicographic optimization approach requires a sorting of the exchange fluxes of interest by a fixed order, which is not always biologically meaningful. This comes to be a limitation of this approach, especially when working with a large number of metabolites of interest.

Chapter 3

Materials and methods

3.1 Experiments

3.1.1 Cell line

In this work the cell line CHO DP-12 clone#1934 (ATCC CRL-12445), previously adapted to growth in suspension, was used. The cell line was obtained by transfection of CHO-DUXB11 cells with a bicistronic DHFR intron expression vector, responsible for the expression of a recombinant humanized anti-IL-8 antibody (Gonzalez et al., 2000; Lucas et al., 1996). This IgG1-type antibody inhibits Interleukin 8 (IL-8) mediated neutrophil chemotaxis. After transfection the cells were cultivated in medium lacking glycine, hypoxanthine and thymidine (GHT-free medium). Methotrexate (MTX) was added to increase selection pressure and amplify gene expression. CHO DP-12 clone#1934 was selected due to its high antibody productivity (Gonzalez et al., 2000).

3.1.2 Culture medium

The chemically-defined and animal-component free culture medium TC-LECC (Xell AG) was used as basal medium. TC-LECC was prepared by dissolving the medium powder in ultrapure water (MilliQ, Millipore), followed by 0.2 µm sterile-filtration. The medium was stored at 4 °C and prior to the cultivation of CHO-

DP12 cells it was supplemented with 8 mM L-Glutamine (Gibco) and 200 nM MTX (Hytas).

As feed medium the also chemically-defined and animal-component free nutrient concentrate TCX2D (Xell AG) was used. Its nutrient concentrations are around threefold increased in regard to the basal medium. Fresh TCX2D was prepared the day before the feeding was initiated, supplemented with 24 mM L-Glutamine, 0.2 µm sterile filtered, and stored at 4 °C. A sterility test was performed and checked before initiation of the feeding.

As both basal and feed medium were prepared manually, small lot-to-lot variations (around 5 %) were observed when measuring the substrate concentrations.

3.1.3 Cell maintenance and propagation

CHO DP-12 cell suspensions were maintained in 125 mL Erlenmeyer style cell culture flasks without baffles (Corning, 431143) with a working volume between 15 and 30 mL in an incubator at 37 °C and 5 % CO_2. Agitation on an orbital shaker at 185 rpm allowed homogenization and sufficient oxygen supply. Passages were always done at a concentration of around 10×10^6 cells mL^{-1}.

For the inoculation of the bioreactor the cells were propagated in 250 mL Erlenmeyer style cell culture flasks without baffels (Corning, 431144) with a working volume of 100 mL.

During cell propagation, samples were taken every other day cell to survey cell concentration and viability.

3.1.4 Bioreactor operation

The fed-batch cultures were carried out in a 3 L Applikon bioreactor (Applikon Biotechnology) with an initial working volume of 1 L and a seeding density of 0.5×10^6 cells mL^{-1}. The ez-control unit of the Applikon bioreactor was set to use the PID control to keep pH at 7.1, temperature at 37 °C and dissolved oxygen concentration (DO) at 40 % of air saturation. Agitation and aeration were

accomplished with a pitched-blade impeller at a rotation of 150 rpm and an open pipe L-sparger positioned below the impeller. A gas mixture of pure oxygen and carbon dioxide was injected through the sparger while a constant air flow rate was applied to the headspace for surface aeration. Carbon dioxide injection and a 7.5 % sodium bicarbonate solution (HyClone, SH30033.01) were used for pH control, and a heating blanket for temperature control. The oxygen partial pressure and thus the DO were measured with a polarographic electrode (Mettler Toledo), whereas for potentiometric pH measurements an ion selective electrode (AppliSens) was used. Temperature was measured with a PT100 temperature sensor. All operational data was logged with the BioXpert software (Applikon Biotechnology). Pulse and continuous feeding were applied with an external peristaltic pump (Watson Marlow, 520U). The feeding strategies for pulse and continuous feeding can be found in Table 3.2 and Table 3.3, respectively. A feeding strategy suggested by the media manufacturer can be found in Table 3.1. The results of the fed-batch cultivations were compared with previous results of a batch cultivation with the same cell line (Bettinardi, 2017).

Table 3.1: Feeding strategy suggested by the media manufacturer.

culture time (hours)	0	24	48	72	96	120	144	168	192	216
feeding volume (mL)	0	0.4	0.4	0.6	0.6	0.8	0.8	0.8	0.8	0.8
working volume (mL)	20.0	20.4	20.8	21.4	22.0	22.8	23.6	24.4	25.2	26

Table 3.2: Feed times and volumes of the fed-batch cultivation with pulse feeding. The working volume after the feed additions is also shown.

culture time (h)	0	96	119	143	167	192	216
feeding volume (mL)	0	80	120	120	160	240	240
working volume (L)	1.00	1.08	1.20	1.32	1.48	1.72	1.96

Table 3.3: Feed times and rates for the fed-batch cultivation with continuous feeding. The time represents the culture time at which the respective feed rate was initiated, and maintained until the next higher feed rate.

culture time (h)	0	72	95	119	144	167	190	224
feeding rate (mL/day)	0	40	80	120	160	200	240	0
working volume (L)	1.00	1.00	1.04	1.12	1.24	1.40	1.60	1.97

3.1.5 Analytical methods

Daily samples were analyzed for viable (X_V) and dead (X_D) cell densities with a Vi-CELL Cell Counter (Beckman Coulter) using the trypan blue dye exclusion method (Strober, 2001). Total cell density (X_T) was calculated as the sum of viable and dead cell densities, and viability (Via) as the fraction of viable over total cells. Additional samples were centrifuged and the supernatant analyzed for glucose and lactate (Biochemistry Analyzer, YSI). Further, supernatant aliquots were stored in a $-20\,°C$ freezer for later amino acid, monoclonal antibody and ammonia assays (to avoid ammonia evaporation, aliquots for ammonia assay were acidified with hydrochloric acid before freezing).

Amino acids

Amino acids were analyzed using high-performance liquid chromatography system (Prominence HPLC, Shimadzu). A reversed phase column (Lichrocart, Merck) with a C18 stationary phase was used to separate the amino acids based on differences in their polarity.

For pre-column derivatization, 100 µL of each sample was vacuum dried at room temperature (Concentrator plus, Eppendorf) and resuspended in 20 µL of a 50 % methanol, 25 % ultrapure water and 25 % triethylamine mixture. After vacuum-drying again, 20 µL of 70 % methanol, 10 % ultrapure water, 10 % triethylamine and 10 % phenyl isothiocyanate (PITC, Thermo) was added for amino acid derivatization. After 20 minutes the samples were vacuum dried and then resuspended in solution A, a mixture of 2 % acetonitrile and 98 % 85 mM sodium

acetate at pH 5.2. Solution B was composed of 70 % acetonitrile and 30 % 85 mM sodium acetate at pH 5.2.

The column was heated to 46 °C and peak area was detected at 254 nm. The percentage of solution B in the mobile phase was gradually increased (Table 3.4), resulting in a decrease of polarity and gradual elution of amino acids from the column (hydrophilic amino acids first). Peaks were integrated manually using the LC Solution software (Shimadzu) and compared to a standard. The amino acid cysteine was not quantified.

Table 3.4: Elution gradient method for amino acid quatification using HPLC

Time (min)	Buffer B (%)
0.0	0
13.5	3
24.0	6
30.0	9
50.0	34
62.5	100
67.0	0

Monoclonal antibody

Monoclonal antibody titer was analyzed using protein A affinity chromatography. For details about this method the reader is referred to Bettinardi (2016, item. 4.3.3). Briefly, an affinity column (2100200, Applied Biosystems) was used in a high-performance liquid chromatography system (Prominence HPLC, Shimadzu). IgG from human serum (I4506, Sigma) was used as external standard for calibration. Standard and samples were filtered with a 0.45 µm syringe filter (Millex-GV, Millipore). The sample, dilution and loading buffer was composed of 10 mM monosodium phosphate and 150 mM sodium chloride, pH 7.20; the elution buffer of 150 mM sodium chloride and 12 mM hydrochloric acid, pH 2. Elution peak areas were determined at a wavelength of 280 nm. The software LC Solution (Shimadzu)

was used for standard curve creation and antibody quantification.

Cell dry mass

CHO DP-12 cells were cultured to a concentration of approximately 10×10^6 cells mL^{-1}. The cell concentration was measured with the Vi-CELL Cell Counter and 10 mL of the cell suspension (well homogenized) were transferred to a 15 mL conical tube. After centrifugation (1000×g, 5 minutes, room temperature) the supernatant was discarded carefully and the cell pellet resuspended in 1 mL ultrapure water. This concentrated cell suspension was transferred to a filter paper and dried overnight in the drying oven at 70 °C. The specific dry mass per cell $\gamma_{cell,dry}$ was calculated by dividing the mass difference of the filter paper (without cell suspension and with dried cell suspension) by the number of total cells in the suspension.

$$\gamma_{cell,dry} = \frac{m_{filter} - m_{dried}}{[X_T]\, V_{sample}} \tag{3.1}$$

All experimental procedures and measurements were done in triplicates.

3.2 Modeling

3.2.1 CHO genome scale metabolic model

Hefzi et al. (2016) presented a detailed genome scale-metabolic model of CHO cell metabolism. By analyzing the genome of CHO.K1 cells and *C.griseus* they established a global model, and using RNA sequencing, proteomic and microarray data, cell-line specific models for CHO.K1, CHO-S and CHO-DG44 cell lines. The global model, iCHO1776, contains 6663 metabolic reactions and 4456 metabolites in 9 cellular compartments (cytosol, extracellular space, golgi apparatus, mitochondria, lysosome, nucleus, endoplasmatic reticulum, intermembrane space of mitochondria and peroxisome/glyoxysome). Figure 3.1 shows the sparsity pattern of the stoichiometric matrix of this global model, showing the connectivity of metabolites and reactions.

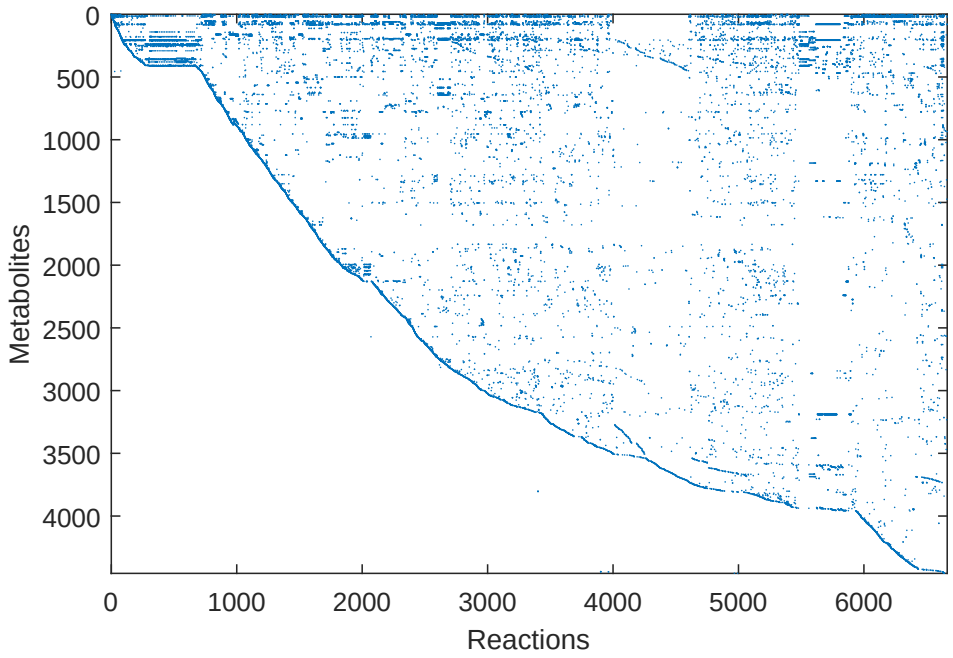

Figure 3.1: Sparsity pattern of iCHOv1776 stoichiometric matrix. The dimensions of this matrix are $m = 4456$ metabolites and $n = 6663$ reactions, resulting in 29 690 328 elements in the matrix. Of these, 27 648, or 0.0931 % are non-zero.

This model is freely available for academic and non-profit use and was obtained from the BiGG data base under `http://bigg.ucsd.edu/models/iCHOv1` (King et al., 2016). More detailed information about the reconstruction process of the metabolic model can be found under Hefzi et al. (2016).

3.2.2 Dynamic flux balance analysis

For the different sets of experimental data (batch, fed-batch with pulse feeding, fed-batch with continuous feeding) both the static and direct approaches of dynamic flux balance analysis (DFBA) were applied. Basically, the structured and unsegregated model consists of three major components:

(i) a dynamic, reactor-scale model of 26 process state variables of interest,

(ii) a steady state, 6663-reaction genome-scale metabolic model of CHO cell metabolism (iCHO1776), embedded within the dynamic model, and

(iii) a kinetic model based on enzyme-substrate interactions, to define the lower bounds for the uptake rates and effectively connect the dynamic extracellular and the steady state intracellular models.

All simulations were done using the software MATLAB (version 2008a). The ODEs were solved using MATLABs implicit solver *ode15s*, which is appropriate for the solution of stiff differential equations. This integrator uses a variable step size and chooses dynamically between solution methods of different orders to control the local error to the desired accuracy. To guarantee that in no moment of the integration the state variables can become negative, the option *'NonNegative'* was set. The optimization problems were solved externally using the Gurobi-Matlab interface (Gurobi Optimization, 2017). This provided a way faster and stable solution than other solvers tried, such as MATLABs internal solvers or the external solver CPLEX. The Gurobi solver was called to solve both LP and QP problems with the simplex method. The optimality and feasibility tolerances were set to their minimum value 1×10^{-9}. For the simplex algorithm, Gurobi allows to pass an

advanced starting basis for both variables (*vbasis*) and linear constraints (*cbasis*). As the optimization problem was solved a great number of times during integration, both (*vbasis*) and (*cbasis*) of the previous solution could be passed as an advanced starting basis for the consecutive solution. Doing so, the computational time could be reduced to a almost one tenth of what it was before.

Bioreactor model

The bioreactor was modeled as a system of ordinary differential equations (ODE), representing the mass balances of the process state variables: the reactor volume V, the concentration of viable cells $[X_V]$, and the metabolite concentrations (products and substrates) M_i. The metabolites observed are glucose (Glc), lactate (Lac), ammonium (Amm), monoclonal antibody (mAb) and 20 aminoacids. A complete list of the state variables and their description can be found in Table 3.5.

Thus, the ODE system consists of a total of 26 differential equations. The volume V is a function of the continuous feed rate Q_{feed}, and the concentration of viable cells $[X_V]$ is described as a function of a net growth rate μ. The change in volume due to media feed implies a dilution of the cell concentration, which is expressed by adding the volume on the left-hand (derivative) side of the EDO. The net growth rate μ was defined as difference between the biomass flux $v_{biomass}$ and the specific death rate k_d. The death rate was mathematically described using Monod-type structures (Monod, 1949) for limiting phenomena, and Aiba and Shonda-type structures (Aiba and Shoda, 1969) for inhibitory behavior. Ammonia was considered as limiting, and the main substrates glucose and glutamine as inhibitory for cell death. This is described in the following equation:

$$k_d = k_{d,max} \frac{[Amm]}{k_{d,Amm} + [Amm]} \frac{k_{i,Glc}}{k_{i,Glc} + [Glc]} \frac{k_{i,Gln}}{k_{i,Gln} + [Gln]} \tag{3.2}$$

where $k_{d,max}$ is the maximum specific death rate, and k_d and k_i are the constants for death stimulating and inhibiting metabolite concentrations, respectively. The parameter values for $k_{d,max}$, $k_{d,Amm}$ and $k_{i,Gln}$ were retrieved from Bree et al. (1988),

and $k_{i,Glc}$ was assumed to be similar to $k_{i,Gln}$.

Then, all the mass balances of all metabolites were described in a similar manner: the concentration change of metabolite m_i was calculated as product of the exchange flux v_{M_i} of the metabolic model for this metabolite and the viable cell concentration $[X_V]$. As the fluxes of a GEM are given as a function of the biomass dry mass (they have the unit mmol $\mathrm{gDM}^{-1}\,\mathrm{h}^{-1}$) and not the viable cell concentration, a constant k_{gDM/X_V} must be included in the product to account for the conversion from viable cell density to dry mass. The metabolite feed is introduced by the product of feed rate Q_{feed} and the concentration $[M_{i,feed}]$ of the respective metabolite i in the feed medium. The dilution effect due to media feed is included as described earlier. The volume derivatives can be passed to the right-hand side of the ODE by applying the product rule, leading to the following EDO:

$$\begin{aligned} \frac{dV}{dt} &= Q_{feed} \\ \frac{d[X_V]}{dt} &= \mu[X_V] - \frac{[X_V]}{V}\frac{dV}{dt} \\ \frac{d[M_i]}{dt} &= v_{M_i}[X_V]k_{gDM/X_V} + [M_{i,feed}]\frac{Q_{feed}}{V} - \frac{[M_i]}{V}\frac{dV}{dt} \end{aligned} \tag{3.3}$$

As the state variables glucose, lactate and monoclonal antibody were measured in $\mathrm{g\,L}^{-1}$, the fluxes of these metabolites needed to be converted from mmol to g using their molar mass. For glucose and lactate, these factors were $0.180\,16\,\mathrm{g\,mmol}^{-1}$ and $0.090\,08\,\mathrm{g\,mmol}^{-1}$, respectively. IgG type antibodies consist of around 150 kDa, thus a molecular mass of $150\,\mathrm{g\,mmol}^{-1}$ was considered.

The values for the fluxes v were obtained from the flux balance analysis (FBA) of the genome scale metabolic model (GEM). This procedure is described in the following text.

Flux balance analysis

The stoichiometric genome-scale metabolic model of the CHO cell, *iCHO1776*, was described earlier in this chapter. However, some modifications had to be made to the model in order to be representative for the CHO-DP12 cell line. First, the

Table 3.5: Process state variables of the model and the corresponding reaction IDs of the iCHOv1 metabolic model

Number	State Variable	Unit	Reaction ID	Symbol
1	Volume	L	NaN	V
2	Viable cell density	10^9 cells L^{-1}	6628	X_V
3	D-Glucose	g L^{-1}	4289	Glc
4	L-Lactate	g L^{-1}	4402	Lac
5	Ammonia	mM	4444	Amm
6	Monoclonal Antibody	g L^{-1}	6636	mAb
7	L-Alanine	mM	4098	Ala
8	L-Arginine	mM	4114	Arg
9	L-Asparagine	mM	4416	Asn
10	L-Aspartate	mM	4418	Asp
11	L-Cysteine	mM	4209	Cys
12	L-Glutamate	mM	4295	Glu
13	L-Glutamine	mM	4292	Gln
14	Glycine	mM	4297	Gly
15	L-Histidine	mM	4380	His
16	L-Isoleucine	mM	4391	Ile
17	L-Leucine	mM	4405	Leu
18	L-Lysine	mM	4422	Lys
19	L-Methionine	mM	4436	Met
20	L-Phenylalanine	mM	4476	Phe
21	L-Proline	mM	4487	Pro
22	L-Serine	mM	4529	Ser
23	L-Threonine	mM	4560	Thr
24	L-Tryptophan	mM	4569	Trp
25	L-Tyrosine	mM	4578	Tyr
26	L-Valine	mM	4589	Val

iCHO1776 accounts for both a producing (EPO or monoclonal antibody) and a not-producing cell line. As CHO-DP12 is a monoclonal antibody (mAb) producing cell line, the reactions for the other cases must be blocked. This was done by setting the lower and upper bound of these reactions to zero. Further, the reactions for the synthesis of the monoclonal antibody (heavy and light chain) were unblocked by setting their upper bound to 1000 (which is technically unbound). The flux balance analysis model formulation was stated as follows:

$$\begin{aligned} \max_{v} \quad & Z = \tfrac{1}{2} v^{\intercal} Q v + c^{\intercal} v \\ \text{subject to} \quad & Sv = 0 \\ & lb \leq v \leq ub \end{aligned} \tag{3.4}$$

where c is the vector of linear objectives, containing the weights for the fluxes considered in the linear objective function, v is the flux distribution, and S is the stoichiometric matrix describing the reaction network topology. Q is the matrix of quadratic objectives, important for the maximization of the enzymatic efficiency. Further, flux v_i is constrained by the lower and upper bounds lb_i and ub_i, respectively.

As objectives for the flux balance analysis (FBA) problem, the maximization of the fluxes for biomass and monoclonal antibody was chosen. Due to the large molar mass of the antibody (150 kDa) its flux in mmol was extremely small in comparison to all other fluxes. Consequently, the weight for this flux was required to be much greater in order to be recognized in the objective function. To guarantee a simultaneous production of biomass and monoclonal antibody, a three-hundredfold greater weight was given to the antibody flux. Further, the maximization of the uptake rates for glucose and glutamine were considered, in order to simulate the overflow metabolism observed in continuous cell lines. To maximize an uptake rate, its weight in the objective function must be negative, as nutrient uptake always implies a negative flux value.

The Gurobi solver requires the quadratic objective matrix Q to be positive semi-definite (PSD) for minimization, and negative semi-definite (NSD) for maximization problems. For the approach of maximal enzymatic efficiency, as described in Section 2.6.1, the square of the Euclidean norm of the flux vector must be minimized. This is done by defining Q as a negative identity matrix, which is necessarily NSD. The weight for all entries of the matrix was set as -1×10^{-3}.

Exchange reaction kinetics

The iCHO1776 GEM contains 6663 reactions. The lower and upper bounds of the reactions are set by default to -1000 and $1000\,\mathrm{mmol\,gDM^{-1}\,h^{-1}}$, respectively. Irreversible reactions have the lower bound set to 0.

Substrate uptake was considered to be active transport and the maximal allowable substrate uptake rate was assumed to follow Michaelis–Menten kinetics:

$$lb_i = -\frac{v_{max,i}[S_i]}{K_{m,i} + [S_i]} \tag{3.5}$$

Here, lb_i is the updated lower bound for exchange reaction v_i of metabolite S_i in the FBA problem. The values of the maximum reaction rates v_{max} and Michaelis-Menten constants K_m for the measured substrates S_i can be found in Table 4.1. It is important to note that these parameters do not represent the actual properties of the transporter proteins, they are rather empirical fits of the observed uptake behavior.

Static and direct DFBA

As mentioned earlier, both static and direct DFBA approaches were used for model simulation. For the static approach, the cultivation time was divided into intervals of 6 h. At the start of each interval, the uptake reaction bounds were updated according to the enzyme kinetics, based on the extracellular metabolite concentrations. Then, the FBA problem was solved and the ODE integrated for the time horizon with fixed flux values. In the dynamic approach, the FBA problem and the uptake reaction

kinetics were put on the right-hand side of the ODE. Then, the system was integrated with an adaptive step size.

The batch process was simulated in a single integration. For the fed-batch process with pulse feeding the time period between two successive feedings was considered as a batch culture: The system was integrated until the next feed time, then the state variables were updated according to the feed volume and concentration. Metabolites that were fed were increased by the appropriate concentration, and the dilution effect on all state variables was adjusted:

$$[Y]_{after} = [Y]_{before}\frac{V_{before}}{V_{after}} + [Y]_{feed}\frac{V_{feed}}{V_{after}} \tag{3.6}$$

In this equation, Y_{after} is the concentration of the state variable Y after, and Y_{before} before the feeding; V_{before} and V_{after} the volume, and V_{feed} and $[Y]_{feed}$ the feed volume and concentration of state variable Y in the feed medium. These values formed the starting point for the consecutive simulation.

In the fed-batch run with continuous feeding, the feed rate was adjusted each day. For the simulation, the cultivation was separated in time intervals for which the feed rate was constant.

3.2.3 Parameter Estimation

This CHO cell DFBA model has 32 kinetic parameters. The parameter values were estimated by fitting the model to the measured data, using the extended flexible polyhedron method. The objective function that was minimized was the sum of the squared difference between the simulated and measured concentrations, summed over all time points and extracellular metabolites. This parameter estimation

problem was proposed as follows:

$$\begin{aligned} \min_{p} \quad & Z = \sum_{k} \sum_{t} \left(Y_{k,t}^{sim} - Y_{k,t}^{meas} \right)^2 \\ \text{subject to} \quad & p_{min} \leq p \leq p_{max} \\ & DFBA\ equations \end{aligned} \tag{3.7}$$

where Z is the objective function to be minimized, $Y_{k,t}^{sim}$ and $Y_{k,t}^{meas}$ are the values of the simulated and measured state variable k at time point t, respectively. The parameters were bound between the lower bounds p_{min} and upper bounds p_{max}. The parameter estimate was dependent on its seed values. Thus, the v_{max} and K_m values for each substrate were first estimated separately, isolating the substrate concentration in the objective function. With this advanced seed values, the estimation of all parameters was performed.

3.2.4 Flux variability analysis

Flux variability analysis (FVA) is used to find the minimum and maximum flux for reactions in the network while maintaining the biological state of the network, such as the biomass and product maximization. After obtaining the optimal solution $\frac{1}{2} v^\intercal Q v + c^\intercal v = Z_{FBA}$ of the FBA problem stated in Equation 3.4, FVA solves two optimization problems for each flux v_i of interest:

$$\begin{aligned} \max_{v} / \min_{v} \quad & v_i \\ \text{subject to} \quad & Sv = 0 \\ & \tfrac{1}{2} v^\intercal Q v + c^\intercal v \geq Z_{FBA} \\ & lb \leq v \leq ub \end{aligned} \tag{3.8}$$

The minimum and maximum flux values for v_i are obtained under the constraint that the biological state defined by the objective function value Z_{FBA} of the FBA is maintained. FVA was performed for all exchange fluxes used in the mass balance

equations (Equation 3.3), after every FBA solution.

FVA was applied for FBA solutions of both linear (FBA-LP) and quadratic programming (FBA-QP) approaches. For FBA-LP solutions the FVA constraint defining the biological state is linear, and the FVA for each flux are solved as a LP. These LP were solved with the simplex algorithm. For FBA-QP solutions the constraint is quadratic, thus transforming the FVA in a second-order cone optimization problem (SOCP). SOCP problems were solved using the homogeneous barrier algorithm from Gurobi.

3.2.5 Pathway visualization

Graphical visualization of pathways of the metabolic model is important in order to facilitate analysis and understanding of interconnections and processes in the biochemical network. `Paint4Net` (Kostromins and Stalidzans, 2012), an extension of the COBRA Toolbox (Heirendt et al., 2017), was used for automatic generation of pathway maps. In these maps, flux data of FBA simulations can be shown, which enables the analysis of flux distributions in the network and allows to track metabolite fluxes.

Chapter 4

Results and Discussion

4.1 Cell cultures

For this study, CHO cells were cultivated in a 3 L bioreactor with an initial working volume of 1 L. First, the cells were cultivated in fed-batch mode with daily pulse feeding (FBpulse): a certain volume of feed media was added to replenish the nutrients in the culture media. Then, a fed-batch cultivation with a continuous feeding (FBcont) was performed.

Before conducting the fed-batch cultivations in a bioreactor, a feeding strategy recommended by the media manufacturer was tested (small-scale) in conical cell culture tubes. For this experiment, data was obtained only for viable cell, dead cell, glucose and lactate concentrations. This recommended feeding strategy was found to maintain the glucose level high in the initial phase of the cultivation, but glucose depleted after approximately 170 hours in culture, resulting in cell death. These results can be found in Appendix C, in Figure C.1. A high glucose concentration in the medium has been associated with an inefficient metabolism and high lactate production (Zagari et al., 2013), thus many fed-batch processes use a feeding strategy to control glucose at low levels (Craven et al., 2014; Li et al., 2005). Consequently it was opted for the cultivations in the bioreactor to delay the initiation of the feeding and adjust the feeding volumes daily based on the specific glucose consumption rate. The feeding strategies for FBpulse and FBcont can be found in Table 3.2 and

Table 3.3, respectively. During cell maintenance and propagation the viability was always above 99 %.

During the fed-batch cultivation with pulse feeding, almost one liter of the feed media TCX2D was added (for more details, see Table 3.2). It reached a peak cell density of 27.4×10^9 cells L^{-1} on its ninth day in culture. The culture was maintained for two more days until the viability dropped below 50 %. At the end of the cultivation, the antibody titer was $0.66\,\mathrm{g\,L^{-1}}$.

During the fed-batch cultivation with continuous feeding the highest viable cell concentration (30.5×10^9 cells L^{-1}) and antibody titer $0.74\,\mathrm{g\,L^{-1}}$ were achieved. The feed rate was adjusted daily based on the specific glucose consumption rate observed in the preceding 24 hours with the aim to assuring a sufficient supply of glucose. After 224 hours, the feeding was stopped as the culture volume came close to the maximum reactor working volume of 2 L. The cultivation was stopped when the viability dropped below 40 % after 247 hours. In Table 3.3 the feed rates for the different time intervals are listed.

These cultivation data were compared to the work of Bettinardi (2017), who performed a batch cultivation of the same cell line in a RALF bioreactor (Bioengineering AG) with a seeding cell density of approximately 0.3×10^9 cells L^{-1}. The batch cultivation reached a peak cell density of approximately 16.5×10^9 cells L^{-1} after nine days in culture. At the end of this cultivation, an antibody titer of almost $0.28\,\mathrm{g\,L^{-1}}$ was achieved.

The main characteristics (viable cell, glucose, lactate and antibody concentrations) of the different operation modes are compared in Figure 4.1. In all cultivations, significant lactate accumulation in the medium was observed during the initial phase of the culture, when the cells were growing exponentially and the glucose concentration was high. However, after the cells were around 100 hours in culture, the lactate concentration decreased rapidly, indicating that the cells underwent a metabolic shift from lactate production to lactate consumption. It can be observed that in all three cases the glucose concentration was approximately

$2\,\mathrm{g\,L^{-1}}$ when the metabolic shift occurred.

In general, these data represent the typical characteristics of batch and fed-batch cultures: fed-batch cultures are known to allow a significantly higher peak cell density, culture longevity and most important, recombinant protein production (Veliz et al., 2008). Here, the peak cell density almost doubled ($16.5 \times 10^9\,\mathrm{cells\,L^{-1}}$ in the batch culture vs. 27.4×10^9 and $30.5 \times 10^9\,\mathrm{cells\,L^{-1}}$ in FBpulse and FBcont, respectively) and the antibody titer at the end of the culture more than doubled ($0.28\,\mathrm{g\,L^{-1}}$ vs. 0.66 and $0.74\,\mathrm{g\,L^{-1}}$).

In Figure 4.2 the amino acid profiles of all three cultivations are shown. In the batch culture, most amino acid concentrations were decreasing, and thus being consumed by the cells. The concentration of several amino acids (asparagine, glutamine, methionine, phenylalanine, serine and tryptophan) dropped to zero during the batch cultivation, glutamine being the first. Both alanine and glutamate were strongly produced by the cells. The concentration of arginine was constant during the batch cultivation.

Interestingly, all amino acids, including glutamine, accumulated in great amounts in both fed-batch strategies. Only glucose concentration was decreasing steadily during the whole culture period, and glutamine started to drop after feeding ceased after 224 hours. This suggests that the feed medium composition and the feeding strategy were not well adjusted: the amino acids were fed excessively and rather the essential carbon/energy sources (especially glucose, then lactate and glutamine towards the end of the cultures) were limiting for growth and antibody production. Amino acids are expensive components of chemically defined media and their accumulation in the culture implies an economically suboptimal production process. Also, it is not known if the accumulation of any of the aminoacids to a certain level can be inhibitory or deleterious to the cell metabolism or cause undesired changes in the culture environment (pH, osmolality, etc.).

In Appendix A, all the experimental data for all state variables can be found (Table A.1, Table A.3, Table A.4 for the batch, FBpulse and FBcont cultivations,

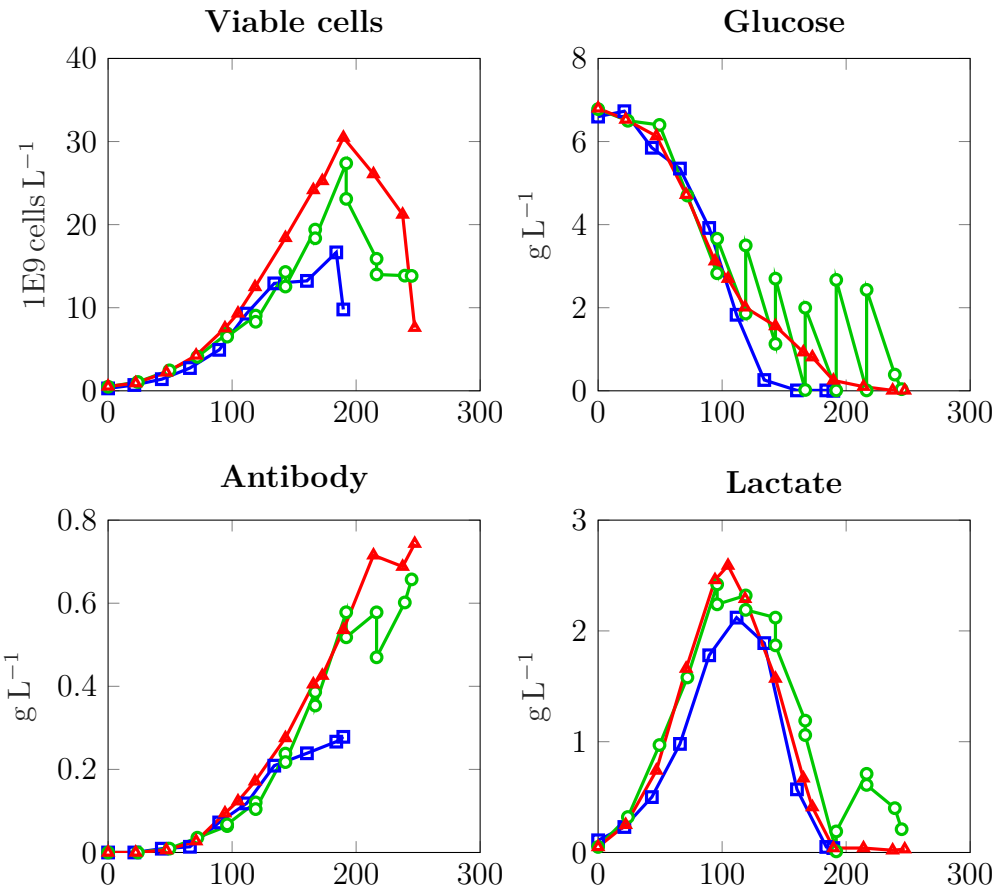

Figure 4.1: Comparison of the different culture strategies: batch (blue squares) (Bettinardi, 2017), fed batch with pulse feeding (green circles) and fed batch with continuous feeding (red triangles). The values on the x-axis represent the culture time in hours.

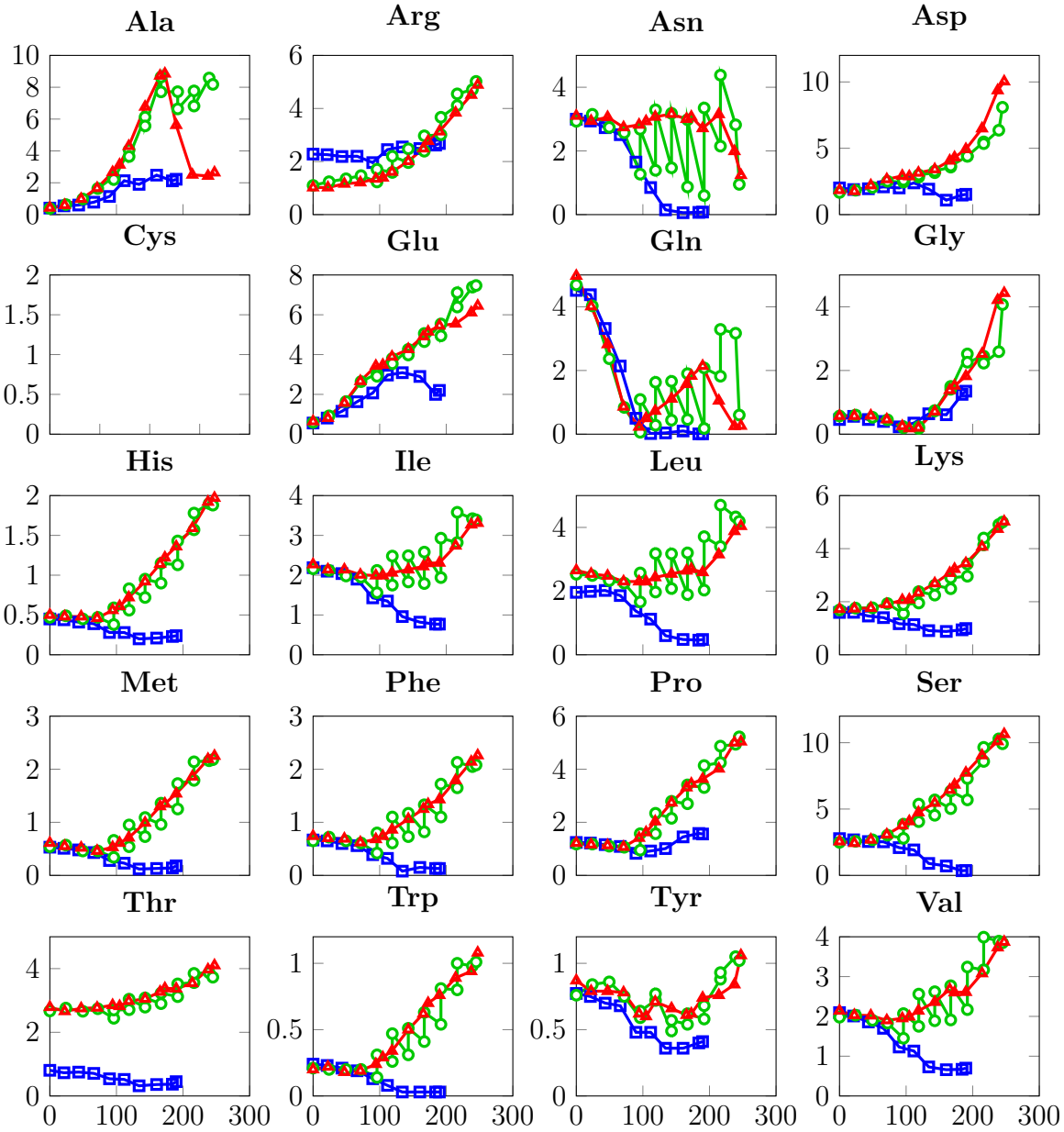

Figure 4.2: Comparison of the different culture strategies: batch (blue squares) (Bettinardi, 2017), fed batch with pulse feeding (green circles) and fed batch with continuous feeding (red triangles). Cystein was not measured. The concentrations on the y-axis are in mmol L^{-1} and the culture time on the x-axis in hours.

respectively). In Table A.2 the measured metabolite concentrations of the feed medium TCX2D are shown.

During the cultivations, the pH, dissolved oxygen concentration (DO) and temperature were kept closely to the setpoints of 7.1, 40 % (of air saturation) and 37 °C, respectively. Thus, they can be considered as constant values for the modeling of the process. The logged data for pH, temperature and dissolved oxygen can be found in Appendix B.

The determination of cell dry mass of the CHO-DP12 cells resulted in a value of $128 \pm 5\,\mathrm{pg\,cell^{-1}}$. This value is smaller than other values reported in literature: Nolan and Lee (2011) reported a measured dry mass of $350\,\mathrm{pg\,cell^{-1}}$ for CHO.K1 cells and Niklas et al. (2009) $419\,\mathrm{pg\,cell^{-1}}$ for HEP G2 cells. However, Berrios et al. (2011) reported a variation of cell mass of CHO TF 70R cells between 196 and $281\,\mathrm{pg\,cell^{-1}}$, depending on the experimental conditions. Considering these variations between different cell lines and culture conditions, the value obtained for CHO-DP12 can be regarded as consistent. However, the method could be improved by using a isotonic saline solution such as PBS for washing the cells, as ultrapure water could damage the cells. Determining the cell dry mass was necessary in the present work for the modeling of the process.

4.2 Modeling

In order to validate the modeling and simulation strategies, the theoretical results were compared with the experimental data obtained. First, different objective functions and constraints were evaluated using the data of the batch cultivation. For each of these simulations flux variability analysis (FVA) was applied to investigate the influence of alternative optimal solutions (AOS) on the DFBA simulation. Then, the modeling strategy was applied to the fed-batch cultivations.

4.2.1 Parameter estimation

Parameter estimation was performed on the batch cultivation data (Bettinardi, 2017). Table 4.1 shows the estimated maximum reaction rates v_{max} and Michaelis-Menten constants K_m for the 16 metabolites used as substrates by the cells.

Table 4.1: Estimates of the kinetic model parameters obtained by empirical fitting to the data

Substrate	v_{max} [mmol gDM^{-1} h^{-1}]	K_m [mM]
D-Glucose	5.4795	4.6703
L-Asparagine	0.0654	0.9818
L-Aspartate	0.0197	1.8001
L-Glutamine	0.3706	1.1270
L-Histidine	0.0186	1.0979
L-Isoleucine	0.0565	1.0193
L-Leucine	0.0585	1.2359
L-Lysine	0.0489	1.1685
L-Methionine	0.0588	1.0469
L-Phenylalanine	0.1447	0.9746
L-Proline	0.0112	2.0000
L-Serine	0.0169	0.0166
L-Threonine	0.0109	0.0281
L-Tryptophan	0.0198	0.9738
L-Tyrosine	0.0298	1.0970
L-Valine	0.0642	1.9924

4.2.2 Biomass and antibody objective function

The first approach made was the maximization of the biomass and antibody fluxes as an linear problem (LP) with the weights 1 and 300 in the objective function, respectively.

This relatively easy approach was able to accurately simulate the culture dynamics of the initial part of the batch culture. In Figure 4.3 it can be seen that the cell growth (in the exponential phase) and glucose consumption were well represented. However, this configuration of objective function and constraints did not predict lactate production nor consumption. Further, ammonia production was not predicted by the model at all and monoclonal antibody production was strongly underestimated. As the predicted concentration of ammonia was zero, the term for cell death (Equation 3.2) was always zero and thus no cell death was predicted.

The predictions of the amino acid concentrations can be seen in Figure 4.4. The metabolic trend (consumption or production) for most amino acids is correct, however the consumption of some amino acids was under- or overpredicted. Well represented amino acids were aspartate, glutamine, histidine, leucine, proline, threonine and tyrosine. The consumption of asparagine, isoleucine, methionine, serine, tryptophan and valine was underpredicted, and the consumption of arginine, lysine and phenylalanine overpredicted. The experimental data show a production of alanine and glutamate during the whole culture, and of glycine and proline towards the end of the cultivation. In the simulation results, glutamate is not produced at all and alanine minimally. The production of glycine and proline is anticipated, and glycine production is overestimated in the simulation.

The early stop of cell growth in the simulation can be associated to the depletion of phenylalanine. Phenylalanine is an essential amino acid which cannot be synthesized by the cell and is required for cell growth. Consequently, phenylalanine is compromised in the biomass reaction of the stoichiometric model, so that upon its depletion the stoichiometry does not allow further growth (Figure 4.3). Interesting is that at this exact moment antibody production starts. This can be explained

based on the objective function of the FBA: both biomass and antibody reactions are in the objective function, however the weight for the antibody reaction was set three-hundredfold greater than the biomass weight, as the value of the antibody flux was observed to be much smaller. These weights were chosen as they allowed simultaneous growth and antibody expression in a FBA applied on the iCHO1776 model without changing the bounds on the uptake fluxes (tested prior to the DFBA formulation). In this DFBA simulation, however different (dynamic) constraints were applied, and these weights did not assure simultaneous growth and antibody expression: the antibody was only produced when further growth became impossible. A greater weight for the antibody flux would be necessary to achieve simultaneous growth and expression. Nevertheless, the weights of the objective function must be set delicately, as a too high weight implies growth suppression. Further, the weights are sensible to changes of the model, such as the introduction of new constraints or terms in the objective function. Thus, a readjustment of the weights is required after any change.

4.2.3 Flux variability analysis

In order to verify the influence of alternative optimal solutions (AOS) on the result of this modeling approach, a flux variability analysis (FVA) was performed at each time step during the static approach. FVA was performed after obtaining the optimal solution of the FBA problem. An inequality constraint was introduced to limit the solution space to optimal FBA solutions, and then each exchange flux was minimized and maximized separately. Thus, the minimum and maximum flux ranges for each exchange flux were obtained.

The result of this dynamic FVA is shown in Figure 4.5. Most exchange fluxes show a high variability for the objective function of biomass and antibody maximization. For the same value of the objective function all exchange fluxes could have different values. Thus, overconsumed substrates could be consumed less, and products not sufficiently produced could be expressed more. Lactate, alanine,

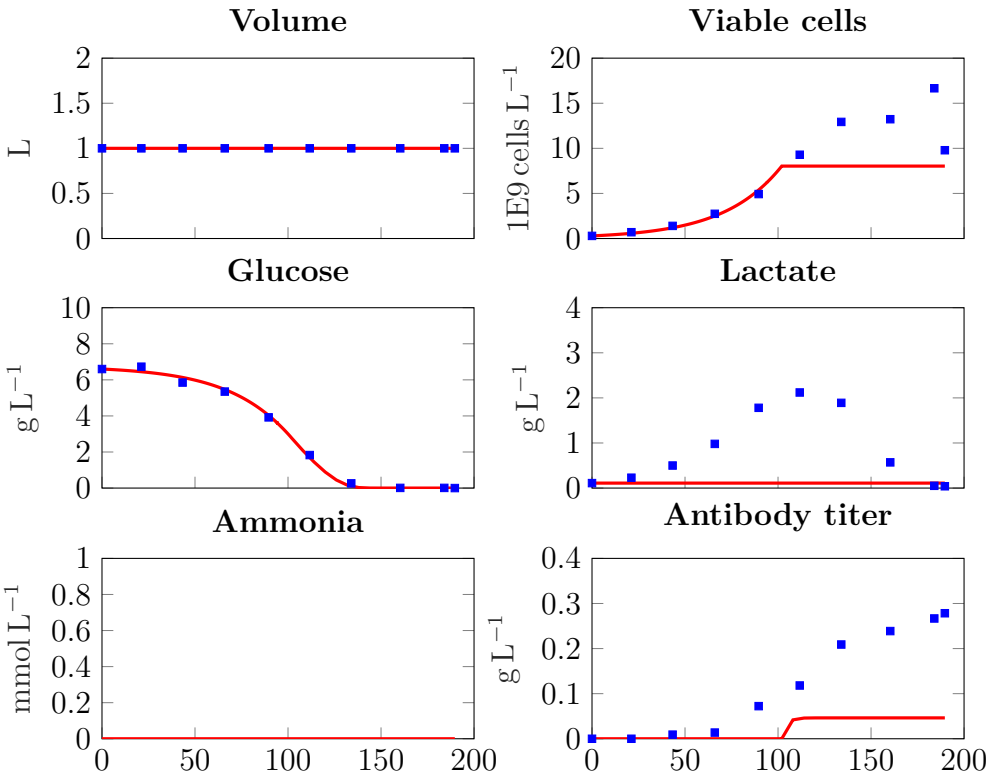

Figure 4.3: Batch cultivation with linear objective function: plot of simulation (red line) vs. experimental data (blue squares). The values on the x-axis represent the culture time in hours. Experimental data from (Bettinardi, 2017).

glutamate and ammonia production would be possible for this objective function, however a different functional state of the metabolic network was selected by the mathematical solution method. In order to limit the optimal solution space to the functional state actually represented by the cells in culture, the introduction of more constraints showed to be necessary.

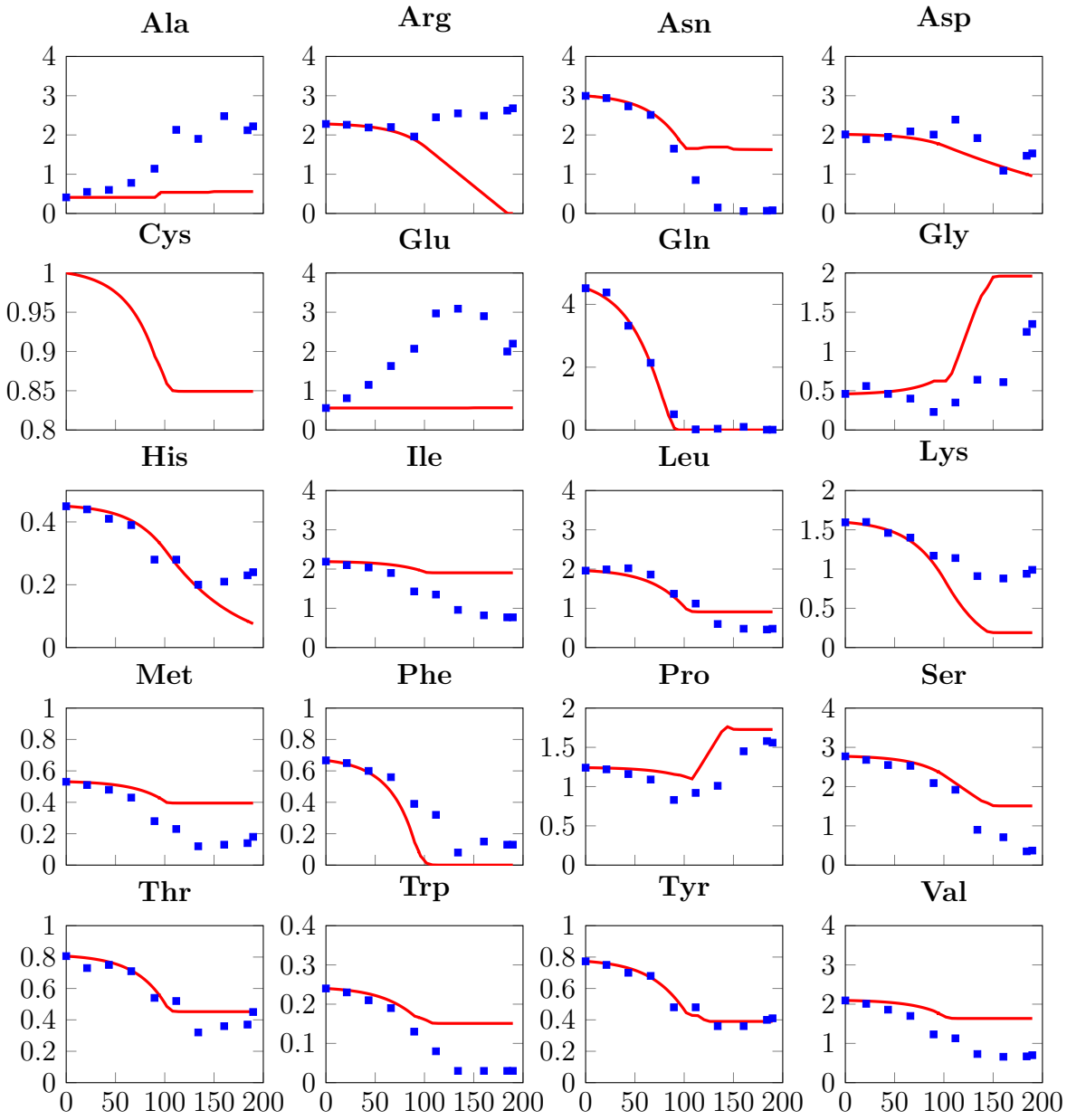

Figure 4.4: Batch cultivation: plot of the simulation results (red lines) vs. experimental data (blue squares) of the aminoacids measured. The concentrations on the y-axis are in mmol L^{-1} and the culture time on the x-axis in hours. Experimental data from Bettinardi (2017).

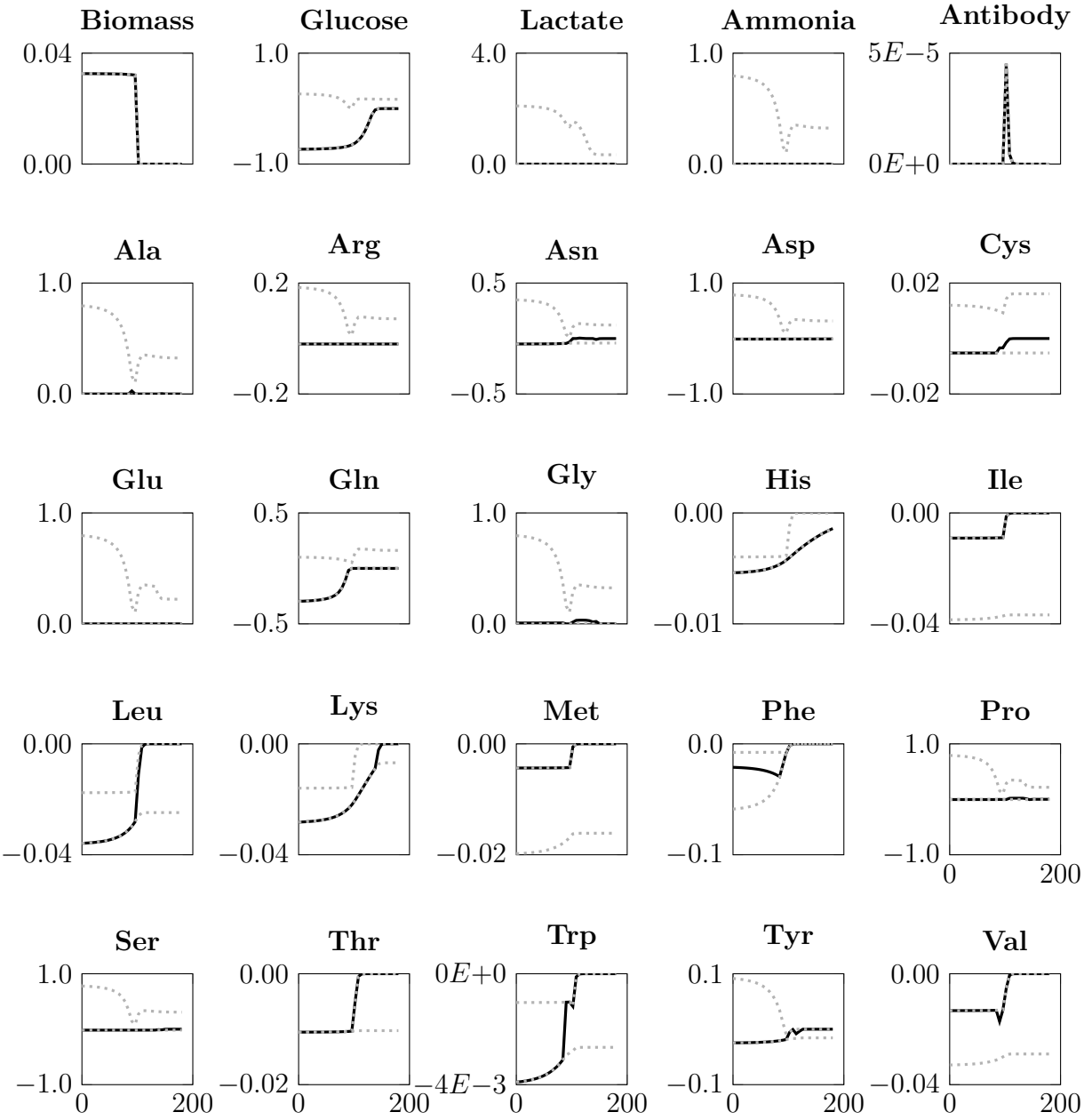

Figure 4.5: Batch cultivation with linear objective function: Flux variability analysis for the 24 exchange fluxes and the biomass function of all time intervals of the static approach. The flux values on the y-axis are in mmol $\mathrm{gDM}^{-1}\,\mathrm{h}^{-1}$, only the biomass flux is in h^{-1}. The dashed gray lines are the minimal and maximal possible fluxes, and the continuous black line is the flux used in the DFBA simulation. The culture time on the x-axis is in hours.

4.2.4 Enzyme efficiency maximization

The principle of enzyme efficiency maximization was applied in a second modeling approach. It was assumed that the metabolism of the cell follows the pathway for which it requires the minimal enzymatic activity, and thus has the highest enzyme efficiency. In terms of the metabolic model this is the lowest overall flux which can be described mathematically as the minimization of the square of the Euclidean norm of the flux vector. This quadratic term was added to the linear terms of the objective function for biomass and antibody maximization. Further, the lower bound of the arginine exchange flux was set to zero as arginine was not consumed by the cells.

Figure 4.6 shows the comparison of the simulated data with the experimental data for the concentrations of viable cells, glucose, lactate, ammonia, and monoclonal antibody. Cell growth is better represented than before as it does not stop prematurely. Ammonia, which was not produced at all in the LP simulation, showed a realistic production. Furthermore, lactate and the monoclonal antibody are as well better represented than before. Glucose, however, is consumed far less than shown by the experimental data.

Consequently, the cell does not require the full energetic potential of glucose to sustain growth and antibody production. This goes along with the altered metabolism of transformed cell lines *in vitro* and confirms the excessive glucose consumption. The most efficient pathway that leads to the maximum of biomass and antibody production does not require the high glucose uptake observed experimentally, consequently the actual glucose metabolism of the cells exceeds purely biosynthetic requirements.

In Figure 4.7 the amino acid profiles are shown. The metabolism of most amino acids shows a similar behavior as in the LP approach (Figure 4.4). However, the produced amino acids show a different profile: alanine production is predicted accurately in the initial phase of the culture. Glycine, proline and glutamate are not produced in the model simulation. Phenylalanine and threonine, both essential

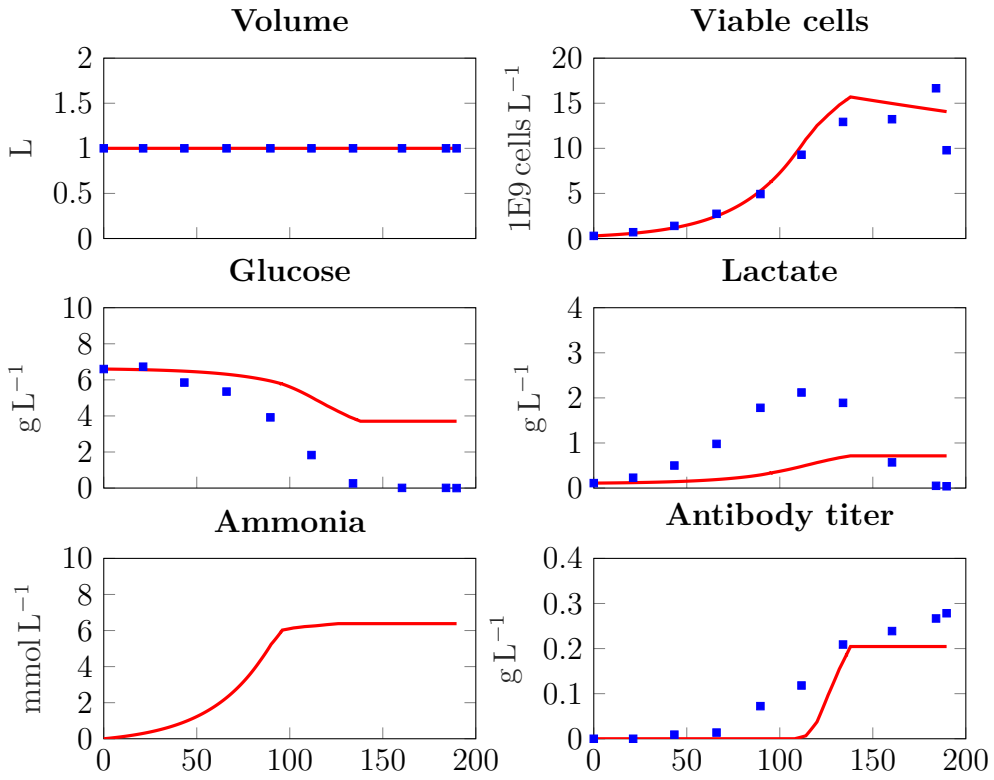

Figure 4.6: Batch cultivation with quadratic objective: plot of simulation (red lines) vs. experimental data (blue squares). The values on the x-axis represent the culture time in hours. Experimental data from Bettinardi (2017).

amino acids required for growth, depleted at the same time. Thus, the maximum growth was assured.

Figure 4.8 shows the result of the dynamic FVA for this quadratic approach. The solution space shows a great variability for most fluxes. Interesting is that the lactate flux is most of the time at its maximum value, thus the principle of enzyme efficiency does not allow a higher lactate production, even though a higher glucose consumption is possible. This result shows that lactate production is not possible when considering an optimal energy metabolism of the cells, and thus implies that the cells *in vitro* use a suboptimal metabolic state producing lactate. This goes in hand with the experimental results by Martínez et al. (2013); Zagari et al. (2013) and Luo et al. (2011).

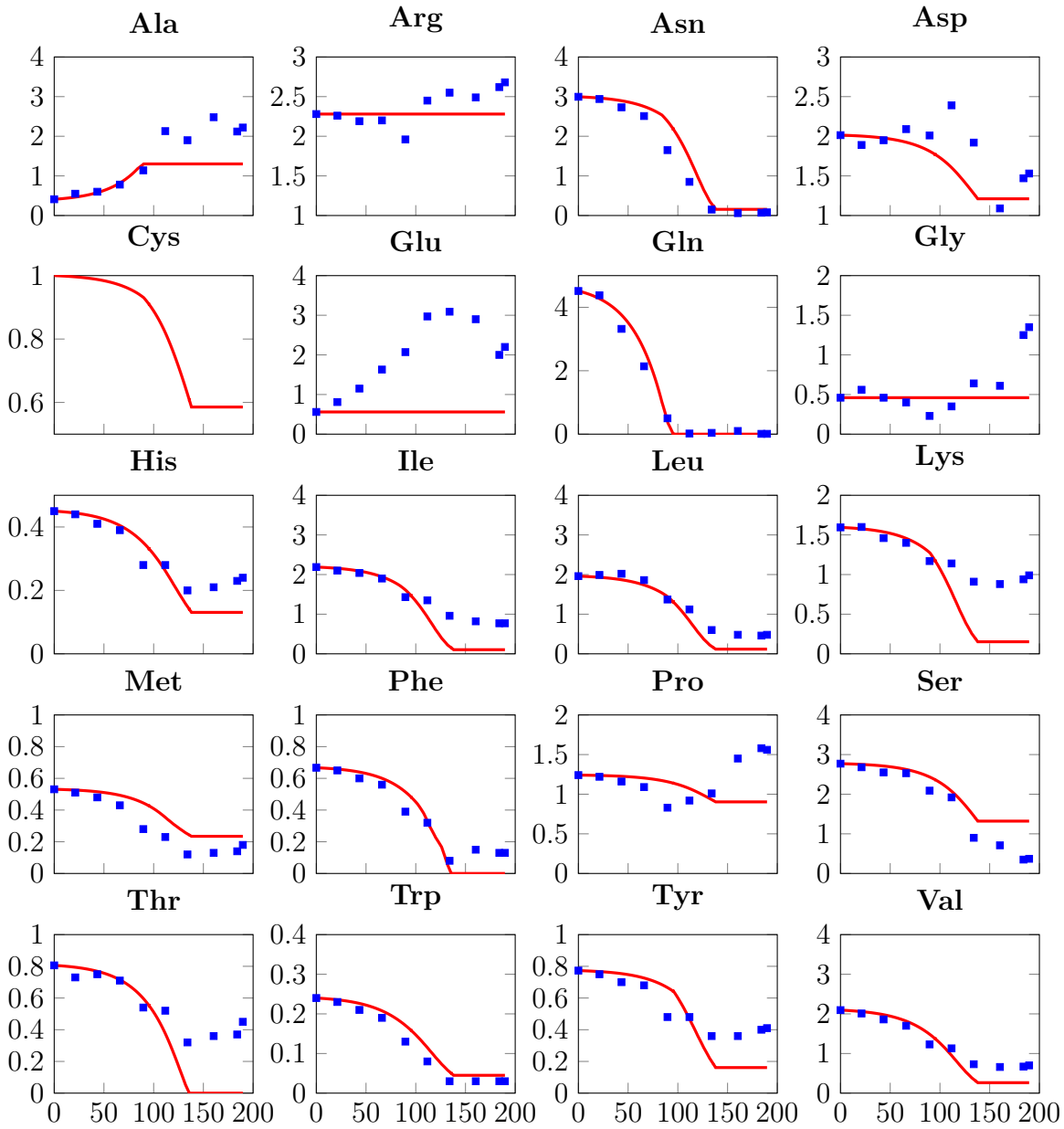

Figure 4.7: Batch cultivation with quadratic objective: plot of the simulation results (red lines) vs. experimental data (blue squares) of the aminoacids measured. The concentrations on the y-axis are in mmol L^{-1} and the culture time on the x-axis in hours. Experimental data from Bettinardi (2017).

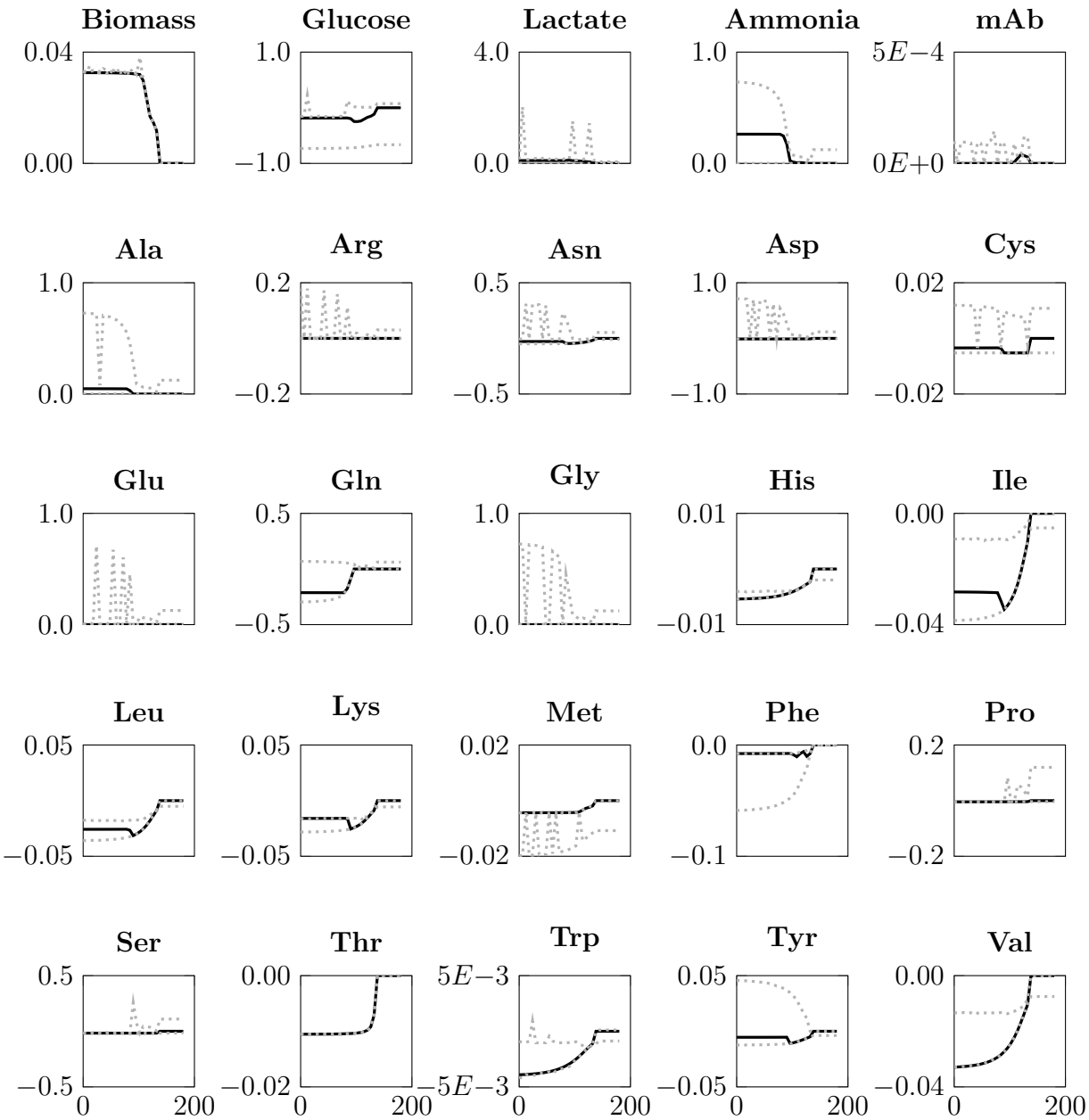

Figure 4.8: Batch cultivation with quadratic objective function: Flux variability analysis for the 24 exchange fluxes and the biomass function of all time intervals of the static approach with a quadratic objective function. The flux values on the y-axis are in mmol $\mathrm{gDM}^{-1}\,\mathrm{h}^{-1}$, only the biomass flux is in h^{-1}. The dashed gray lines are the minimal and maximal possible fluxes, and the continuous black line is the flux used in the DFBA simulation. The values on the x-axis represent the culture time in hours.

4.2.5 Other modeling attempts

In order to reduce the solution space and better represent the experimental data, additional constraints were tested. Thereby any hard constraints were avoided, such as imposed lower bounds for production fluxes (Meadows et al., 2010), or conditional statements (Xing et al., 2010), for example to force the metabolic shift of lactate metabolism. Constraints of these types would allow an easy adjustment of the model to experimental data, however they would limit the predictive capacity of the model.

The results of the enzyme efficiency maximization showed some flaws: first, glucose was less consumed as by the cell *in vitro*; second, lactate was less produced and not consumed; and third, glutamate was not produced. As discussed earlier, lactate formation *in vitro* is associated with a a high glycolytic flux and excessive glucose metabolism (Häggström, 2000). Thus, as a first attempt, the maximization of glucose uptake was added to the objective function with a weight of -1. This lead to a glucose consumption as represented by the experimental data, however neither lactate production nor the profile of any of the other state variables changed. Nevertheless, considering the stoichiometry constraint of the FBA, a higher glucose inflow must necessarily lead to an increase in any outflow of the metabolic model. Using `Paint4Net` the pathway map around glucose was visualized and the flux tracked to find the sink: glucose was converted to isomaltose in a single reaction and then left the network by the isomaltose exchange reaction. Mathematically this can be explained as it is the easiest way to assure a maximal glucose uptake and a minimal overall flux, as demanded by the objective function. To avoid this, the upper bound of the isomaltose exchange reaction was set to zero and, consequently, this pathway blocked. However, successive attempts led to similar results: a great part of the glucose flux left the network as D-sorbitol, upon blocking this reaction as D-Fructose, then glycerol, and so forth. The iCHO1776 model has more than 600 exchange reactions that allow the export of metabolites from the network. The manual blocking of the reactions exporting glucose showed to be not viable. Further, it would turn the model more empiric as these metabolites were not measured and

a flux through these reactions could be possible.

Several other attempts were made to include the attributes of the cell metabolism observed in *in vitro* cell cultures and discussed in the literature (Altamirano et al., 2013; Häggström, 2000). These involved blocking or limiting certain reactions which were reported to be inactive or limited in continuous cell lines, such as: pyruvate carboxylase (Neermann and Wagner, 1996), PEPCK (Fitzpatrick et al., 1993) or pyruvate dehydrogenase (Häggström, 2000). All these modifications and combinations did not alter the results significantly. An attempt to track the reaction fluxes by visualizing the network with `Paint4Net` was made in order to better understand what was happening within the cell, however the pure size of the network solely made this impossible. Fluxes through a lot of reactions, which do not constitute to the well studied core-metabolism (glycolysis, TCA cycle, pentose phosphate cycle, glutamine pathways and oxidative phosphorylation), were observed. No evidence for the expression of the enzymes catalyzing these reactions was found in literature. It is possible that the iCHO1776 GEM contains a great number of enzymes and thus metabolic pathways that are not expressed in the culture conditions *in vitro*.

Other attempts involved the addition to the objective function of enzymes that were reported to be overexpressed in continuous cell lines - such as L-lactate dehydrogenase or glutaminase (Amable and Butler, 2008). A weight of 0.004 for glutaminase in the objective function, implying an overactivity of the enzyme in the direction of glutamine to glutamate, led to a high lactate production and then consumption, as described by the experimental data. However, biomass and antibody production were underestimated. These simulation results are found in Figure 4.9 and Figure 4.10.

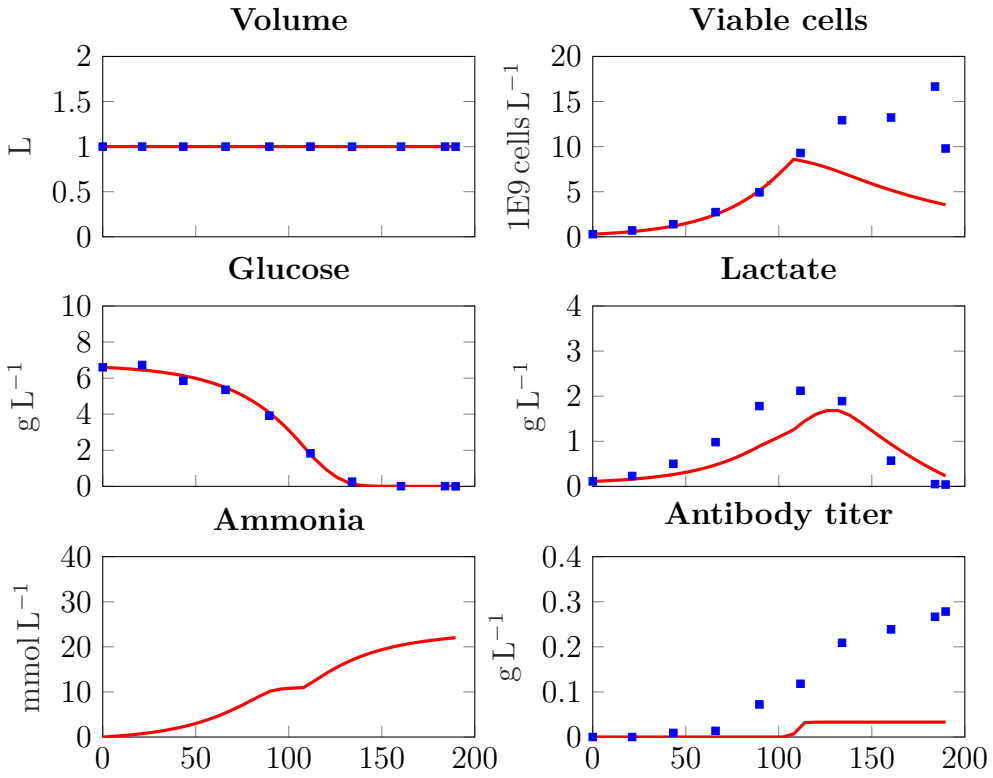

Figure 4.9: Batch simulation with glutaminase in the objective function. Plot of simulation (red lines) vs. experimental data (blue squares). The values on the x-axis represent the culture time in hours. Experimental data from Bettinardi (2017).

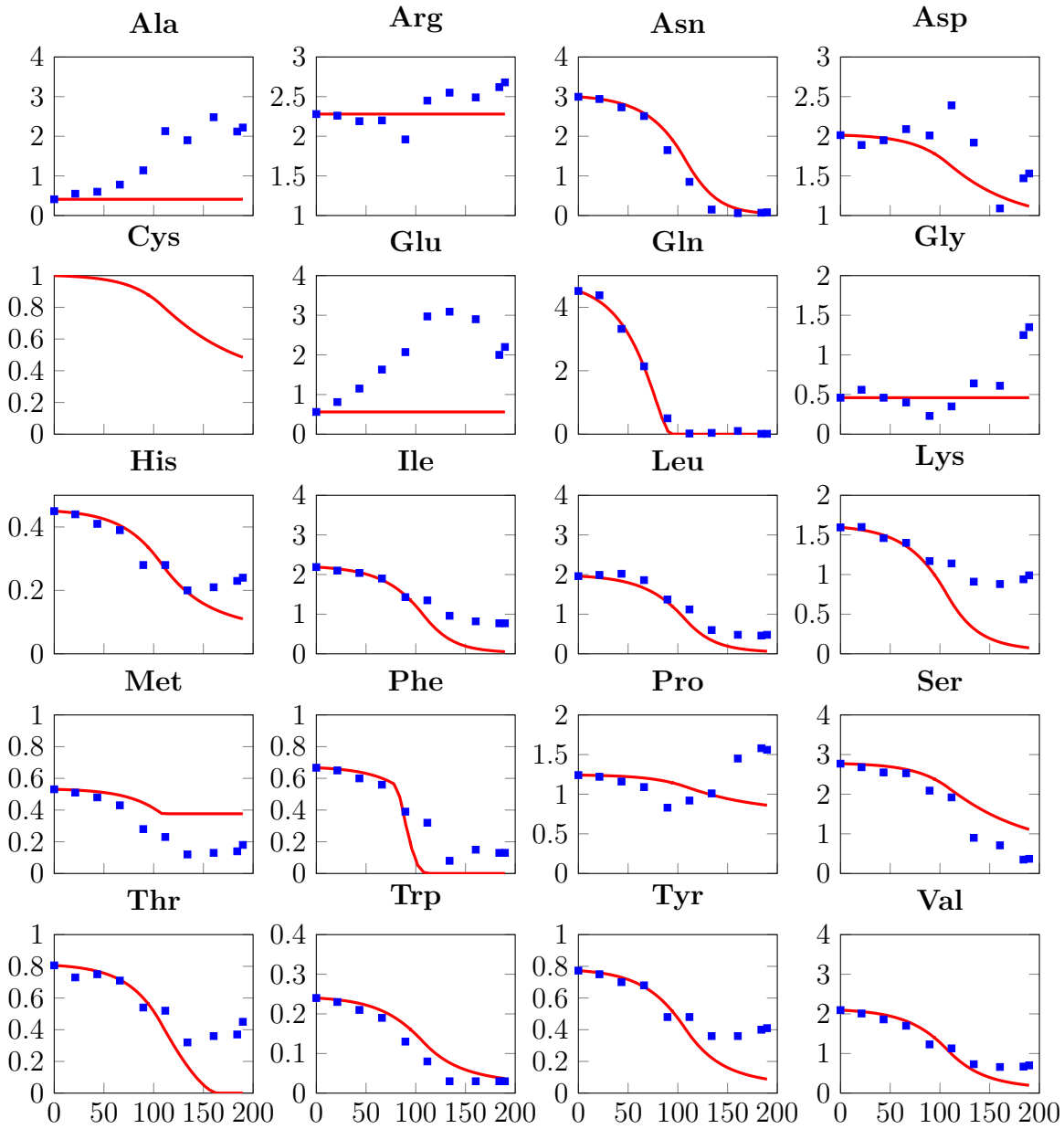

Figure 4.10: Batch simulation with glutaminase in the objective function. Plot of the simulation results (red lines) vs. experimental data (blue squares) of the aminoacids measured. The concentrations on the y-axis are in mmol L^{-1} and the culture time on the x-axis in hours. Experimental data from Bettinardi (2017).

4.2.6 Fed-batch cultivations

The fed-batch cultivations were simulated with the same set of parameters which was determined for the batch-cultures. As objective function the linear approach as in Section 4.2.2 was used, and arginine consumption was constrained to zero.

The simulation results for FBpulse can be found in Figures 4.11 and 4.12. The viable cell concentration and antibody titer were satisfactorily represented. However, the simulation over-predicted glucose consumption slightly and did not foresee the metabolic shift from lactate production to lactate consumption. Furthermore, the experimental data showed an accumulation of most amino acids during the fed-batch culture. The simulation was not able to represent this, and most amino acids were predicted to almost deplete.

For FBcont, the simulation results are shown in Figures 4.13 and 4.14, and were similar to the results of FBpulse. Glucose consumption was overestimated and no lactate shift occurred. The model showed a too high production of antibody, and ammonia accumulated during the simulation to toxic levels. As in FBpulse simulation, most amino acids were consumed much more than showed by the experimental data.

It is important to emphasize that only the experimental data of the batch cultivations was used to estimate the parameters of the model. Fed-batch cultivations, compared to batch cultivations, show a significantly different time profile of metabolite concentrations and other metabolic pathways are activated (Dorka et al., 2009). Empiric kinetic models are not able to describe batch and fed-batch data with the same set of parameters, and often they require different parameters for different phases of a cultivation (Dorka et al., 2009; Gao et al., 2007). This indicates that these models depend on the operation mode and further implies for the GEM that different parts of the metabolic network are active during a cultivation.

However, one must consider that all these results shown here are still subject to flux variability. As there exist multiple optimal solutions, the selection of the

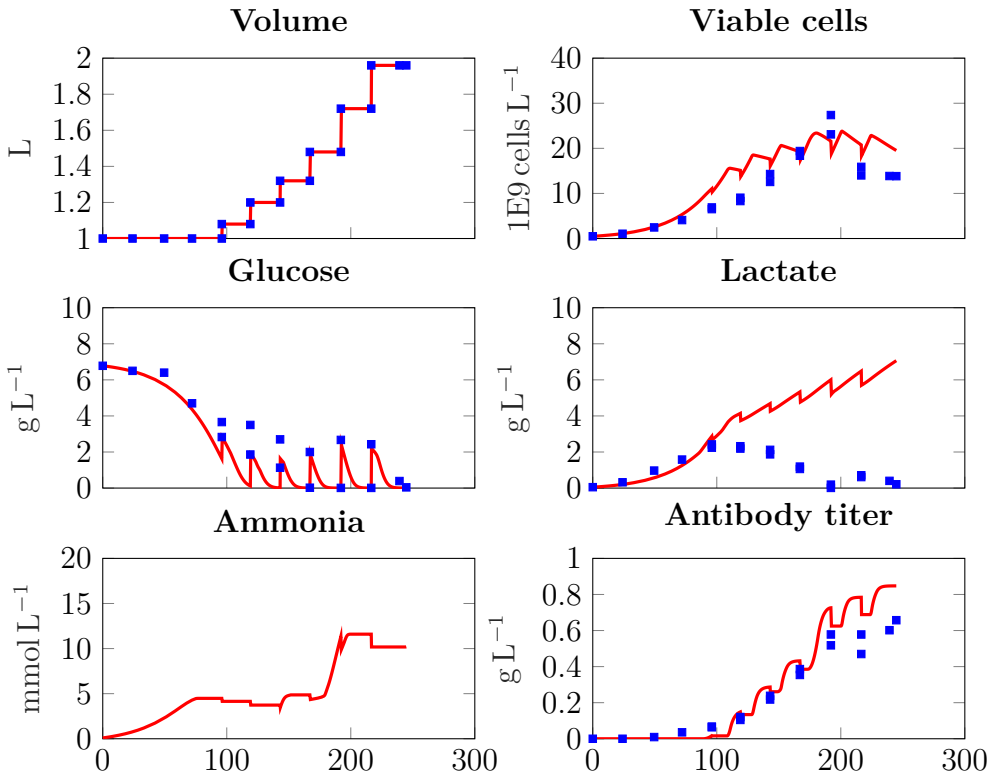

Figure 4.11: Fed-batch simulation with pulse feed: plot of simulation (red line) vs. experimental data (blue squares). The values on the x-axis represent the culture time in hours

phenotype of the cell *in silico* depends only on the solution method of the optimizer and is not based on biologically meaningful assumptions. This problem must first be handled in order to advance and use the model as a predictive tool.

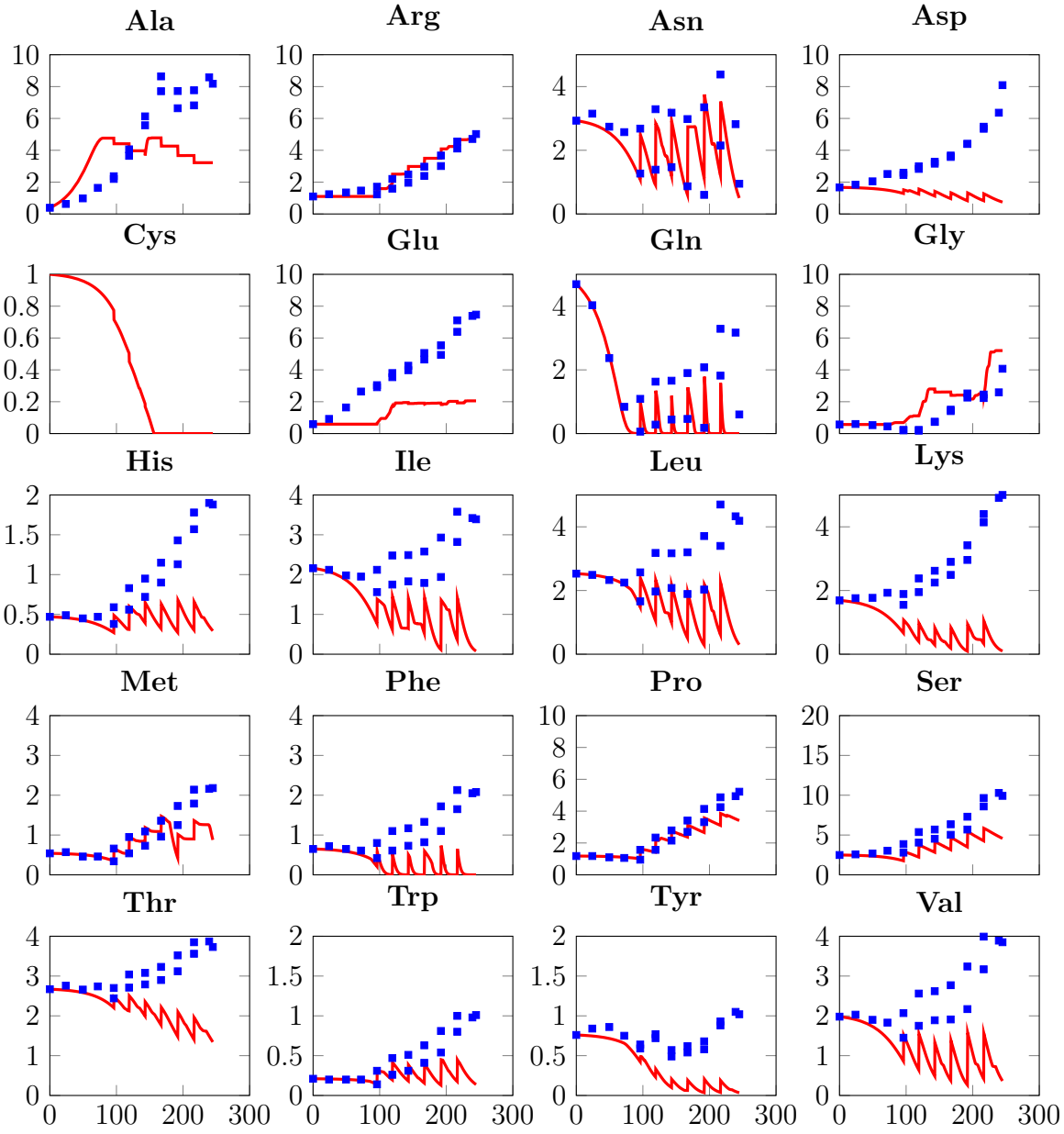

Figure 4.12: Fed-batch simulation with pulse feed: plot of the simulation results (red line) vs. experimental data (blue squares) of the aminoacids measured. All concentrations are in mmol L^{-1} and the culture time on the x-axis in hours.

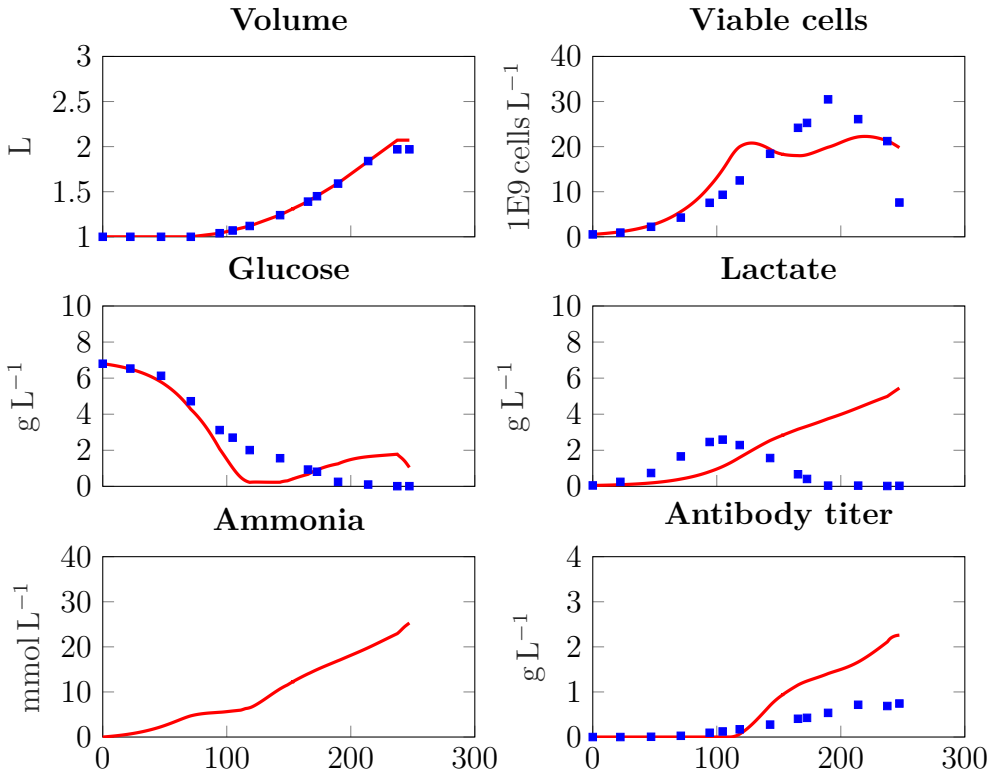

Figure 4.13: Fed-batch simulation with continuous feed: plot of simulation (red line) vs. experimental data (blue squares). The values on the x-axis represent the culture time in hours.

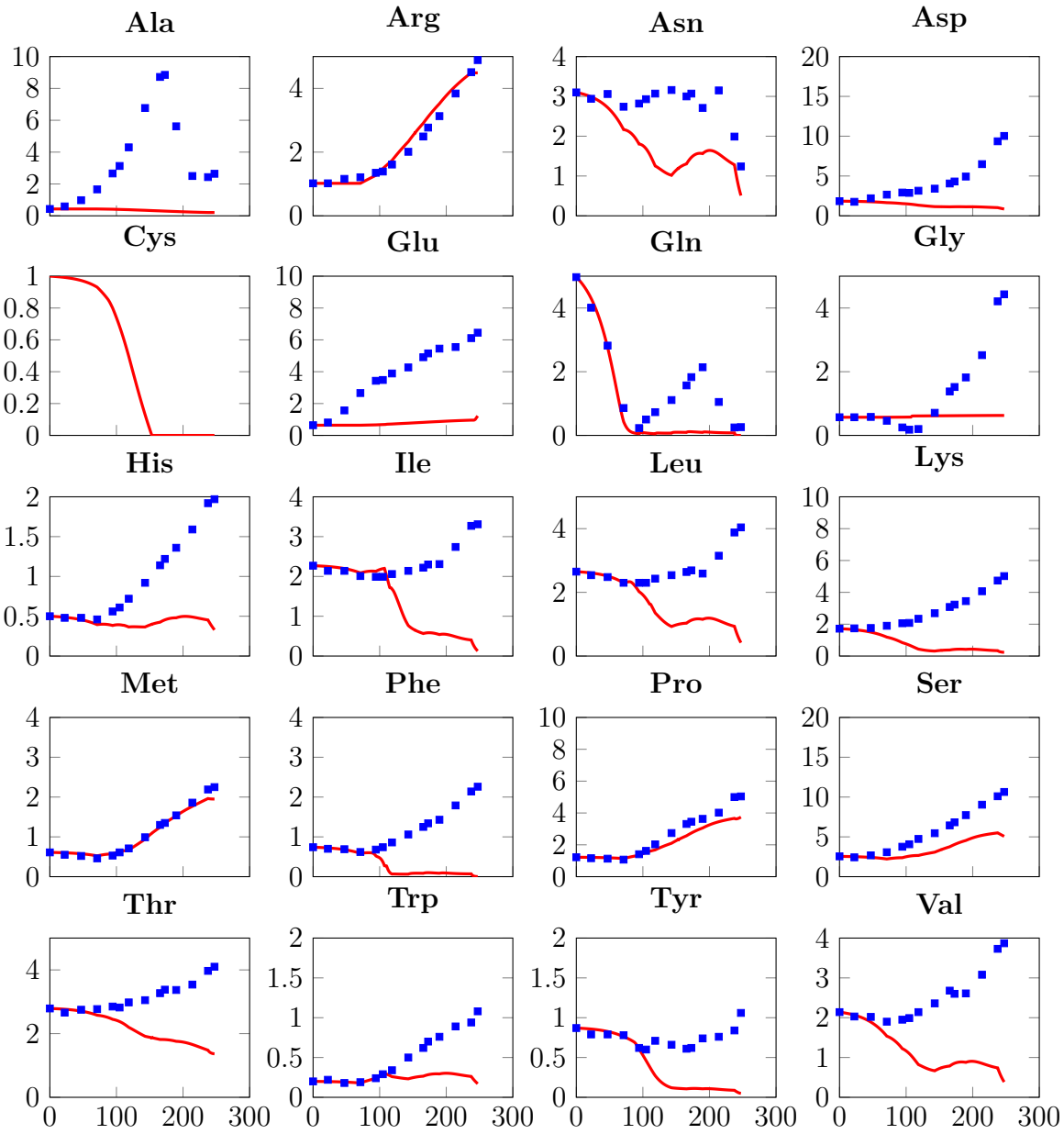

Figure 4.14: Fed-batch simulation with continuous feed: plot of the simulation results (red line) vs. experimental data (blue squares) of the aminoacids measured. All concentrations are in mmol L^{-1} and the culture time on the x-axis in hours.

Chapter 5

Conclusions and outlook

This work represents, to the best of the author's knowledge, the first study of the modeling of CHO cell batch and fed-batch cultures using a dynamic flux balance analysis approach and a genome-scale metabolic model. Even though the current model is not able to perfectly represent the experimental data and consequently cannot be used as predictive tool in this form, important knowledge has been gained and documented. This knowledge will pave the path for further studies, as the future of modeling of cell culture processes seems to lie on the use of genome-scale models. Most interesting is that an extremely simple DFBA formulation with only a few constraints was able to represent the culture dynamics of cell growth and 24 extracellular metabolites considerably well. However, the current study was limited due to the lack of biological meaningful data, such as genomic and proteomic data for the specific cell line and clone. These data would allow a further definition of the phenotype of the cell. Caution must be taken as a GEM, which is intended to provide the most possible accurate information about the organism, can easily become a difficult-to-understand and difficult-to-manipulate black box model when not enough input data is available.

Based on the knowledge acquired in the present work are two ways to make dynamic flux balance analysis with a genome-scale metabolic model viable for mammalian cell cultures: complete the model with biological meaningful data; or reduce its size so that the data available is sufficient to define the phenotypic behavior

of the modeled cell line.

Data of more extracellular metabolites, especially oxygen and carbon dioxide, would give important information about the oxidative metabolism of the cell. However, more profound biologic data would be necessary to unleash the full potential of the genome-scale metabolic model: genomic, proteomic, metabolomic and transcriptomic data for the specific cell line and clone. These -omics data would allow to better define the metabolic model, delivering information about which genes exist, which proteins are expressed and which pathways are active in the cell. Thus the model could be simplified and constraints introduced on the basis of biological meaningful information.

Another option is the reduction of the GEM using pure computational methods. Algorithms to reduce GEMs to core-networks have been presented by Vlassis et al. (2014), Erdrich et al. (2015) and Röhl and Bockmayr (2017). Of these, Erdrich et al.'s `NetworkReducer` method allows to specify protected reactions, metabolites and functional states, and Röhl and Bockmayr's `MinimalNetwork` method speeds the reduction process up and further guarantees network minimality.

Once is obtained a good adjustment to the experimental data in a representative form, the model can be used for diverse *in silico* studies. The dynamic optimization of the feeding strategy - as originally intended to do in this work - is one of them. Furthermore, the feed media composition could be subject to optimization as well: with an economic objective function the use of expensive amino acids could be minimized. Metabolic engineering could also be applied to optimize genetic and regulatory processes within the cell.

List of References

Aiba, S. and Shoda, M. (1969). Reassessment of the product inhibition in alcohol fermentation. *Journal of Fermentation Technology*, 47(12):790–794.

Alizadeh, F. and Goldfarb, D. (2003). Second-order cone programming. *Mathematical Programming*, 95(1):3–51.

Altamirano, C., Berrios, J., Vergara, M., and Becerra, S. (2013). Advances in improving mammalian cells metabolism for recombinant protein production. *Electronic Journal of Biotechnology*, 16(3):10–10.

Amable, P. and Butler, M. (2008). Cell metabolism and its control in culture. In Castilho, L., Moraes, A., Augusto, E., and Butler, M., editors, *Animal Cell Technology: From Biopharmaceuticals to Gene Therapy*, pages 75–110. Taylor & Francis.

Antoniewicz, M. R. (2013). Dynamic metabolic flux analysis—tools for probing transient states of metabolic networks. *Current Opinion in Biotechnology*, 24(6):973–978.

Bates, R. G. and Pinching, G. (1949). Acidic dissociation constant of ammonium ion at 0 to 50 C, and the base strength of ammonia. *Journal of Research of the National Bureau of Standards*, 42:419–430.

Berg, J., Tymoczko, J., and Stryer, L. (2002). *Biochemistry, Fifth Edition*. W.H. Freeman, New York.

Berrios, J., Altamirano, C., Osses, N., and Gonzalez, R. (2011). Continuous CHO cell cultures with improved recombinant protein productivity by using mannose as carbon source: Metabolic analysis and scale-up simulation. *Chemical Engineering Science*, 66(11):2431–2439.

Bettinardi, I. W. (2016). Desenvolvimento de estratégias de alimentação com meios concentrados para cultivo de células animais em perfusão. MSc dissertation, Alberto Luiz Coimbra Institute for Graduate Studies and Research in Engineering (COPPE/UFRJ).

Bettinardi, I. W. (2017). Estratégias de alimentação e de diferentes equipamentos de retenção celular para a produção de um anticorpo monoclonal em perfusão. Exame de qualificação da candidatura ao grau de doutor em ciências em engenharia química, Alberto Luiz Coimbra Institute for Graduate Studies and Research in Engineering (COPPE/UFRJ). Unpublished data.

Blank, L. M., Kuepfer, L., and Sauer, U. (2005). Large-scale 13 C-flux analysis reveals mechanistic principles of metabolic network robustness to null mutations in yeast. *Genome Biology*, 6(6):R49.

Bonarius, H. P., Özemre, A., Timmerarends, B., Skrabal, P., Tramper, J., Schmid, G., and Heinzle, E. (2001). Metabolic-flux analysis of continuously cultured hybridoma cells using 13-CO_2 mass spectrometry in combination with 13C-lactate nuclear magnetic resonance spectroscopy and metabolite balancing. *Biotechnology and Bioengineering*, 74(6):528–538.

Bordbar, A., Monk, J. M., King, Z. A., and Palsson, B. O. (2014). Constraint-based models predict metabolic and associated cellular functions. *Nature Reviews Genetics*, 15(2):107–120.

Bree, M. A., Dhurjati, P., Geoghegan, R. F., and Robnett, B. (1988). Kinetic modelling of hybridoma cell growth and immunoglobulin production in a large-scale suspension culture. *Biotechnology and Bioengineering*, 32(8):1067–1072.

Bro, C. and Nielsen, J. (2004). Impact of 'ome'analyses on inverse metabolic engineering. *Metabolic Engineering*, 6(3):204–211.

Bussolati, O., Uggeri, J., Rotoli, B. M., Franchi-Gazzola, R., and Gazzola, G. C. (1993). The relationship between sodium-dependent transport of anionic amino acids and cell proliferation. *Biochimica et Biophysica Acta*, 1151(2):153–160.

Castilho, L. (2016). Biopharmaceutical Products: An Introduction. In Thomaz-Soccol, V., Pandey, A., and Resende, R., editors, *Current Developments in Biotechnology and Bioengineering*, pages 3–21. Elsevier.

Chuang, H.-Y., Hofree, M., and Ideker, T. (2010). A decade of systems biology. *Annual Review of Cell and Developmental Biology*, 26:721–744.

Covert, M. W., Schilling, C. H., and Palsson, B. (2001). Regulation of gene expression in flux balance models of metabolism. *Journal of Theoretical Biology*, 213(1):73–88.

Craven, S., Whelan, J., and Glennon, B. (2014). Glucose concentration control of a fed-batch mammalian cell bioprocess using a nonlinear model predictive controller. *Journal of Process Control*, 24(4):344–357.

Dorka, P., Fischer, C., Budman, H., and Scharer, J. M. (2009). Metabolic flux-based modeling of mAb production during batch and fed-batch operations. *Bioprocess and Biosystems Engineering*, 32(2):183–196.

Ecker, D. M., Jones, S. D., and Levine, H. L. (2015). The therapeutic monoclonal antibody market. *MAbs*, 7(1):9–14.

Erdrich, P., Steuer, R., and Klamt, S. (2015). An algorithm for the reduction of genome-scale metabolic network models to meaningful core models. *BMC Systems Biology*, 9(1):48.

Feist, A. M., Herrgård, M. J., Thiele, I., Reed, J. L., and Palsson, B. Ø. (2009). Reconstruction of biochemical networks in microorganisms. *Nature Reviews Microbiology*, 7(2):129–143.

Fitzpatrick, L., Jenkins, H., and Butler, M. (1993). Glucose and glutamine metabolism of a murine b-lymphocyte hybridoma grown in batch culture. *Applied Biochemistry and Biotechnology*, 43(2):93–116.

Gao, J., Gorenflo, V. M., Scharer, J. M., and Budman, H. M. (2007). Dynamic metabolic modeling for a MAB bioprocess. *Biotechnology Progress*, 23(1):168–181.

Ghaderi, D., Zhang, M., Hurtado-Ziola, N., and Varki, A. (2012). Production platforms for biotherapeutic glycoproteins. occurrence, impact, and challenges of non-human sialylation. *Biotechnology and Genetic Engineering Reviews*, 28(1):147–176.

Gianchandani, E. P., Chavali, A. K., and Papin, J. A. (2010). The application of flux balance analysis in systems biology. *Wiley Interdisciplinary Reviews: Systems Biology and Medicine*, 2(3):372–382.

Glacken, M. W. (1988). Catabolic control of mammalian cell culture. *Nature Biotechnology*, 6(9):1041–1050.

Gomez, J. A., Hoffner, K., and Barton, P. I. (2014). Dfbalab: a fast and reliable matlab code for dynamic flux balance analysis. *BMC Bioinformatics*, 15(1):409.

Gonzalez, T. N., Leong, S. R., and Presta, L. G. (2000). Humanized anti-IL-8 monoclonal antibodies. US Patent 6133426A.

Gurobi Optimization, I. (2017). Gurobi optimizer reference manual. URL `http://www.gurobi.com`. Last accessed on Dez 03, 2017.

Häggström, L. (2000). Cell metabolism, animal. *Encyclopedia of Cell Technology*, 1:392–411.

Hefzi, H., Ang, K. S., Hanscho, M., Bordbar, A., Ruckerbauer, D., Lakshmanan, M., Orellana, C. A., Baycin-Hizal, D., Huang, Y., Ley, D., Martinez, V. S., Kyriakopoulos, S., Jiménez, N. E., Zielinski, D. C., Quek, L.-E., Wulff, T., Arnsdorf, J., Li, S., Lee, J. S., Paglia, G., Loira, N., Spahn, P. N., Pedersen, L. E., Gutierrez, J. M., King, Z. A., Lund, A. M., Nagarajan, H., Thomas, A., Abdel-Haleem, A. M., Zanghellini, J., Kildegaard, H. F., Voldborg, B. G., Gerdtzen, Z. P., Betenbaugh, M. J., Palsson, B. O., Andersen, M. R., Nielsen, L. K., Borth, N., Lee, D.-Y., and Lewis, N. E. (2016). A consensus genome-scale reconstruction of chinese hamster ovary cell metabolism. *Cell Systems*, 3(5):434–443.

Heirendt, L., Arreckx, S., Pfau, T., Mendoza, S. N., Richelle, A., Heinken, A., Haraldsdottir, H. S., Keating, S. M., Vlasov, V., Wachowiak, J., et al. (2017). Creation and analysis of biochemical constraint-based models: the COBRA Toolbox v3.0. *arXiv preprint arXiv:1710.04038*.

Hjersted, J. and Henson, M. (2009). Steady-state and dynamic flux balance analysis of ethanol production by saccharomyces cerevisiae. *IET Systems Biology*, 3(3):167–179.

Hjersted, J. L., Henson, M. A., and Mahadevan, R. (2007). Genome-scale analysis of saccharomyces cerevisiae metabolism and ethanol production in fed-batch culture. *Biotechnology and Bioengineering*, 97(5):1190–1204.

Höffner, K., Harwood, S. M., and Barton, P. I. (2013). A reliable simulator for dynamic flux balance analysis. *Biotechnology and Bioengineering*, 110(3):792–802.

Holzhütter, H.-G. (2004). The principle of flux minimization and its application to estimate stationary fluxes in metabolic networks. *The FEBS Journal*, 271(14):2905–2922.

Ideker, T., Galitski, T., and Hood, L. (2001). A new approach to decoding life: systems biology. *Annual Review of Genomics and Human Genetics*, 2(1):343–372.

Jayapal, K. P., Wlaschin, K. F., Hu, W., and Yap, M. G. (2007). Recombinant protein therapeutics from CHO cells - 20 years and counting. *Chemical Engineering Progress*, 103(10):40–47.

Jenkins, N. and Curling, E. M. (1994). Glycosylation of recombinant proteins: problems and prospects. *Enzyme and Microbial Technology*, 16(5):354–364.

Kildegaard, H. F., Baycin-Hizal, D., Lewis, N. E., and Betenbaugh, M. J. (2013). The emerging CHO systems biology era: harnessing the 'omics revolution for biotechnology. *Current Opinion in Biotechnology*, 24(6):1102–1107.

Kim, J. Y., Kim, Y.-G., and Lee, G. M. (2012). CHO cells in biotechnology for production of recombinant proteins: current state and further potential. *Applied Microbiology and Biotechnology*, 93(3):917–930.

King, Z. A., Lu, J., Dräger, A., Miller, P., Federowicz, S., Lerman, J. A., Ebrahim, A., Palsson, B. O., and Lewis, N. E. (2016). BiGG Models: A platform for integrating, standardizing and sharing genome-scale models. *Nucleic Acids Research*, 44(D1):D515–D522.

Kitano, H. (2002). Systems biology: a brief overview. *Science*, 295(5560):1662–1664.

Kostromins, A. and Stalidzans, E. (2012). Paint4net: Cobra toolbox extension for visualization of stoichiometric models of metabolism. *Biosystems*, 109(2):233–239.

Koumpouras, G. (2012). Dynamic Optimization of Bioprocesses. *Applied Mathematics*, 3(10A):1487–1495.

Krömer, J., Nielsen, L., and Blank, L. (2014). *Metabolic Flux Analysis: Methods and Protocols*. Methods in Molecular Biology. Springer New York, 233 Spring St, New York, NY 10013, USA.

Ledford, H. (2010). 'biosimilar' drugs poised to penetrate market. *Nature*, 468(7320):18–19.

Li, L., Mi, L., Feng, Q., Liu, R., Tang, H., Xie, L., Yu, X., and Chen, Z. (2005). Increasing the culture efficiency of hybridoma cells by the use of integrated metabolic control of glucose and glutamine at low levels. *Biotechnology and Applied Biochemistry*, 42(1):73–80.

Longo, N., Franchi-Gazzola, R., Bussolati, O., Dall'Asta, V., Nucci, F. A., and Gazzola, G. C. (1988). Amino acid and sugar transport in mouse 3t3 cells expressing activated ras and neu oncogenes. *Annals of the New York Academy of Sciences*, 551(1):374–377.

Lucas, B. K., Giere, L. M., DeMarco, R. A., Shen, A., Chisholm, V., and Crowley, C. W. (1996). High-level production of recombinant proteins in CHO cells using a dicistronic DHFR intron expression vector. *Nucleic acids research*, 24(9):1774–1779.

Luo, J., Vijayasankaran, N., Autsen, J., Santuray, R., Hudson, T., Amanullah, A., and Li, F. (2011). Comparative metabolite analysis to understand lactate metabolism shift in chinese hamster ovary cell culture process. *Biotechnology and Bioengineering*, 109(1):146–156.

Mahadevan, R., Edwards, J. S., and Doyle, F. J. (2002). Dynamic flux balance analysis of diauxic growth in Escherichia coli. *Biophysical Journal*, 83(3):1331–1340.

Mahadevan, R. and Schilling, C. (2003). The effects of alternate optimal solutions in constraint-based genome-scale metabolic models. *Metabolic Engineering*, 5(4):264–276.

Mancuso, A., Sharfstein, S. T., Tucker, S. N., Clark, D. S., and Blanch, H. W. (1994). Examination of primary metabolic pathways in a murine hybridoma with carbon-13 nuclear magnetic resonance spectroscopy. *Biotechnology and Bioengineering*, 44(5):563–585.

Martínez, V. S., Dietmair, S., Quek, L.-E., Hodson, M. P., Gray, P., and Nielsen, L. K. (2013). Flux balance analysis of CHO cells before and after a metabolic switch from lactate production to consumption. *Biotechnology and Bioengineering*, 110(2):660–666.

Meadows, A. L., Karnik, R., Lam, H., Forestell, S., and Snedecor, B. (2010). Application of dynamic flux balance analysis to an industrial *Escherichia coli* fermentation. *Metabolic Engineering*, 12(2):150–160.

Michaelis, L. and Menten, M. L. (1913). Die Kinetik der Invertinwirkung. *Biochemische Zeitschrift*, 49(1):333–369.

Monod, J. (1949). The growth of bacterial cultures. *Annual Reviews in Microbiology*, 3(1):371–394.

Nam, J. H., Zhang, F., Ermonval, M., Linhardt, R. J., and Sharfstein, S. T. (2008). The effects of culture conditions on the glycosylation of secreted human placental alkaline phosphatase produced in chinese hamster ovary cells. *Biotechnology and Bioengineering*, 100(6):1178–1192.

Neermann, J. and Wagner, R. (1996). Comparative analysis of glucose and glutamine metabolism in transformed mammalian cell lines, insect and primary liver cells. *Journal of Cellular Physiology*, 166(1):152–169.

Neto, J. S. (2016). Quase metade (51%) dos gastos do Ministério da Saúde é feito com biofármacos. `http://epocanegocios.globo.com/Brasil/noticia/2016/08/remedios-ja-concentram-metade-dos-gastos-do-ministerio-da-saude.html`. Last accessed on Dez 03, 2017.

Niklas, J., Noor, F., and Heinzle, E. (2009). Effects of drugs in subtoxic concentrations on the metabolic fluxes in human hepatoma cell line Hep G2. *Toxicology and Applied Pharmacology*, 240(3):327–336.

Nolan, R. P. and Lee, K. (2011). Dynamic model of cho cell metabolism. *Metabolic Engineering*, 13(1):108–124.

Oddone, G. M., Mills, D. A., and Block, D. E. (2009). A dynamic, genome-scale flux model of lactococcus lactis to increase specific recombinant protein expression. *Metabolic Engineering*, 11(6):367–381.

Orth, J. D., Thiele, I., and Palsson, B. Ø. (2010). What is flux balance analysis? *Nature Biotechnology*, 28(3):245–248.

Pál, C., Papp, B., Lercher, M. J., Csermely, P., Oliver, S. G., and Hurst, L. D. (2006). Chance and necessity in the evolution of minimal metabolic networks. *Nature*, 440(7084):667.

Palsson, B. Ø. (2015). *Systems biology: constraint-based reconstruction and analysis*. Cambridge University Press, Cambridge CB2 8BS, UK.

Petch, D. and Butler, M. (1994). Profile of energy metabolism in a murine hybridoma: glucose and glutamine utilization. *Journal of Cellular Physiology*, 161(1):71–76.

Philippidis, A. (2017). The top 15 best-selling drugs of 2016. `https://www.genengnews.com/the-lists/the-top-15-best-selling-drugs-of-2016/77900868`. Last accessed on Dez 03, 2017.

Quek, L.-E., Dietmair, S., Krömer, J. O., and Nielsen, L. K. (2010). Metabolic flux analysis in mammalian cell culture. *Metabolic Engineering*, 12(2):161–171.

Röhl, A. and Bockmayr, A. (2017). A mixed-integer linear programming approach to the reduction of genome-scale metabolic networks. *BMC Bioinformatics*, 18(1):2.

Sánchez, B. J., Pérez-Correa, J. R., and Agosin, E. (2014). Construction of robust dynamic genome-scale metabolic model structures of saccharomyces cerevisiae through iterative re-parameterization. *Metabolic Engineering*, 25(C):159–173.

Santos, F., Boele, J., and Teusink, B. (2011). A practical guide to genome-scale metabolic models and their analysis. *Methods in Enzymology*, 500:509–532.

Schuetz, R., Zamboni, N., Zampieri, M., Heinemann, M., and Sauer, U. (2012). Multidimensional optimality of microbial metabolism. *Science*, 336(6081):601–604.

Strober, W. (2001). Trypan blue exclusion test of cell viability. *Current Protocols in Immunology*, pages A3–B.

Teusink, B., Wiersma, A., Molenaar, D., Francke, C., de Vos, W. M., Siezen, R. J., and Smid, E. J. (2006). Analysis of growth of lactobacillus plantarum wcfs1 on a complex medium using a genome-scale metabolic model. *Journal of Biological Chemistry*, 281(52):40041–40048.

Trewavas, A. (2006). A brief history of systems biology. *The Plant Cell*, 18(10):2420–2430.

Tziampazis, E. and Sambanis, A. (1994). Modeling of cell culture processes. *Cytotechnology*, 14(3):191–204.

Vargas, F. A., Pizarro, F., Pérez-Correa, J. R., and Agosin, E. (2011). Expanding a dynamic flux balance model of yeast fermentation to genome-scale. *BMC Systems Biology*, 5(1):75.

Veliz, E. C., Rodríguez, G., and Cardero, A. F. (2008). Bioreactors for animal cells. In Castilho, L., Moraes, A., Augusto, E., and Butler, M., editors, *Animal Cell Technology: From Biopharmaceuticals to Gene Therapy*, pages 221–258. Taylor & Francis.

Vlassis, N., Pacheco, M. P., and Sauter, T. (2014). Fast reconstruction of compact context-specific metabolic network models. *PLoS Computational Biology*, 10(1):e1003424.

Vriezen, N. and van Dijken, J. P. (1998). Fluxes and enzyme activities in central metabolism of myeloma cells grown in chemostat culture. *Biotechnology and Bioengineering*, 59(1):28–39.

Walsh, G. (2014). Biopharmaceutical benchmarks 2014. *Nature biotechnology*, 32(10):992–1000.

Wiebe, M., Becker, F., Lazar, R., May, L., Casto, B., Semense, M., and Fautz, C. (1989). A multifaceted approach to assure that recombinant tpa is free of adventitious virus. *Advances in Animal Cell Biology and Technology*, pages 68–71.

Wurm, F. M. (2005). Manufacture of recombinant biopharmaceutical proteins by cultivated mammalian cells in bioreactors. In Knäblein, J., editor, *Modern Biopharmaceuticals: Design, Development and Optimization*, pages 723–759. Wiley-VCH Verlag GmbH, Weinheim, Germany.

Xing, Z., Bishop, N., Leister, K., and Li, Z. J. (2010). Modeling kinetics of a large-scale fed-batch CHO cell culture by Markov chain Monte Carlo method. *Biotechnology Progress*, 26(1):208–219.

Yahia, B. B., Malphettes, L., and Heinzle, E. (2015). Macroscopic modeling of mammalian cell growth and metabolism. *Applied Microbiology and Biotechnology*, 99(17):7009–7024.

Zagari, F., Jordan, M., Stettler, M., Broly, H., and Wurm, F. M. (2013). Lactate metabolism shift in cho cell culture: the role of mitochondrial oxidative activity. *New Biotechnology*, 30(2):238–245.

Zhang, C. and Hua, Q. (2016). Applications of genome-scale metabolic models in biotechnology and systems medicine. *Frontiers in Physiology*, 6:413.

Zhuang, K., Izallalen, M., Mouser, P., Richter, H., Risso, C., Mahadevan, R., and Lovley, D. R. (2011). Genome-scale dynamic modeling of the competition between rhodoferax and geobacter in anoxic subsurface environments. *The ISME Journal*, 5(2):305.

Appendices

Appendix A

Experimental data

Table A.1: Experimental data of the batch cultivation (Bettinardi, 2017). The units are described in Table 3.5.

t (h)	V	Xv	Glc	Lac	mAb	Ala	Arg	Asn	Asp	Glu	Gln	Gly
0.00	1.00	0.29	6.60	0.11	0.00	0.41	1.97	2.63	1.70	0.56	4.25	0.46
21.17	1.00	0.70	6.73	0.23	0.00	0.55	2.26	2.94	1.89	0.81	4.38	0.56
43.33	1.00	1.40	5.85	0.50	0.01	0.60	2.19	2.73	1.95	1.15	3.32	0.46
66.00	1.00	2.74	5.35	0.98	0.02	0.78	2.20	2.51	2.09	1.63	2.14	0.40
89.58	1.00	4.93	3.92	1.78	0.07	1.14	1.96	1.65	2.01	2.07	0.50	0.23
111.67	1.00	9.29	1.83	2.12	0.12	2.13	2.45	0.85	2.39	2.97	0.02	0.35
134.00	1.00	12.93	0.26	1.89	0.21	1.90	2.55	0.15	1.92	3.09	0.04	0.64
160.33	1.00	13.23	0.01	0.57	0.29	2.48	2.49	0.06	1.09	2.90	0.10	0.61
184.00	1.00	16.66	0.01	0.05	0.27	2.12	2.62	0.07	1.47	2.00	0.01	1.25
189.67	1.00	9.79	0.00	0.04	0.28	2.22	2.68	0.08	1.53	2.20	0.01	1.35
t (h)	**His**	**Ile**	**Leu**	**Lys**	**Met**	**Phe**	**Pro**	**Ser**	**Thr**	**Trp**	**Tyr**	**Val**
0.00	0.42	1.93	1.96	1.34	0.51	0.60	1.15	2.32	0.55	0.22	0.70	1.84
21.17	0.44	2.10	1.99	1.60	0.51	0.65	1.22	2.68	0.73	0.23	0.75	2.01
43.33	0.41	2.04	2.02	1.46	0.48	0.60	1.16	2.55	0.75	0.21	0.70	1.86
66.00	0.39	1.90	1.86	1.40	0.43	0.56	1.09	2.53	0.71	0.19	0.68	1.70
89.58	0.28	1.43	1.37	1.17	0.28	0.39	0.83	2.09	0.54	0.13	0.48	1.23
111.67	0.28	1.35	1.12	1.14	0.23	0.32	0.92	1.92	0.52	0.08	0.48	1.13
134.00	0.20	0.96	0.60	0.91	0.12	0.08	1.01	0.90	0.32	0.03	0.36	0.73
160.33	0.21	0.82	0.48	0.88	0.13	0.15	1.45	0.71	0.36	0.03	0.36	0.66
184.00	0.23	0.77	0.46	0.94	0.14	0.13	1.58	0.35	0.37	0.03	0.40	0.67
189.67	0.24	0.77	0.48	0.99	0.18	0.13	1.56	0.37	0.45	0.03	0.41	0.70

Table A.2: Measured feed media composition for both fed-batch cultivations. Small variations can be explained as error during measurement and lot-to-lot variation.

TCX2D	V	Xv	Glc	Lac	mAb	Ala	Arg	Asn	Asp	Glu	Gln	Gly
FBpulse	1.00	0.00	18.70	0.00	0.00	0.00	7.73	20.34	4.44	1.24	13.84	0.64
FBcont	1.00	0.00	20.03	0.00	0.00	0.00	6.28	27.53	5.18	2.75	12.99	0.43
TCX2D	**His**	**Ile**	**Leu**	**Lys**	**Met**	**Phe**	**Pro**	**Ser**	**Thr**	**Trp**	**Tyr**	**Val**
FBpulse	3.23	9.08	14.02	6.25	4.68	5.57	9.26	17.24	5.97	2.43	1.28	9.87
FBcont	3.12	9.86	15.74	6.53	5.35	5.84	8.25	13.39	5.26	2.45	1.29	9.93

Table A.3: Experimental data of the fed-batch cultivation with pulse feeding. The units are described in Table 3.5. Amino acid concentrations after the pulse feeding were not measured but calculated by Equation 3.6.

t	V	Xv	Glc	Lac	mAb	Ala	Arg	Asn	Asp	Glu	Gln	Gly
0.00	1.00	0.49	6.78	0.05	0.00	0.39	1.10	2.93	1.67	0.59	4.69	0.57
24.00	1.00	1.06	6.50	0.32	0.00	0.63	1.24	3.15	1.84	0.92	4.03	0.60
49.50	1.00	2.46	6.40	0.97	0.01	0.98	1.35	2.74	2.05	1.64	2.37	0.53
72.00	1.00	4.09	4.70	1.58	0.04	1.64	1.47	2.57	2.51	2.64	0.84	0.45
96.00	1.00	6.89	2.83	2.42	0.06	2.37	1.23	1.27	2.45	3.04	0.06	0.20
96.00	1.08	6.52	3.66	2.24	0.07	2.20	1.71	2.68	2.59	2.91	1.09	0.23
119.00	1.08	9.05	1.86	2.32	0.12	4.06	1.59	1.39	2.83	3.80	0.28	0.18
119.00	1.20	8.31	3.50	2.19	0.10	3.65	2.20	3.29	2.99	3.54	1.63	0.23
143.00	1.20	14.30	1.13	2.12	0.24	6.13	1.96	1.47	3.16	4.26	0.44	0.74
143.00	1.32	12.55	2.70	1.87	0.22	5.57	2.48	3.18	3.28	3.98	1.66	0.73
167.00	1.32	19.40	0.02	1.19	0.39	8.64	2.39	0.87	3.58	5.06	0.46	1.50
167.00	1.48	18.36	2.00	1.06	0.35	7.71	2.97	2.98	3.67	4.65	1.90	1.41
192.00	1.48	27.38	0.01	0.01	0.58	7.72	3.01	0.60	4.40	5.54	0.18	2.52
192.00	1.72	23.10	2.67	0.19	0.52	6.64	3.67	3.35	4.40	4.94	2.08	2.26
216.50	1.72	15.89	0.01	0.71	0.58	7.77	4.11	2.15	5.48	7.11	1.82	2.45
216.50	1.96	14.00	2.43	0.61	0.47	6.82	4.55	4.38	5.35	6.39	3.29	2.23
239.25	1.96	13.86	0.39	0.40	0.60	8.58	4.71	2.82	6.36	7.39	3.17	2.59
244.75	1.96	13.83	0.04	0.21	0.66	8.18	5.02	0.95	8.09	7.47	0.60	4.07

t	His	Ile	Leu	Lys	Met	Phe	Pro	Ser	Thr	Trp	Tyr	Val
0.00	0.47	2.16	2.53	1.69	0.54	0.65	1.18	2.49	2.67	0.21	0.76	1.98
24.00	0.49	2.12	2.49	1.76	0.57	0.72	1.18	2.57	2.76	0.20	0.84	2.03
49.50	0.45	1.98	2.33	1.77	0.46	0.65	1.10	2.68	2.66	0.20	0.86	1.90
72.00	0.47	1.95	2.25	1.93	0.46	0.61	1.06	3.03	2.74	0.20	0.75	1.83
96.00	0.38	1.56	1.66	1.55	0.34	0.42	0.95	2.79	2.44	0.14	0.59	1.45
96.00	0.59	2.12	2.57	1.89	0.66	0.80	1.57	3.86	2.70	0.31	0.64	2.07
119.00	0.56	1.75	1.97	1.95	0.54	0.61	1.57	4.05	2.71	0.26	0.72	1.75
119.00	0.83	2.48	3.18	2.38	0.95	1.10	2.34	5.37	3.04	0.47	0.77	2.56
143.00	0.72	1.83	2.08	2.25	0.73	0.73	2.15	4.53	2.79	0.31	0.49	1.89
143.00	0.95	2.49	3.17	2.62	1.09	1.17	2.79	5.69	3.08	0.51	0.57	2.62
167.00	0.90	1.79	1.89	2.49	0.96	0.82	2.70	5.03	2.90	0.41	0.54	1.91
167.00	1.15	2.58	3.20	2.90	1.36	1.33	3.41	6.35	3.23	0.63	0.62	2.77
192.00	1.13	1.94	2.03	2.96	1.25	1.10	3.31	5.69	3.12	0.54	0.58	2.17
192.00	1.43	2.93	3.71	3.42	1.73	1.72	4.14	7.30	3.52	0.81	0.68	3.24
216.50	1.57	2.82	3.40	4.14	1.79	1.65	4.25	8.59	3.56	0.80	0.88	3.17
216.50	1.78	3.58	4.70	4.40	2.14	2.13	4.87	9.65	3.85	1.00	0.93	3.99
239.25	1.90	3.42	4.33	4.91	2.16	2.05	4.94	10.29	3.87	0.98	1.05	3.89
244.75	1.88	3.39	4.19	5.00	2.18	2.08	5.22	9.92	3.73	1.01	1.02	3.85

Table A.4: Experimental data of fed-batch cultivation with continuous feeding. The units are described in Table 3.5.

t (h)	V	Xv	Glc	Lac	mAb	Ala	Arg	Asn	Asp	Glu	Gln	Gly
0.00	1.00	0.53	6.80	0.05	0.00	0.43	1.02	3.10	1.84	0.64	4.97	0.57
22.25	1.00	0.93	6.53	0.25	0.00	0.59	1.02	2.94	1.76	0.81	4.01	0.57
47.00	1.00	2.22	6.13	0.74	0.01	0.98	1.16	3.06	2.20	1.57	2.82	0.58
71.00	1.00	4.26	4.72	1.66	0.03	1.66	1.21	2.74	2.66	2.66	0.86	0.46
94.25	1.04	7.54	3.12	2.46	0.09	2.66	1.35	2.82	2.92	3.43	0.23	0.25
104.75	1.07	9.32	2.70	2.59	0.12	3.13	1.39	2.93	2.88	3.48	0.50	0.18
118.50	1.12	12.50	2.01	2.29	0.17	4.30	1.61	3.07	3.15	3.89	0.73	0.20
143.00	1.24	18.41	1.56	1.57	0.28	6.77	2.01	3.16	3.41	4.27	1.11	0.71
165.50	1.39	24.17	0.93	0.67	0.40	8.72	2.49	3.00	4.06	4.91	1.57	1.38
172.75	1.45	25.26	0.81	0.41	0.43	8.85	2.77	3.07	4.31	5.15	1.83	1.52
189.75	1.59	30.48	0.25	0.04	0.54	5.62	3.13	2.71	4.93	5.45	2.14	1.82
214.00	1.84	26.09	0.10	0.04	0.72	2.50	3.84	3.15	6.49	5.55	1.05	2.52
237.50	1.97	21.22	0.01	0.02	0.69	2.43	4.51	1.99	9.36	6.11	0.25	4.21
247.25	1.97	7.60	0.01	0.03	0.74	2.64	4.89	1.24	10.03	6.45	0.26	4.43
t (h)	**His**	**Ile**	**Leu**	**Lys**	**Met**	**Phe**	**Pro**	**Ser**	**Thr**	**Trp**	**Tyr**	**Val**
0.00	0.50	2.27	2.65	1.72	0.61	0.74	1.22	2.55	2.79	0.20	0.87	2.14
22.25	0.48	2.14	2.54	1.74	0.55	0.70	1.16	2.43	2.66	0.22	0.79	2.03
47.00	0.48	2.14	2.48	1.76	0.52	0.69	1.13	2.68	2.75	0.18	0.79	2.02
71.00	0.46	2.01	2.30	1.90	0.46	0.62	1.07	3.07	2.77	0.19	0.78	1.90
94.25	0.56	1.99	2.30	2.06	0.53	0.68	1.41	3.76	2.85	0.24	0.62	1.95
104.75	0.61	1.99	2.30	2.08	0.61	0.74	1.62	4.07	2.82	0.29	0.60	1.99
118.50	0.72	2.06	2.43	2.34	0.71	0.86	2.03	4.74	2.98	0.34	0.71	2.14
143.00	0.92	2.14	2.54	2.69	0.99	1.06	2.74	5.46	3.05	0.50	0.66	2.36
165.50	1.14	2.22	2.64	3.08	1.30	1.25	3.31	6.44	3.27	0.62	0.61	2.68
172.75	1.22	2.30	2.69	3.23	1.35	1.34	3.45	6.83	3.38	0.70	0.62	2.60
189.75	1.36	2.31	2.59	3.45	1.54	1.43	3.63	7.73	3.37	0.76	0.74	2.61
214.00	1.59	2.74	3.15	4.07	1.86	1.79	4.02	9.04	3.54	0.89	0.76	3.08
237.50	1.92	3.27	3.88	4.74	2.19	2.14	5.00	10.10	3.97	0.94	0.84	3.73
247.25	1.97	3.31	4.04	5.02	2.25	2.26	5.04	10.64	4.10	1.08	1.06	3.87

Appendix B

Datalogs

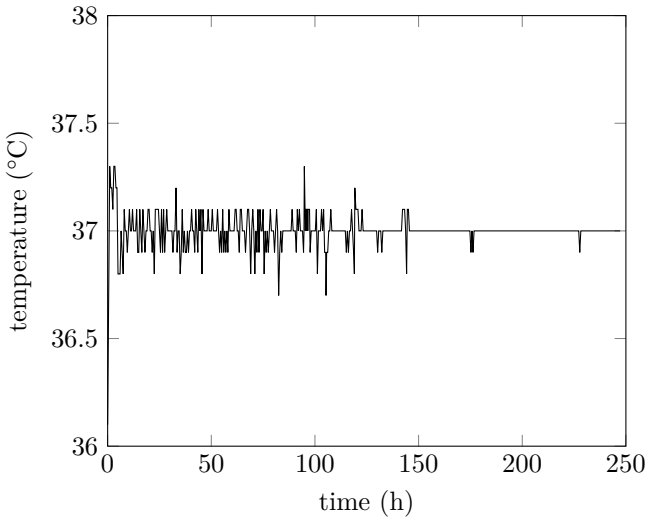

Figure B.1: Temperature data logged of the fed-batch cultivation with continuous feeding.

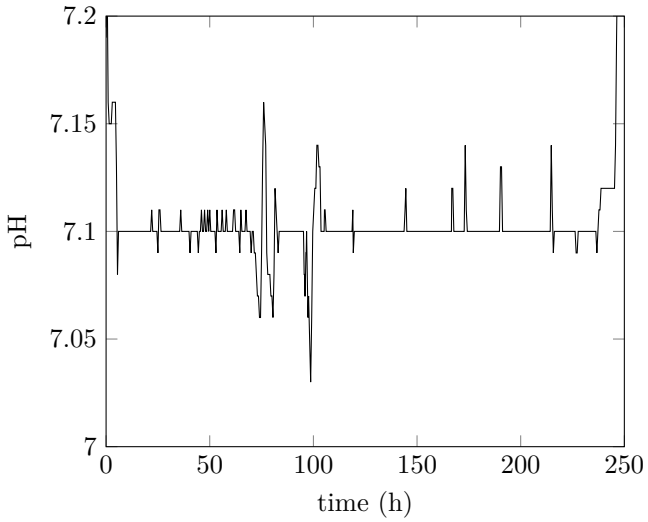

Figure B.2: pH data logged of the fed-batch cultivation with continuous feeding.

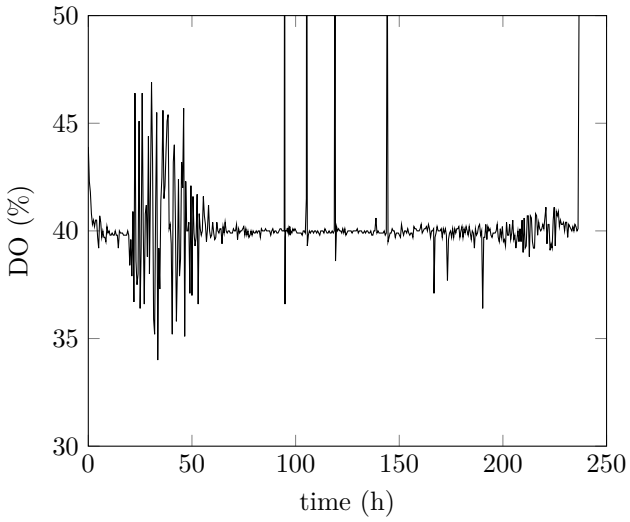

Figure B.3: Dissolved oxygen data logged of the fed-batch cultivation with continuous feeding.

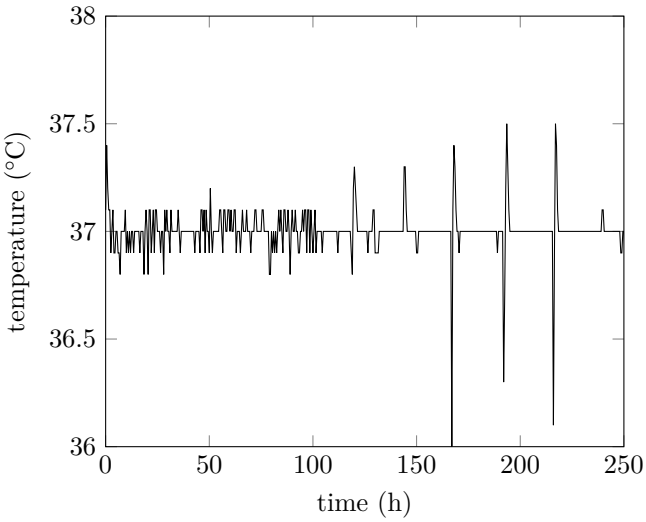

Figure B.4: Temperature data logged of the fed-batch cultivation with pulse feeding.

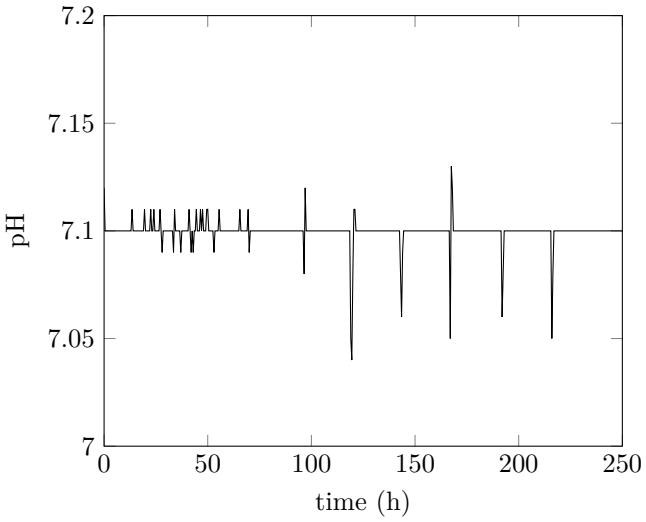

Figure B.5: pH data logged of the fed-batch cultivation with pulse feeding.

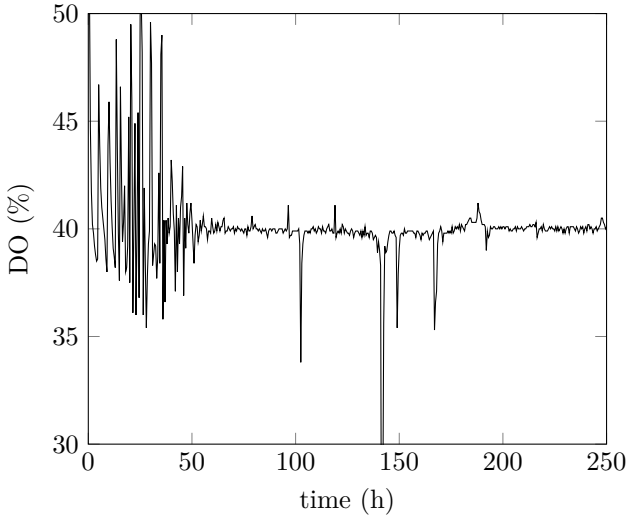

Figure B.6: Dissolved oxygen data logged of the fed-batch cultivation with pulse feeding.

Appendix C

Additional experiments

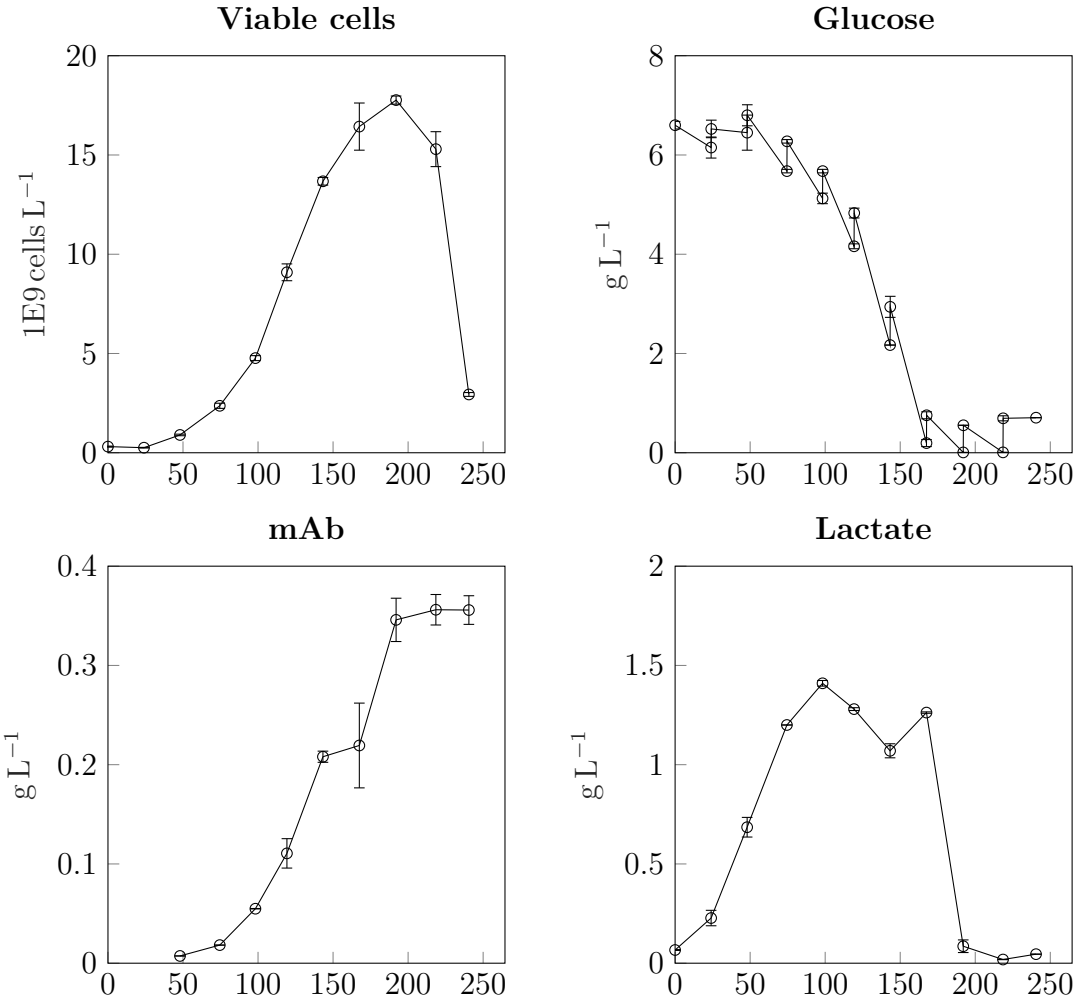

Figure C.1: Fed-batch experiment in conical cell culture tubes to test the feeding strategy recommended by the medium manufacturer. Starting volume was 20 mL. The feeding strategy is shown in Table 3.1. The x-axis represents the culture time in hours.